NASA/CR—2005-213134

Cold Aero Performance of a Two-Dimensional Mixer Ejector Nozzle

C. Balan
GE Aircraft Engines, Cincinnati, Ohio

January 2005

The NASA STI Program Office . . . in Profile

Since its founding, NASA has been dedicated to the advancement of aeronautics and space science. The NASA Scientific and Technical Information (STI) Program Office plays a key part in helping NASA maintain this important role.

The NASA STI Program Office is operated by Langley Research Center, the Lead Center for NASA's scientific and technical information. The NASA STI Program Office provides access to the NASA STI Database, the largest collection of aeronautical and space science STI in the world. The Program Office is also NASA's institutional mechanism for disseminating the results of its research and development activities. These results are published by NASA in the NASA STI Report Series, which includes the following report types:

- TECHNICAL PUBLICATION. Reports of completed research or a major significant phase of research that present the results of NASA programs and include extensive data or theoretical analysis. Includes compilations of significant scientific and technical data and information deemed to be of continuing reference value. NASA's counterpart of peer-reviewed formal professional papers but has less stringent limitations on manuscript length and extent of graphic presentations.

- TECHNICAL MEMORANDUM. Scientific and technical findings that are preliminary or of specialized interest, e.g., quick release reports, working papers, and bibliographies that contain minimal annotation. Does not contain extensive analysis.

- CONTRACTOR REPORT. Scientific and technical findings by NASA-sponsored contractors and grantees.

- CONFERENCE PUBLICATION. Collected papers from scientific and technical conferences, symposia, seminars, or other meetings sponsored or cosponsored by NASA.

- SPECIAL PUBLICATION. Scientific, technical, or historical information from NASA programs, projects, and missions, often concerned with subjects having substantial public interest.

- TECHNICAL TRANSLATION. English-language translations of foreign scientific and technical material pertinent to NASA's mission.

Specialized services that complement the STI Program Office's diverse offerings include creating custom thesauri, building customized databases, organizing and publishing research results . . . even providing videos.

For more information about the NASA STI Program Office, see the following:

- Access the NASA STI Program Home Page at ***http://www.sti.nasa.gov***

- E-mail your question via the Internet to help@sti.nasa.gov

- Fax your question to the NASA Access Help Desk at 301–621–0134

- Telephone the NASA Access Help Desk at 301–621–0390

- Write to:
  NASA Access Help Desk
  NASA Center for AeroSpace Information
  7121 Standard Drive
  Hanover, MD 21076

NASA/CR—2005-213134

Cold Aero Performance of a Two-Dimensional Mixer Ejector Nozzle

C. Balan
GE Aircraft Engines, Cincinnati, Ohio

Prepared under Contract NAS3–26617

National Aeronautics and
Space Administration

Glenn Research Center

January 2005

Document History

This research was originally published internally as HSR055 in August 1997.

Available from

NASA Center for Aerospace Information
7121 Standard Drive
Hanover, MD 21076

National Technical Information Service
5285 Port Royal Road
Springfield, VA 22100

Available electronically at http://gltrs.grc.nasa.gov

Table of Contents

Summary

Since 1986, NASA and the U.S. aerospace industry have been assessing the economic viability and environmental acceptability of a second-generation supersonic civil transport, or *High Speed Civil Transport* (HSCT). Environmental acceptability in terms of airport community noise and economic viability are critical elements in this endeavor. Development of a propulsion system that satisfies strict airport noise regulations (FAR36 Stage III levels), at acceptable performance and weight, is critical to the success of any HSCT program. 2D Mixer–Ejector exhaust systems are one approach in achieving this goal. In support of HSCT development, GEAE (GE Aircraft Engines), under contract to the NASA Lewis Research Center (Contract NAS3–26617), conducted this test program, at the NASA Langley 16-ft transonic wind tunnel to evaluate the cold aerodynamic performance aspects of the two-dimensional mixer ejector (2DME) exhaust system concept.

The effects of SAR (SAR, suppressor area ratio, = mixed-flow area ÷ primary nozzle throat area.), MAR (MAR = overall exhaust system exit ÷ mixing-plane area), flap length, CER (suppressor chute expansion ratio), chute alignment and free stream Mach number were investigated on a 1/11 th cold aerodynamic scale model of a 2DME exhaust system.

Two modes of ejector operation, subsonic and supersonic, were identified. Transition from subsonic to supersonic mode was associated with improved performance. The Nozzle Pressure ratio (NPR) at which transition takes place was affected by MAR, SAR and free stream Mach number.

Increasing the flap length improved thrust performance by about 1 point at 0.7 Mach, primarily due to associated changes in external boattail angle. Similarly, the staggered chutes performed slightly better than aligned chutes by about 0.5 to 1 points. The convergent chutes with CER of 1.0 performed better than convergent divergent (CD) chutes with CER of 1.22 and 1.38 at NPRs less than 3.5 and the CD chutes performed better at higher NPRs probably due to changes in expansion losses.

Pumping and nozzle performance peaked at MAR less than 1.0. A static gross thrust coefficient Cf_g of 0.99 was obtained under cold-flow conditions at NPR 3.5 and MAR 0.9 for SAR 2.5 (Cf_g = measured ÷ ideal thrust at fully expanded isentropic flow.), in supersonic mode. Significant reduction in thrust minus drag coefficient was observed under wind-on conditions, about 5 points at nozzle pressure ratio of 3.5 to 4 and a free-stream Mach number of 0.32. Increasing SAR increased pumping and Cf_g at static conditions, but the benefits were not realized under wind-on conditions due to increased ram drag and external form and friction drag.

A simple 1 Dimensional approach is used to evaluate the nozzle gross thrust coefficients, which confirms significant thrust augumentation due to secondary flow and the effect of ram drag under wind on conditions.

Introduction

The success of the next generation High Speed Civil Transport (HSCT) is dependant on achieving environmental acceptability and economic viability. Low noise exhaust nozzle technology has significant impact on both these issues. The exhaust system design that meets **FAR 36 Stage 3** takeoff acoustic requirements and provides high levels of cruise and transonic performance, while maintaining adequate takeoff performance at an acceptable weight and reliability is essential to the success of the HSCT program.

The 2D mixer – ejector nozzle represents one approach to reducing the exhaust noise of jet engines at takeoff. This concept incorporates previously demonstrated jet noise suppression technology of multi–element suppressors in concert with a high entrainment ejector to reduce the jet velocity exiting the nozzle, thereby reducing the jet noise during takeoff. This exhaust system was designed to operate along the GE21/F14 study L1M Variable Cycle Engine to power a Mach 2.4 HSCT with a range of 5000 nm and a pay load of 51,900 lbs.

The cold aerodynamic performance of this nozzle on a 1/11th scale model was evaluated at the NASA Langley Research Center 16–Foot Transonic Wind Tunnel and the acoustic performance on a 1/7th scale model was evaluated at the GEAE's Cell41 Anechoic Acoustic test facility (Reference 1). These two scale models of the 2D Mixer–ejector nozzle were designed, fabricated and tested by General Electric Aircraft Engines (GEAE), under NASA Lewis Research Center contract (NAS3–25415), as a part of NASA's High Speed Research (HSR) Phase I – Generation (GEN) 1.0 program.

The aero performance data obtained in GEN 1.0 – Phase I testing was insufficient to optimize the nozzle design from aero performance criteria. However, the limited acoustic data obtained indicates that the 2D Mixer–ejector nozzle is a viable candidate for meeting FAR 36 – Stage 3. To improve the understanding of the various key design parameters on the 2D mixer–ejector performance, additional configurations were designed and tested under NASA Lewis Research Center contract NAS3–26617, task order #19, at the NASA Langley's static thrust stand and the 16–Foot Transonic Wind Tunnel. This test program, referred to as GEN 1.0 – Phase II tests is the subject of this report.

The overall objective of this GEN 1.0 – Phase II test program is to expand the aero performance design data base needed to develop a 2D mixer–ejector exhaust nozzle. The specific objectives addressed in this test program are:

- Effect of primary/Core flow Expansion Ratio (CER) on secondary flow pumping and aero performance.
- The effect of ejector Mixing Area Ratio (MAR) on pumping and aero performance.
- The effect of Suppressor Area Ratio (SAR) on pumping and aero performance.
- The effect of chute stagger between the top and bottom rows of ejector on pumping and aero performance.

This report summarizes the testing carried out under the Task Order# 19 and data analysis performed. For analyses purposes, data from the earlier testing carried out under contract NAS3–25415 is included as required. For clarity, some of the model description, installation and instrumentation details are reproduced here from the final contract report of NAS3–25415. This enables the report to be sufficiently complete to provide necessary understanding of the model hardware and installation.

Exhaust System Description

The basic exhaust system considered in this program is of variable geometry, and the primary objective of the scale-model overall test program was to address acoustic and performance issues related to the takeoff mode configuration. A brief description of the cycle, full-scale preliminary design, and key overall geometric parameters that define the aerodynamic/acoustic performance at takeoff are discussed in this section.

Full Scale Exhaust System Preliminary Design

Figure 1 shows the preliminary design of the 2DCD mixer ejector nozzle evolved in the *Base Program* for the GE21/F14 Study L1M VCE to power a Mach 2.4 HSCT with a 5000-nmi range and a payload of 51,900 lbm. The nozzle is depicted in the takeoff position; the mixer chutes are deployed to break up the primary jet with alternating ambient flow entrained through the ejector inlet. Figure 2 shows the nozzle in supersonic and subsonic cruise modes; the mixer chutes are retracted from the primary stream and stowed.

Design point for the baseline exhaust system was selected to be the cycle condition that produced a net thrust of 50,000 lbf at an altitude of 689 ft and an airplane Mach number of 0.32 at a nominal airflow of 700 lbm/s, based on the airplane takeoff thrust requirements assumed in the preliminary design studies conducted in Reference 2. The cycle conditions corresponding to this thrust setting for the GE21/F14 Study L1M cycle are shown in Table 1.

Nozzle throat area is varied during takeoff as well as cruise conditions to accommodate engine flow variations. During takeoff, engine flow is held at the nominal value of 700 lbm/s as engine throttle is reduced from the sideline thrust setting to takeoff thrust (also commonly called community noise measurement). This thrust reduction is achieved by decreasing jet velocity, at an approximately constant engine air flow of 700 lbm/s, to help abate jet noise at the takeoff monitor. Such a thrust modulation requires an increase in nozzle throat area.

The required throat area variation for the engine operation is achieved in the full-scale preliminary design by two schemes as shown in Figure 3. In the scheme shown at the top, the primary nozzle throat area A_{P8} is controlled by holding the chutes fixed and rotating the convergent flap; this limits the nozzle SAR to 2.27 at the takeoff condition. In the scheme shown at the bottom, A_{P8} is controlled by holding the flap and rotating the chutes, which yields an SAR of 2.8 at the takeoff condition. However, this configuration yields a center streak of high-velocity flow in the primary stream, 2.72-in thick in full scale. From a noise-reduction consideration, a large SAR with no center streak of high-velocity jet is preferred. The decision to entrain larger amounts of ambient air at the risk of having a center streak of high-velocity primary jet was chosen as the preferred design feature based acoustic considerations.

Scale Model Exhaust System Design

Figure 4 is a photo of the exhaust system scale model with one sidewall removed, and Figure 5 is a schematic of the exhaust system model. The 2D mixer–ejector exhaust system in the suppressed mode consist of an upstream plenum in the primary flow path representing the mixed flow turbofan exhaust and suppressor chutes forming the primary flow path, followed by the mixing chamber formed by the two side walls and the upper and lower flaps, where the ambient secondary flow is entrained and mixed with the primary flow. The secondary flow inlets are located on the top and bottom upstream of the flaps. The secondary flow enters the mixing

chamber through the passages formed by adjacent suppressor chutes. It was recognized early in the program that efficient induction of ambient air into the ejector system is very essential. The mechanical implementation proposed in the preliminary design required the chutes to be rotated away from the main engine flow after takeoff, and such a scheme did not permit an aerodynamically "clean" ejector inlet — particularly at the confluence of the ejector inlet and chute geometries. The scale-model ejector inlet ramp has a very gentle radius and a shallow angle of approximately 26° to the horizontal. More recent mechanical designs and installation considerations near the wing trailing edge for these types of mixer/ejector nozzles probably will dictate shorter and steeper inlet ramps that may reduce the inlet recovery and also secondary mass flow entrained relative to the inlet tested under this test series.

All of the scale models under this test program employ a fixed-position, flush-inlet-lip design with a large radius, designed to accommodate the large variations in mass flow ratios to be encountered in the test configurations due to changes in suppressor area ratio (SAR range of 2.5 to 3.9) as well as large variations in primary nozzle pressure ratio (NPR range of 1.5 to 4.0).

Key Geometric Parameters

The overall exhaust system nomenclature are identified in Figure 6. The key overall dimension is flap/ ejector length *(Lej)* measured from the suppressor exit to the exit of the nozzle. The primary dimensions at the exhaust-system exit (station 9) are width from sidewall to sidewall (w_9) and the half height of the nozzle measured from the center line to the flap trailing edge (h_9). The number of chutes in each half of the suppressor *(n)* is an important overall parameter.

Figure 7. shows the key dimensions of the suppressor chutes. The three planes of importance are the primary throat (station 8), the suppressor exit (station 89), and the mixing plane (station "mix" or *m*). Correspondingly, three heights of the suppressor as measured from the centerline of the nozzle are identified as h_8, h_{89}, and h_{mix}. The gap between the centerline of the nozzle and the suppressor chute foot (h_{gap}) is another important dimension. The key dimensions along the width of the suppressor are the primary and secondary flow passage widths at the throat plane, w_{p8} and w_{s8} respectively, and at the suppressor exit plane, w_{p89} and w_{s89} respectively. In all of these key geometric definitions, the wall thickness of the suppressor chutes is included as a part of the secondary flow passage.

Based on these key dimensions, the following overall geometric parameters are defined.

Primary Nozzle Throat Area: $$A_{p8} = (h_8 - h_{gap}) \times w_{p8} \times 2n + 2 \times h_{gap} \times w_9$$

Secondary Flow Area at Throat Plane: $$A_{s8} = (h_{mix} - h_{gap}) \times w_{s8} \times 2n$$

By definition, the wall thicknesses of the chutes are included in the secondary flow chute width. Note that the height of the secondary flow passage used in the above definition is based on h_{mix}.

Total Mixed-Flow Area: $$A_m = A_{p8} + A_{s8} = 2 \times h_{mix} \times w_9 - 2n \times (h_{mix} - h_8) \times w_{p8}$$

The total mixed-flow area is defined as the sum of the primary and secondary flow areas at the throat plane. This is also equivalent to the total flow area at the mixing-plane location minus the projected areas of the fingers or primary-chute extensions. A simpler definition could have been the total area downstream of the finger/primary chute extensions $(2 \times h_m \times w_9)$. For the purpose of this report, the differences between the definitions are insignificant and do not alter the conclusions.

Primary Flow Area at Suppressor Exit: $A_{p89} = (h_{89} - h_{gap}) \times w_{p89} \times 2n + 2 \times h_{gap} \times w_9$

Exhaust Nozzle Exit Area: $A_9 = 2 \times h_9 \times w_9$

Suppressor Area Ratio: $SAR = A_{mix} / A_{p8}$

The suppressor area ratio is defined as the ratio of the mixed-flow area to the primary nozzle throat area. SAR plays an important role in the pumping characteristics. Larger SAR's lead to higher pumping and correspondingly reduced exhaust jet velocities. However, for a given primary mass flow/throat area, a larger SAR also implies a larger and heavier nozzle.

Chute Expansion Ratio: $CER = A_{p89} / A_{p8}$

The chute expansion ratio is defined as the ratio of the primary flow area at the suppressor exit to the primary throat area. CER represents the degree of expansion achieved by the primary flow inside the suppressor chutes. An ideally expanded primary jet that matches the internal back pressure is expected to reduce internally generated shock noise and improve performance. A CER of 1.0 implies that the primary flow throat is located at the exit of the suppressor chutes. Please note, this definition is based on gross parameters defined at the throat and exit of the chute primary flowpath; any significant variation in local chute geometry should be considered in evaluating the effect of CER.

Mixing Area Ratio: $MAR = A_9 / A_{mix}$

The mixing area ratio is defined as the ratio of the overall exhaust system exit area to the mixing plane area.

Ejector Length: L_{ej} is the length of the ejector (divergent flap) as measured from the suppressor exit plane to the exit of the overall nozzle. Longer ejectors increase acoustic-treatment area, which can effectively suppress the internally generated noise and aid in meeting the noise goals, at some increase in overall exhaust system weight and performance penalty.

Model And Test Setup

Model Description

The scale model slightly deviated from the full scale design as the need for variability of basic geometric parameters had to be addressed while maintaining the simplicity of construction and test procedures. A cross section of the cold aero performance scale model exhaust system is shown in figure 8. As explained in the previous section the scale model ejector inlet ramp has a very gentle radius and a shallow angle of approximately 26 degrees to the horizontal. The ejector inlet lip/ flap leading edge also has a fairly large radius. Both the scale model inlet ramp and the inlet lip/flap leading edge were fixed for all configurations tested. The three piece flap consisted of the leading edge, flap adjusting wedge piece and the flap, as shown in Figure 8. By installing different wedge pieces between the leading edge and the flap, the flap divergence angle can be changed. The ejector side walls were of fixed design for a given flap length. The bottom and top suppressor chute racks are of single piece construction and can be changed independently. The primary variation in configurations was achieved by changing the suppressor chutes or the flap angle. The ejector pumping can be changed significantly by the design of the suppressor chutes and the flow area available for the secondary flow can be controlled. As the scale model nozzle width between the side walls and the height at the suppressor chute exit was fixed for all configurations any change in the secondary flow area through the suppressor chutes resulted in a corresponding change in the primary flow areas. Consequently the various designs tested had different primary throat areas and the scale factor relative to full scale was slightly different for each configuration.

All of the scale model aero–performance testing was carried out using cold (ambient temperature) primary flow. The data needs to be corrected for temperature effects when applied to full scale.

Model Design Parameters

Phase I Model

The aero performance model built under NAS3–25415 was designed to represent the corresponding acoustic model that was tested in the GEAE's Cell41 Anechoic acoustic test facility. Many variations of this configurations to reduce the overall acoustic risk in meeting the program goals were tested. The full scale preliminary design parameters explored had the following attributes:

20 Convergent Divergent aligned chutes with a full scale primary throat area of 1086 sq inches.
Two SARs of 2.8 and 3.3.
Two flap lengths of 80" and 120" in full scale.
Center gap from chute bottom to chute bottom of 2.72" full scale.
Center wedges of two different lengths, at the center of the nozzle to eliminate the center gap, there by reducing the high velocity center streak, as well as, providing for more acoustic treatment.

In addition, the scale model suppressor chutes for both SARs were designed with two different CERs to provide for reasonably matched static pressure at the chute exit. The flap adjusting wedges corresponding to 4 different MAR variations were also designed. The variations in CERs and MARs possible with this scale model hardware were as follows:

CER – 1.22 & 1.38
MAR – 1.40, 1.20, 1.00 & 0.80 (with primary focus on MAR=1.4 & 1.2)

A summary of the model design parameters and test configurations investigated in this test series is given in Table 2.

Phase II Model

The overall performance data obtained during the GEN1.0 aero performance testing (Ref. 1) indicates that significant performance improvements may be possible with MARs less than 1.0 i.e. convergent flaps.

Another primary candidate identified for investigation was the CER. The overall performance was significantly improved for a given geometry going from a CER of 1.38 to 1.22. One of the primary reasons for CERs greater than one i.e. convergent divergent primary chute flow path was to match the static pressure at the ejector mixing plane there by reducing any shock losses as well as associated shock noise. However, the acoustic data obtained in Cell41 indicated that the overall contribution of the shock noise was not significant (Ref. 1). Consequently, fully convergent primary chute i.e. CER of 1.0 was identified at the end of the GEN1.0 testing as a prime candidate for further investigation.

The effect of chute alignment/stagger was also selected for further investigation as the staggered chutes have the potential to enhance the mixing of the primary and secondary flows there by providing a means of either reducing the acoustic signature or for a given noise level reducing the flap length. The stagger was obtained by translating the bottom chute rack by half a period. A comparison of the staggered and aligned chute geometry at the exit is given in Figure 9.

The acoustic data obtained on the GEN1.0 testing also indicated that at the operating conditions of interest, the nozzle with SAR of 2.8 was quieter than SAR of 3.3. The optimum SAR from acoustic requirements could be lower than 2.8 for the cycle operating points of interest and it was decided to include an additional SAR of 2.5 for aero performance evaluation.

The hardware designed and procured under phase II program are the following:

SAR 2.8 Aligned suppressor chutes with CER of 1.00.
SAR 2.8 Staggered suppressor chutes with CER of 1.22.
SAR 2.5 Staggered suppressor chutes with CER of 1.00.
Flap Wedges for MARs – 0.85,0.90,0.95, & 0.975.

A summary of the model design parameters and test configurations investigated in this test program are given in Table 3.

Test Facility & Test Setup

The performance test was conducted in the NASA Langley 16 foot transonic wind tunnel. This facility is a single return, continuous flow exchange air cooled, atmospheric pressure wind tunnel with an octagonal, slotted throat test section. The wall divergence is adjusted as function of the air stream dew point and Mach Number to reduce the impact of any longitudinal static pressure gradient in the test section. Test section Mach number is continuously variable to a maximum of 1.3. The average Reynold's number per foot ranges from about 1.4×10^6 at a free stream Mach number of 0.20 to about 4.0×10^6 at a free stream Mach number of 1.30. Further details on this test facility can be obtained in Reference 3.

The Langley non–axisymmetric single engine propulsion simulator (Reference 3) was used to evaluate the performance of the exhaust system models under investigation. A detailed sketch of the propulsion simulation system is presented in Figure 10. As illustrated in Figure 10, this simulator/model consisted of five major components namely a nose–fore body, a low pressure plenum, an instrumentation section, a transition section, and the test nozzle.

The nose–fore body section was nonmetric and all of the sections downstream of the nose–forebody were metric. The five component force balance was located in the low pressure plenum section. A low friction teflon seal was inserted at the metric break between the nose–forebody and the low pressure plenum to eliminate cross flow through the nonmetric – metric interface with out transmitting axial force across the interface.

The primary flow of the exhaust nozzle was supplied by a high pressure air system external to the simulator. A continuos flow of clean, dry, high pressure air at a stagnation temperature of 80^0F entered the high pressure plenum located in the nose–forebody through six supply lines located in the support strut as shown in Figure 10. The high pressure air was discharged radially outward from the high pressure plenum to the low pressure plenum through eight equi–spaced sonic nozzles located around the circumference of the high pressure discharge pipe. This arrangement minimizes the effect of any forces resulting from the transfer of axial momentum as the air passes from the non metric to the metric part of the simulator. Two flexible metal bellows were used to seal the low pressure plenum and compensate for any axial forces resulting from pressurization.

The air flow in the low pressure plenum was diffused over the balance housing and straightened by a 79 percent open area baffle plate. The air flow then passed through the instrumentation section, were the stagnation temperature and pressure of the air supply entering the test hardware was measured. The airflow, then passed through the transition section. In the transition section, the internal geometry changed from circular to rectangular, compatible with the 2D mixer–ejector nozzle test hardware. From the transition section the air flow was exhausted through the test hardware.

The single engine propulsion simulator with the 2D mixer–ejector exhaust system model was supported in the tunnel by a sting–strut support system as shown in Figure 10. The nose–forebody of the simulator at its 12 o'clock position, was attached to the bottom of the support strut. The centerline of the simulator/model was located along the test section center line and the centerline of the sting was located 22.0 inches above the test section centerline. The simulator/model blockage was approximately 0.23 percent of the test section cross section and the maximum blockage including the model support was approximately 0.31 percent. The photographs of the installation and the model hardware are given in Figure 11 through 13.

Test Configurations & Procedure

Test Configurations

Table 2. presented earlier, gives a summary of configurations tested during the GEN1.0 – Phase I series of tests under NAS3–25415. Some of these configurations were repeated in the current GEN1.0 –Phase II test program to establish repeatability as well as for further investigation. The configurations tested under the Phase II series of tests are given in Table 3, discussed earlier.

Test Procedure

The Phase II testing was conducted at two different locations. Static tests of selected configurations were conducted in the static test stand located in the Model Preparation Area (MPA). This helped in acquiring significant volume of data on selected configurations, especially the effect of MAR on the performance characteristic. For a given suppressor geometry i.e. SAR & CER, the MAR was changed by adjusting the flap angle and performance of the nozzle was evaluated as a function of primary nozzle pressure ratio NPR. The wind tunnel data was gathered in a similar fashion. For a given suppressor chute geometry, flap length and MAR the performance data was acquired at constant wind tunnel Mach numbers, by changing the primary nozzle pressure ration NPR. All of the wind tunnel performance data were acquired at Mach numbers of 0.0, 0.32, 0.40, 0.55, and 0.70.

Additional testing was conducted at both locations to determine the momentum tares of the high pressure air on the measured forces. This consisted of jet–off and jet–on loadings of the installed model in the model preparation area. The jet–off model calibrations were performed on axial force, normal force and pitching moment. The jet on calibrations in the model preparation area were performed using three calibration nozzles having a range of throat areas of 5.711, 8.501 & 11.352 in^2. For each throat area, at various levels of normal force and pitching moment, the jet–on calibration was performed upto a NPR of 6.0. The jet–on calibration, using the 8.501 in^2 calibration nozzle was repeated in the wind tunnel immediately after installation and just prior to removal of the model to insure that the calibrations performed in the MPA are valid and no significant changes occurred during the test program.

Instrumentation and Data Reduction

Instrumentation

Basic model instrumentation included the five-component force balance shown in Figure 10. A rake of 12 total-pressure probes in the instrumentation section was used to measure the primary nozzle flow total pressure. An iron-constantan thermocouple in the instrumentation section also provided the total temperature of the primary nozzle flow. In addition, the test facility instrumentation measured parameters to define the test conditions: wind tunnel test section total pressure, total temperature, and Mach number. The primary nozzle mass flow supplied by the test facility was also measured using a *Multiple Critical Venturi* system (Reference 3).

Ejector Inlet Conditions – The parameters of interest for the secondary flow are the total pressure, total temperature, and secondary mass flow. The total temperature of the secondary flow was assumed to be that of the tunnel free-stream; no separate measurements were made. The secondary flow total pressure at the ejector inlet was measured using 15 probes. The instrumentation consisted of three rakes with five total-pressure probes each. Two of the rakes were located at the top inlet and the other was located in the lower inlet. The average rake total pressure were used to define the ejector inlet secondary flow total pressure.

A total of six wall static pressure taps, two at each rake location, one on the inlet ramp and the other on the inlet scoop/flap leading edge, were used to define the local static pressure. These wall static pressure taps were located to coincide with the tip of the total-pressure probes as shown in Figure 14. Measurements from the rake total pressure probes and corresponding wall static pressures were used to calculate local Mach numbers and the total secondary mass flow rate.

Ejector Inlet Wall Static Pressures – A total of 17 wall static pressure taps were located in the ejector inlet. Of these, six were located at the inlet total pressure rake locations, as mentioned above, and were used for evaluating the mass flow. The remaining 11 static pressures were located in the inlet ramp and scoop/flap leading edge. These provided additional diagnostic information on the inlet flow quality. A total of Four of these eleven static pressures were located along the upper surface of the inlet ramp, see Figure 14. The remaining seven static pressures were distributed over the leading edge of the flap/internal surface of the inlet scoop.

Mixer Chute Static Pressures – Referring to Figure 15, a total of 21 static pressure taps were distributed over the mixer chutes. Six were located on the primary flow side, and the remaining 15 were located on the secondary flow side of the chutes.

Flap/Ejector Shroud Static Pressures – Both the short and the long upper flaps were instrumented with two rows of static pressure taps along the length of the flaps. The long flap had a total of 14 taps, and the short flap had a total of 10. Referring to Figure 16, one row was aligned with the primary flow exiting the suppressor chute, and the other row was aligned with the secondary flow exiting the chute.

Data Reduction:

From the measured quantities various performance parameters were calculated by the facility data reduction program. The primary calculations carried out based on measured parameters were limited to the following:

1) Calculation of wind tunnel free stream conditions – i.e. free stream Mach M_0
2) Calculation of balance forces corrected for balance and metric support tares – i.e. $(F–D_{noz})$
3) Calculation of the actual primary flow based on multiple choked Ventury data – i.e. W_p
4) Calculation of the primary ideal flow and jet velocity – i.e. W_{pi}, V_j
5) Calculation of secondary flow entrainment through integration of mass flow across the inlet, from measured rake total pressures, wall static pressures and free stream total temperature. These calculations assume no significant spanwise variation of secondary flow properties.

Key Performance Parameters

Key performance parameters are listed in this section. Data-reduction procedures are not discussed in detail due to the simple nature of the calculations.

Free stream conditions

The free-stream conditions defined below include directly measured as well as calculated parameters.

M_0	Free-stream Mach number, calculated
P_{T0}	Free-stream total pressure, measured (psia)
P_0	Free-stream or ambient static pressure, measured (psia)
T_{T0}	Free-stream total temperature, measured (°R)
T_0	Free-stream static temperature, calculated (°R)

Primary flow parameters

P_{Tp}	Primary nozzle inlet total pressure, measured (psia)
T_{Tp}	Primary nozzle inlet total temperature, measured (°R)
W_p	Primary nozzle weight flow (lbm/s), measured using choked flow venturi
W_{pi}	Primary nozzle ideal weight flow, calculated (lbm/s)
NPR	Primary nozzle pressure ratio, calculated as P_{Tp} / P_0
V_j	Primary nozzle ideal jet velocity, calculated based on NPR and T_{tp}
F_i	Primary nozzle ideal thrust based on measured weight flow rate, $W_p \times V_j$

Secondary flow parameters

P_{Ts}	Secondary inlet total pressure, measured (psia)
W_s	Secondary inlet weight flow, calculated (lbm/s)

Overall system performance

F–D	Measured thrust minus drag corrected for balance tares
$F–D_{noz}$	Measured thrust minus nozzle drag (deduced from above)
W_T	Total nozzle flow rate: sum of primary + secondary, $W_p + W_s$ (lbm/s)

Coefficients

From the above parameters, the following coefficients are determined.

C_{D8}	Primary nozzle flow coefficient defined as the ratio of measured primary nozzle flow rate to the ideal primary nozzle flow rate: W_p / W_i
$C_{f–Dnoz}$	Thrust minus nozzle drag coefficient defined as the ratio of measured nozzle thrust minus drag to the primary nozzle ideal thrust: $(F–D_{noz}) / F_i$
Cf_g	Nozzle thrust coefficient, estimated for the static case only. (Total external drag and ram drag due to secondary flow entrainment are zero at static conditions.) Same as $C_{f–Dnoz}$ for static case.
ω	Pumping ratio, defined as the ratio of secondary to primary flow rates: W_s / W_p
$\omega\sqrt{\tau}$	Corrected pumping ratio: $(W_s / W_p) \sqrt{(T_{Ts} / T_{Tp})}$

Aeroperformance Data Analyses

This investigation on the mixer–ejector nozzle performance was comprehensive enough to establish the effect of Mixer exit to nozzle exit plane exit are MAR, the effect of primary chute expansion ratio CER, the effect of chute alignment, the effect of Suppressor Area Ratio SAR, and flap length. In addition some of the basic phenomena on the two possible modes of operation of the ejector i.e. subsonic and supersonic modes were also established. All of these aspects of ejector performance and their impact on both the nozzle performance is discussed. The comprehensive data report will be published by NASA Langley and not included here as a part of this report.

Basic ejector characteristics

Typical static performance of the ejector in terms of the thrust coefficient, pumping and secondary flow entrainment are presented in Figure 17 as a function of the nozzle pressure ratio, for SAR=3.3, CER=1.22, MAR=0.9. Note that the thrust–drag coefficient and thrust coefficient are the same for static case, since the total drag (sum of ram drag and external drag) is zero under static conditions. In this figure the data is presented for both increasing as well as for decreasing pressure ratios. The various data points of interest along the thrust performance characteristics given in Figure 17a are identified as A,B,C,D,E & F for clarity of discussion. The thrust coefficient continuously increases with increasing NPR from a pressure ratio of 1.5 to 3.5 denoted as points A, & B respectively. As the pressure ratio is increased from point B to C there is a significant increase in the C_{fg} for a small change in NPR. Further increase in NPR does not change the C_{fg} significantly and the characteristics is nearly flat from point C to D. As NPR is decreased from its maximum value of about 5.0 for this particular test, the C_{fg} follows the higher levels back to point C. As the pressure ratio is decreased further, the C_{fg} continues to follow the higher levels to point E before transition to the lower levels of curve A–B. There are two significant aspects to the thrust coefficient variation with NPR. First is the general behavior with a significant discontinuity and two distinctly different levels or modes of performance. The other is the overlap in the two performance characteristics. In the particular set of data presented in Figure 17, the thrust coefficient at NPR of 3.5 is not single valued and is a function of how the operating condition is achieved i.e. increasing or decreasing NPR. These two aspects namely the discontinuity in the performance characteristics and the hysterisis – or the non singular performance characteristics observed in approaching a given operating point along increasing or decreasing NPR, can lead to control system stability problems in the full scale exhaust system designs and should be considered from all aspects of the exhaust system operating envelope.

The key observation that can be made from figure 17b is that the pumping ratio decreases with increasing NPR to its lowest values. The primary reason for this behavior being the continuos increase in primary flow with increasing NPR. The secondary flow increases steeply as NPR is increased from its lowest value and reaches a maximum around NPR of 3.5 as shown in Figure 17c. The secondary flow then gradually decreases with increasing NPR. It is important to note that the transition or the discontinuity in performance indicated in Figure 17a, as NPR is increased from its lowest value, occurs at the same pressure ratio where the maximum in secondary flow is observed. No significant discontinuity is observed in either the corrected pumping ratio or the secondary flow. The estimated secondary flow entrainment is probably in significant error, especially under static conditions. The primary reason for the error is the lack of instrumentation to account for any spanwise distribution in the flow properties at the inlet. Referring to Figure 14, the rakes for estimating the secondary flow were located reasonably away from the wall and consequently the distortion in the flow field near the end walls are not captured. This distortion could be significant under static conditions, as the secondary flow is entrained from all directions and the end walls act like sharp

edged inlet resulting in poor flow quality. The secondary flow is probably overestimated in the current calculations. The estimated pumping characteristics should be treated for qualitative evaluation only and not for quantitative analysis.

The flap pressure distributions for all of the above nozzle pressure ratios are given in Figure 18. The flap static pressures have been non dimensionalized by the free stream static pressure P_0 and the corresponding axial locations measured from the suppressor chute exit have been non dimensionalized by the flap length. In evaluating these static pressures it must be understood that the total pressures are not constant along the length of the flap due to the mixing process. However, it may be safe to assume that the primary and secondary flows are essentially unmixed immediately down stream of the suppressor exit. Due to the complicated nature of the flow characteristics and the possibility of significant pressure gradients along the height of the nozzle, the pressure taps located at chute exit and vicinity must be used cautiously.

Figure 18a and 18b give the flap static pressure distribution of pressure taps aligned with primary flow center line and secondary flow center line respectively, for all NPRs. The primary observation is the two distinctly different trends in flap static pressure distribution, one predominantly higher than ambient and other lower than ambient. Also all of the static pressure distributions that are higher than ambient are associated with the lower range of performance. In general, for NPRs less than 3.5 the pressure distribution beyond 20 percent of the flap length is higher than ambient and the pressure distribution indicates primarily accelerating flow characteristics from 50 to 70 percent of the flap length to nozzle exit. The accelerating characteristics towards the exit of the nozzle at MAR of 0.9 i.e. converging nozzle indicates that the flow is primarily subsonic in this region. The secondary flow aligned static pressure taps immediately downstream of the suppressor exit at about 6 percent of the flap length indicate secondary flow static to total pressure ratios less than critical and the secondary flow is primarily subsonic. The static pressure gradient from 6 percent of the flap length to 20 percent of the flap length can not be explained easily as the secondary flow total pressure is not constant due to the mixing process. The primary conclusion based on the pressure distribution is that the mixed flow is subsonic, for NPRs lower than 3.5 at which the discontinuity in performance characteristics is observed. For mixed flow to be subsonic with supersonic primary, it can be expected that both streams are subsonic downstream of the primary chute exit. This implies that the primary must pass through a normal shock down stream of the chute exit. This could explain the significantly poor performance observed in the subsonic mode. For NPRs greater than 3.5, in general, the pressure distribution indicates predominantly lower than ambient static pressures, with a significant pressure rise near the exit of the nozzle beyond 85 percent of the flap length. The steep rise in static pressure near the mixer exit also indicates possible shock presence in the flow. The general flow features reasonably down stream of the suppressor exit indicate that the mixed flow is supersonic. This is consistent with the basic ejector theory (Reference 4), as there are two solutions possible for the mixed flow, one subsonic and other supersonic, based on the mixing chamber geometry and inlet and exit flow conditions. The two operating regions of the ejector are named respectively subsonic and supersonic modes. This transition from subsonic to supersonic mode is observed at all MARs, and there is significant improvement in performance associated with the supersonic mode. At MARs less than one in supersonic mode of ejector operation, the nozzle actually acts as a supersonic diffuser.

Another important feature observed at MARs lower than 1.0 is the hysterisis explained earlier. Figure 19 compares the primary and secondary flow aligned static pressure distributions for the four selected cases corresponding to the four corner points B–C–E–F of the hysterisis loop identified in Figure 17. In all cases the pressure distribution of the two rows of taps are identical beyond 20 per-

cent of the flap length from chute exit. Approaching the NPR of 3.5, from lower pressure ratios, the flap pressure distribution in Figure 19a indicates subsonic mode operation. The secondary flow aligned static pressures at and very close to the exit indicates a diffusing trend with the chute exit secondary flow static to total pressure just above critical. As NPR is increased to 3.8, the secondary flow static to total pressure ratio at chute exit is well below critical and the pressure distribution given in Figure 17b indicates supersonic mode of operation with predominantly lower than ambient static pressures over most of the flap length with a steep rise in static pressure to near ambient levels at the exit of the nozzle. As the pressure ratio is decreased back to 3.5, the flap static pressure distribution given in Figure 19c indicates that the nozzle is still operating in the supersonic mode. Further decrease in NPR to 3.2, results in the nozzle operation in subsonic mode as indicated by Figure 19d. This behavior is typical of the observations on all of the mixer ejector models described in this test series, at MARs less than 1. The only difference is the NPR at which transition occurs, level of discontinuity and hysterisis, which are discussed later, under the effect of MAR on performance.

The performance of the SAR 2.8, CER 1.22 aligned chute long flap configuration at a MAR of 1.2 is presented in Figures 20 through 22. Figure 21a and 21b give the flap static pressure distribution of pressure taps aligned with primary flow center line and secondary flow center line respectively, for all of the NPRs. Figure 22 gives a comparison of primary and secondary chute aligned flap static pressures at selected NPRs.

At nozzle pressure ratios of 1.5 through 3.5 the flap static pressures (Figure 21a) indicate a gradually diffusing pressure distribution downstream of the mixer exit, beyond the first 30 to 40 percent of the flap length. Considering that the flaps are diverging as indicated by a MAR of 1.2, the flow should be subsonic in the mixing area, and down stream along the length of the flap. At nozzle pressure ratios of 2.5 and greater, beyond 5 percent of the flap length, there is a continuos decrease in pressure levels, indicative of accelerating flow, followed by a significant rise in flap static pressure and a region of nearly flat pressure distribution. The location of the sudden raise in static pressure moves down stream towards the exit of the nozzle with increasing nozzle pressure ratio, from approximately 40 percent of the flap length at NPR of 2.5 to 70 percent of the flap length at NPR of 4.0. Once again considering the MAR, it can be postulated that the mixed flow is supersonic and the mixing chamber acts as a supersonic nozzle. In the supersonic mode of operation for a diverging mixing area ratios, i.e. MAR > 1.0, the location of the shock is a function of the nozzle exit back pressure. As the primary nozzle pressure ratio is increased, the mixed flow total pressure also increases and the shock moves towards the exit of the nozzle. At high enough pressure ratios the mixer ejector nozzle exit will be fully supersonic. A significant increase in the nozzle performance is observed associated with the supersonic mode. Significant model vibration/instability was also experienced with the transition from subsonic to supersonic mode.

The comparison of the primary and secondary flow chute aligned pressure taps, as given in Figure 22 indicates that at all NPRs, the static pressures at and beyond 20 percent of the flap length from the suppressor chute exit are nearly identical. The primary chute aligned static pressure at X=0, i.e. at the chute exit for all nozzle pressure ratios of 2.0 and above yield an expansion ratio (primary total to local static pressure ratio) of about 3.8. This could be due to the actual geometry of the scale model. It is also important to note that at NPRs of 1.5 and 2.0 the primary chute aligned pressure taps all indicate diffusing flow characteristics, while the NPRs of 2.5 and 4.0 both indicate rapid acceleration followed by sudden diffusion. The primary reason for the behavior at 2.5 and above could be the shape of the primary chute extensions. The static pressure tap at X/L_{ej} of 0.02 is located on the primary chute extension and the static pressure tap at X/L_{ej} of 0.058 is located down stream of the primary chute extension on the flap. The supersonic flow from the primary chutes are vectored in

this region by 15^0 to the flap and consequently must go through a compression turn. This could be the primary reason for the observed over acceleration and deceleration. At all pressure ratios of 2.0 and above the secondary flow aligned pressure taps at the chute exit indicate possible choking as the local static pressure is equal to or lower than the critical pressure ratio of 0.528 times P_0. Further analysis is needed to evaluate the behavior of these static pressures at NPR of 2.0. This static pressure tap is located in the area between the adjacent primary chute extensions in a region of very high curvature as the flap leading edge blends with the straight portion of the flap. The flow could be locally sonic and may not represent the entire flow field. This reasoning is further substantiated by the fact that at X/L_{ej} of 0.058, the secondary flow aligned static pressure at NPR of 2.0 is reasonable above critical pressure ratio.

Figure 23 illustrates the various operating modes of the mixer ejector nozzle schematically. Transition or mode switch exhibited by the mixer ejector nozzle is associated with the state of the mixed flow i.e. subsonic or supersonic and is experienced at all MARs. However, at MARs less than one , the mixing chamber formed by the flaps and side walls act as a diffuser in the supersonic mode. To establish supersonic flow for this geometry, a normal shock must be passed through the exit. However, once supersonic flow is established in the mixing chamber, it can be sustained at lower pressure ratios. This phenomena is similar to a wind tunnel staring problem and results in the hysterisis observed. A review of the flap static pressures support the general flow features illustrated in Figure 23.

The NPR at which the transition occurs is a function of the geometry and ambient conditions which will be discussed under the effect of MAR. All of the basic characteristics presented in the subsequent discussions are for increasing NPR and includes both the subsonic and supersonic ejector modes of operation. The data acquired in this test series were centered around improving pumping characteristics and performance. The data acquired illustrates the effect of some key design parameters on pumping and nozzle performance. This investigation was comprehensive enough to establish the effects of MAR, SAR, CER, Flap Length, as well as the free–stream Mach number. In addition some of the basic phenomena on the two possible modes of operation of the ejector i.e. subsonic and supersonic modes were also established. All of these aspects of ejector performance and their impact on both the nozzle performance and pumping is discussed.

Effect of Free Stream Mach Number

The effect of free stream Mach number on the thrust performance for SAR 2.8, CER 1.0 Long flap – aligned chute configuration is given in Figure 24, and data are presented for three different MARs. The primary observation is the significant reduction in the thrust minus drag coefficient with external flow by about 5 points at a free stream Mach of 0.32 at NPR of 4.0 relative to static conditions and the penalty associated with external flow at lower NPR is even more significant. The slope of the thrust minus drag coefficient variation with NPR for wind on cases is also steeper relative to the static case, and the slope increases with increasing external Mach number. The external flow also impacts the characteristics some what differently at different MARs. Especially, at MAR of 0.8 the performance at 0.32 Mach is nearly flat, but the static performance is also significantly different compared to other MARs. One significant observation is the absence of transition from subsonic to supersonic mode. The corresponding pumping characteristics given in Figure 25 indicates that there is a slight increase in pumping with free stream Mach number. This increase in pumping is essentially due to the higher value of free stream total pressure P_{ts} with free stream Mach number. For a given NPR and ambient static condition, the primary mass flow is essentially same. The ideal secondary flow total pressure is 7.4, 11.6, 22.8 and 38.7 percent higher than that of the static

condition at free stream Mach numbers of 0.32, 0.40, 0.55 and 0.70 respectively. Consequently, one can expect a corresponding increase in pumping with free stream Mach number. The actual increase in pumping is lower than the increase in secondary flow total pressure as the inlet recovery is significantly lower with increased free stream Mach number.

Referring to Figure 26, the estimated secondary flow corrected for same free stream static pressure and the secondary flow total temperature indicates, at constant NPR the entrainment increases with increasing Mach number, except that Mach 0.32 entrainment is not significantly higher than static, in spite of the significant increase in the secondary flow total pressure (about 7 percent) at Mach 0.32 relative to the static condition. Caution must be exercised in interpreting this data as possible significant flow distortion in the span wise direction, especially under static conditions, was not included in estimating the secondary flow. Under wind on conditions, there is a significant boundary layer development along the model, which is ingested along with the free stream flow. This is illustrated by the total pressure distribution at the inlet as function of the inlet height given in Figure 27. The wall statics at the ramp and scoop side of the inlet are also indicated in this figure. There is a significant reduction in the total pressure over most of the inlet away from the ramp side at Mach 0.32, while the total pressure distribution is flat over most of the inlet at Mach 0.0. Some of this is due to the wall boundary layer over the entire fore body being ingested by the ejector inlet. It can bee seen that at high Mach numbers of 0.55 and 0.7 the ramp side total and static pressures are the same over a good portion of the inlet height indicating separated flow. The overall increase in entrainment observed is not proportional to the increase in free stream total pressure due to the inlet total pressure recovery.

The performance of the nozzle, likewise is affected by two primary sources of losses associated with external flow. First one is the external friction and pressure drag of the entire exhaust system due to the external flow and the second one is the ram drag associated with the secondary flow entrainment. The external friction drag is essentially constant for a given free stream conditions, except for minor effects due to pumping. The ram drag is directly proportional to both the secondary flow and free stream velocity/Mach number. The secondary flow increases from its lowest value to a maximum with increasing NPR. The maximum in secondary flow for this configuration occurs in the nozzle pressure ratio range of 2.5 to 3.5. The secondary flow then drops of gradually with further increase in NPR as indicated by Figure 25. This implies that the highest ram drag is experienced between NPR of 2.5 and 3.5 and the same is true for the total drag, as the nozzle external drag is nearly constant for a given Mach number. Consequently, the significant decrease in performance observed is primarily due to the increased external and ram drag contributions at wind on conditions, both of which are absent at static condition. Simultaneously, both primary flow and ideal thrust increase significantly with increasing NPR resulting in a steeper thrust minus drag coefficient variation with NPR at wind on conditions, since the total drag as a fraction of ideal thrust is smaller at higher NPRs.

There were no significant efforts made to separate the various drag terms described above. A knowledge of these drag terms will enable evaluation of the gross thrust performance of the nozzle and further understanding of the performance characteristics. The primary reason for not including these drag terms in the analysis was the uncertainty in the estimated secondary flow and the lack of good definition of the flap external pressure distribution, at all MARs tested. The scale model flap and side wall also had significantly thick trailing edges of about 0.25 inches in model size. There was insufficient instrumentation to estimate the base drag accurately and the overall uncertainty associated with the total drag is considered to be significant.

The observations made on the effect of free stream Mach number on the performance is typical of all configurations and data is also presented for SAR 2.8 CER 1.22 and SAR 3.3, CER 1.22 configurations in Figures 28 through 33 for comparison. The primary differences are limited to the actual levels of performance and the behavior is similar to the SAR 2.8, CER 1.0 data discussed here.

Inlet Recovery

From the inlet total pressure rake data, the inlet recovery defined as the ratio of average inlet total pressure to the free–stream or ideal secondary flow total pressure can be estimated. This data is discussed in this section.

Figure 34 is a plot of the estimated inlet recovery at the inlet flow metering section as a function of NPR at various free stream Mach numbers tested. This data is for SAR 2.8, CER 1.22 aligned chute, long flap configuration at a MAR of 0.95. The behavior of the inlet under static conditions is quite different than the wind on conditions. Under static conditions inlet recovery characteristic shows a minimum around NPR of 3, while it shows a maximum around the same NPR for wind on conditions. As mentioned earlier, under static conditions, flow separation occurs on the flap side which is largely influenced by secondary mass flow rate. The maximum secondary flow rate under static conditions occurs around this NPR. The rake total pressure profiles presented in Figure 35 confirms the significant changes in the total pressure near both ramp and flap side of the inlet boundary with NPR. For the same reason one can imagine significantly lower total pressures near the end walls and consequently the estimated secondary flow as well as recoveries must be in error due to lack of instrumentation in the span wise direction.

Figure 36 is a plot of the rake total pressure profiles for two different free–stream Mach numbers and selected NPRs. The effect of ejector suction and the resulting changes in the inlet total pressure profile due to favorable pressure gradients generated is obvious from these profiles, relative to the free flowing inlet i.e. NPR=1.0. For this reason the inlet recovery is a maximum under peak mass flow conditions. At higher pressure ratios the secondary flow is limited due to compound choking down stream of the mixer. This results in reduced pumping, which in turn affects the flow distribution and inlet recovery.

Similar inlet recovery characteristics are observed for SAR 2.5 and SAR 3.3 configurations also, as confirmed in Figures 37 and 38.

The estimated inlet recoveries as a function of free stream Mach number at selected pressure ratios are presented in Figure 39 for two different configurations. once again, the effect of both free stream Mach number and NPR or pumping is obvious. Figure 40 compares the inlet recoveries as function of free stream Mach number for three different SARs tested at constant NPRs. The effect of SAR implies effect of pumping. The lower SAR with lower pumping has lower recoveries at the same NPR and free stream Mach.

Finally all of the test data from long flap configurations, for all SARs and MARs are presented as a function of secondary flow in Figure 41. This figure indicates that the inlet recovery characteristics is essentially a function of inlet flow and free stream Mach number. Figure 42 is a plot of the mass averaged inlet recovery defined as the ratio of mass averaged total pressure at the rake plane to the free stream total pressure. The mass averaged inlet recovery characteristics is similar to the simple area averaged inlet recovery characteristics presented in Figure 41, except for the levels. The mass averaged inlet total pressure is higher than the area averaged total pressure. SAR, CER and MAR have no significant impact on the inlet recovery characteristics. This is probably true as all of the data was obtained with one common inlet geometry.

Effect of Chute Expansion Ratio

The primary reason for the variation in CER, is to match the static pressure at the suppressor exit, which can in turn reduce both the losses associated with the under expansion of the primary flow as well as the internal shock noise associated with mismatched static pressure at suppressor exit. The CER 1.22 corresponds to the suppressor exit static pressure of the same magnitude as free stream static at the design nozzle pressure ratio of 4.0. The CER of 1.38 tested in phase–I corresponds to the suppressor exit static pressure of 11.0 psia based on 1D ejector code evaluation of the ejector pumping characteristics. However, the observed performance differences in the phase–I tests between the two CERs > 1 resulted in including a CER of 1.0 in Phase–II. The phase–I data was obtained primarily on MARs > 1, and the data from CER of 1.38 is not included in the current analysis. The phase–I data essentially indicates that at NPRs lower than 3.5 the CER of 1.22 performed better than CER of 1.38, and no significant difference was observed at higher NPRs. The difference between the two was greater at very low nozzle pressure ratios.

The effect of CER on both thrust minus drag coefficient and pumping for two different suppressors, namely aligned and staggered, at the same SAR of 2.8 and selected MARs and free stream conditions, is presented in figures 43 through 50. A close look at this data indicates that in general the lower CER performed significantly better than the higher CER, at low NPRs and the higher CER performed slightly better than the lower CER at high NPRs. The cross–over between the two performance characteristics occurs around an NPR of 3.5 to 4.5 depending on the free stream Mach number and MAR. The difference between the two thrust–drag coefficients at static conditions is nearly 4 to 5 point at NPR of 2.0 and the difference is about 1 to 2 point at NPR of 3.0. There is also a significant difference in pumping, especially at lower pressure ratios.

The possible reasons for this difference at lower pressure ratios could be the losses associated with over–expansion and re–compression of the primary flow in the chutes, in the case of CER=1.22. These losses are similar to any convergent divergent nozzle and the magnitude of losses depends on the area ratio i.e. CER and the back pressure. The internal nozzle pressure ratio i.e. the pressure ratio experienced by the primary flow as given by the primary flow total pressure and the pressure just down stream of the suppressor chute exit is a function of NPR and pumping. For about the same pumping, the static pressure just down stream of the primary nozzle exit should be same. This will imply that the primary nozzle internal pressure ratio should be the same. The area ratios of 1.22 correspond to an internal nozzle pressure ratio of 4.0 and there is always some losses associated with over expansion until the ideal internal pressure ratio is reached. The losses associated with the over–expansion is higher at low NPRs as the internal pressure ratio is significantly lower than the design CER. Consequently at low overall primary nozzle pressure ratios, the higher losses associated with higher CER produces lower performance. This is confirmed by the plot of the static pressure variation with NPR, at the throat and exit of the suppressor chutes along the primary side of the flow as indicated in Figure 51. The static pressures in Figure 51 have been normalized with the primary total pressure. The static pressures at the exit of the suppressor chute is constant for all NPRs above 2.0, indicating that the flow was fully expanded inside the suppressor chutes. There is also a significant gradient at the chute exit between mid height and near the flap. The static pressure tap near the flap was physically located at the exit of the suppressor chute along the finger/extension on the primary side of the flow path as shown in figure 16, and the static pressure is controlled by the local wall curvature especially in supersonic flow. The data presented in Figure 51 also indicates, that the actual expansion ratio at CER 1.22 was about 3.5 at mid chute height and 3.8 near the flap, instead of 4.0. These differences could be due to actual difference in the geometry, where these static pressure taps are physically located. The variation of the throat static pressure as function of NPR presented in

Figure 51 indicates, that the flow is choked at all pressure ratios including NPR of 1.5. Consequently, it can be concluded that there is a shock inside the suppressor chute at NPR of 1.5 and the flow is fully expanded at all NPRs greater than 2.0. Depending on the back pressure downstream of the suppressor chute, additional losses due to over expanded flow must have been incurred at pressure ratios higher than 2.0 and less than about 4.0.

In the case of the convergent chute, the primary flow is under expanded at all flow conditions above a choking internal pressure ratio of 1.89. This under expanded primary jet in the case of CER=1.0, experiences free expansion downstream of the chutes, resulting in some over expansion and re–compression. The losses associated with the over expansion and re–compression is higher at higher nozzle pressure ratios. This also affects the pumping as the secondary flow area available locally is reduced due to the over expansion of the primary flow. Consequently, the simple convergent chutes are further away from optimum at higher NPRs and the convergent divergent chutes with CER of 1.22 is closer to optimum at the same higher NPRs, which explains the performance differences with CER at other than design pressure ratios.

Effect of Chute Alignment

The effect of chute alignment is presented if Figures 52 through 55 and Figures 56 through 59, for two CERs of 1.22 and 1.0 respectively, at a constant SAR of 2.8. A view of the aligned and staggered chutes at the exit of the suppressor is given in Figure 5 for comparison. The CER 1.22, SAR 2.8 performance data for staggered and aligned configurations at three different MARs under static condition is presented in Figure 52 and under wind–on condition is presented in Figures 53 through 55. Figure 52 indicates that the staggered chutes showed a small improvement in pumping relative to the aligned chutes at all test conditions. The thrust minus drag performance was also better by about 0.5 to 1.0 points at most of the nozzle pressure ratios tested. The observations are the same even under wind–on conditions as indicated by Figures 53, 54 and 55. The CER 1.0, SAR 2.8 performance data for staggered and aligned configurations at three different MARs under static condition is presented in Figure 56 and under wind–on condition is presented in Figures 57 through 59. Figures 56 through 59 indicate that the staggered chutes showed basically no difference in pumping characteristics for CER of 1.0 and consistent thrust minus drag performance improvement is limited to a MAR of 0.8. As explained earlier, the staggered chutes were manufactured by translating the bottom half of the suppressor chute rack by half a period. This results in the bottom half of the ejector side walls to be exposed to the secondary flow and the top half to the primary flow in the case of the staggered chutes, while the aligned chutes had all of the side walls were exposed to the primary flow. Consequently the staggered chutes with part of the side walls being exposed to lower velocity secondary stream could perform slightly better due to possible lower wall frictional losses. The mixing process is also significantly altered due to the stagger and it is difficult to separate the various components of the loss mechanisms as a function of both MAR and CER. However, it can be concluded that stagger does not affect the pumping or the thrust minus drag performance adversely and potential benefits of about 0.5 to 1 point in thrust minus drag performance can be expected with stagger. The final conclusions can be arrived at only by detailed evaluation with all of the side walls exposed to similar flow conditions for both aligned and staggered chutes, preferably on a hot model, as the differences in velocities between the secondary and primary stream are greater than the current investigation on the cold aero–performance model.

Effect of Flap Length

The effect of flap length is evaluated at a constant MAR of 0.95 for staggered chute configurations. Figure 60 compares the pumping performance, for the two different flap lengths of 7.40 and 14.10 (80 and 120 inches full scale) for SAR 2.80, CER 1.0 suppressor configuration. Figures 61 and 62 present the effect of flap length on pumping for the SAR 2.80, CER 1.22 suppressor configuration, and SAR 2.5, CER 1.0 suppressor configuration, respectively. The primary observation from figures 60 through 62 is that there are no significant differences in the pumping characteristics between the two flap lengths. The primary variable that controls the pumping are the SAR, MAR and internal losses. The only difference between the two flap lengths are the internal losses associated with the wall friction. One would expect the wall friction losses to be proportional to the flap length and the long flap should have approximately 50 percent more losses due to internal wall friction than the short flap. However, these frictional losses may be only a small part of the total losses and the effect on pumping seems to be negligible.

The effect of flap length on the thrust minus drag performance is presented in figures 63 through 65 for the same three suppressor configurations. The thrust minus drag performance indicates that the short flap is nearly identical to the long flap at static condition for all the three suppressors tested. If any, it can be concluded that for the SAR 2.5 configuration the short flap may be better than the long flap by less than 0.5 points, which is probably within the accuracy of measurements, for this configuration. This is supported by the observations on the pumping, which was not affected by the flap length. Under static conditions there is no external drag consequently the thrust performance should be a function of pumping i.e. total flow at the nozzle exit, ambient static pressure and nozzle exit area. Since constant MAR implies constant nozzle exit area, for the same pumping i.e. same total flow the thrust should be the same, which is the primary observation on thrust performance under static conditions. Under wind–on conditions the long flap seems to perform better consistently by 0.25 points at Mach numbers of 0.32 to 0.55 and significantly better by at least 1 point at 0.7 Mach. Once again, as there was no significant change in pumping, the internal thrust performance should be the same for both flap lengths. The changes in external drag are caused by both skin friction associated with change in external surface area, and pressure drag associated with the change in boattail angle. Increase in flap length leads to an increase in external surface area and a reduction in the boattail angle. These changes especially at the lower free stream Mach numbers seems to be insignificant. Consequently, it can be concluded that the only significant effect of flap length on performance is at 0.7 free–stream Mach and the long flap performs better than the short flap at the high free stream Mach in spite of the higher external skin friction losses, due to the reduction in the external boattail angle. It may be possible to optimize the nozzle performance for all reasonable flap lengths, if the lower flap length is desired from weight considerations.

Effect of Suppressor Area Ratio

The effect of SAR for the two different configurations at selected MARs and M_0 are given in Figures 66 through 73. The first set of figures 66 through 69 compare the performance of aligned CER 1.22 chutes at two different SARs of 3.3 and 2.8, and the second set of figures 70 through 73 compare the performance of staggered CER 1.0 chutes at two different SARs of 2.8 and 2.5. For the same primary throat area A_{p8} the secondary flow area of SAR 3.3 is higher by 28 percent relative to the SAR of 2.8. Consequently one would expect the pumping to be higher by about 28 percent for the SAR of 3.3 relative to SAR of 2.8. Figures 66 through 69 confirms this and the SAR of 3.3 pumps approximately 25 percent more than the SAR of 2.8 at all NPRs. However, the static thrust performance shows only a small improvement of about 1 point with increased SAR over a wide range of

NPRs, as indicated by figure 66. The slight benefit in the observed static thrust performance is not realized under wind on conditions. Figures 67, 68 and 69 indicate that, in general, the performance of SAR 2.8 is always better than SAR 3.3, under wind–on conditions. The level of improvement in thrust minus drag performance under wind–on conditions for the lower SAR is a function of both MAR and M_0. The improvement in thrust performance is about half to 1 point at free stream Mach of 0.32 and is about 2 to 3 points at free stream Mach of 0.7, depending on MAR. For the same throat area, the SAR of 3.3 has a larger external dimensions and hence larger surface area and higher external drag. The ram drag also increases proportional to the pumping. Consequently, under wind on conditions, any improvement in the gross thrust performance due to the higher pumping associated with higher SAR seems to have been more than offset by the increase in the drag associated with the higher SAR. The same conclusions can be arrived at based on the performance trends between SAR 2.8 and SAR 2.5 of the staggered chutes with CER of 1.0, presented in Figures 70 through 73.

The same data are presented as a function of SAR in Figures 74 through 77 for four different MARs of 0.85, 0.9, 0.95 and 1.0 respectively, at selected nozzle pressure ratios. Data are presented at three different free stream Mach numbers of 0.0, 0.32 and 0.55 for all MARs considered. The differences in performance due to CER and chute alignment are included in this comparison. The test data on SAR 2.5 configuration was limited to CER 1.0 staggered chutes and on the SAR 3.3 configuration was limited to CER 1.22 aligned chutes. For SAR 2.8, the data are presented for both CER 1.0 staggered and CER 1.22 aligned configurations. From prior discussions on the effect of CER and chute alignment, the CER 1.0 staggered chutes can be expected to perform better than CER 1.22 aligned chutes, over the nozzle pressure ratios of interest by two to three points of which about half to 1 point is from stagger and the rest is due to CER. This is evident in all of the data presented in Figures 74 through 77. The scatter of about 2 points in performance at SAR of 2.8 is the result of configuration variables CER and stagger. The significant improvement in performance associated with the supersonic mode at all SARs can also be seen from these data, as indicated by the significant changes in trust minus drag coefficients at NPRs of 3.5 and 4.0. Figure 74 indicates that the static thrust performance at a MAR of 0.85 and NPR of 3.0 and 3.5 shows almost no effect of SAR under static condition and a decrease of about 2 to 4 points from a SAR of 2.5 to 3.3 under wind–on conditions. Similarly, at a MAR of 0.9 under static conditions as seen in Figure 75, there is no significant efffect in performance between the SAR of 2.5 and 3.3, for both NPRs of 3 and 4. NPR 3.5 data includes mode shift. The same conclusions can be reached from figures 76 and 77 as well. This implies that the improvement in static thrust performance with SAR from 2.5 to 3.3 is of the same order of magnitude as CER 1.0 to 1.22 and stagger. For all the MARs, the wind on data indicates, 2 to 4 points decrease in performance from a SAR of 2.5 to 3.3, for free stream Mach Number of 0.32 and about 5 points for free stream Mach of 0.55 for NPRs of 3 and 3.5, when mode transition is not experienced. In the cases, where mode transition is experienced, the decrease in performance with SAR, from 2.5 to 3.3 is as high as 10 points. The decrease in performance with SAR is a strong function of both MAR and free stream Mach number. The effect of significant ram drag penalty associated with SAR under wind on conditions is evident from these figures. In addition to the ram drag contribution, for a given primary nozzle throat area, the overall external wetted area for SAR 2.5 is about 24 percent lower relative to SAR of 3.3 which should lead to significantly lower external drag contribution.

Effect Of Mixing Area Ratio

The performance of three of the suppressor configurations i.e. SAR, CER and chute alignment as a function of MAR at constant NPR and free stream Mach number are presented in figures 78 through 80. The nozzle performance or the thrust–drag coefficient, essentially shows a peak at MAR

less than 1.0 for all pressure ratios considered. The pumping characteristics is nearly flat for all MARs higher than the MAR at which peak performance is obtained. Figure 78 presents the performance data for SAR 2.5, CER 1.0, staggered chute, long flap configuration. Referring to Figure 78, the NPR 4.0, at a MAR of 0.85, was at supersonic mode under static conditions and at subsonic mode under wind on conditions. NPR of 3.0 and 3.5 were at supersonic mode for all test conditions for MARs above 0.95 and 0.9 respectively. Significant reduction in thrust minus drag performance with free stream Mach number is also obvious. The highest thrust minus drag performance observed at NPR of 3.5 is nearly 0.99 under static conditions, and 0.94 at Mach 0.32, and 0.9 at Mach 0.55, for SAR 2.5 in supersonic mode at a MAR of 0.9.

Similar data for SAR 2.9, CER 1.22, aligned chute, long flap configuration is presented in figure 79, indicates NPR 4 to perform better than NPR 3.5 and 3 at all test conditions. Once again, NPR 3.5 and 4 were at supersonic mode at a MAR of 0.9 under static conditions, but only NPR 4.0 was at supersonic condition at this MAR at Mach 0.32. At a free stream Mach of 0.55, all NPRs presented were at subsonic mode at a MAR of 0.9. The significant reduction in thrust minus drag performance with free stream Mach number is also obvious. In addition , the poor performance at a MAR of 1.2 can also be seen from this figure.

The performance data for SAR 3.3, CER 1.22, aligned chute, long flap configuration is presented in Figure 80. This data is very similar to SAR 2.8 data presented in Figure 79, and confirms effect of free stream conditions and MAR on mode transition. Once again peak performance of about 0.98 was obtatined at a MAR of 0.9 and NPR of 3.5 was observed under static conditions in supersonic mode.

The transition pressure ratios for both increasing and decreasing NPRs are presented as a function of MAR for three of the suppressor configurations in Figure 81. Transition occurs early at a MAR of 1 relative to a MAR of 0.85. For the SAR 3.3 suppressor, transition at a MAR of 0.85 occurs at a NPR of 5 and at a MAR of 1 it is at NPR of 2.7. Corresponding transition pressure ratios for SAR 2.5 is 4 and 2.55. The lack of hysterisis at a MAR of 1 is also obvious from this figure as the transition pressure ratio is same along both increasing and decreasing NPR. The degree of hysterisis can be evaluated by studying the overlap in performance associated with approaching transition along the subsonic part of the performance characteristic i.e. increasing NPR and the supersonic part of the performance characteristics i.e. decreasing NPRs. SAR 3.3 seems to have larger separation between the two transition pressure ratio curves relative to SAR 2.5 and it can be concluded that SAR 3.3 has significantly stronger hysterisis. The primary reason for higher transition pressure ratio required by the higher SAR is entrainment. In order to establish supersonic flow through the converging duct, the mixed flow Mach number and total momentum per unit mass of mixed flow must be sufficient to pass a normal shock through the duct. The higher SAR with higher entrainment results in lower mixed flow specific momentum. Hence, a higher primary nozzle pressure ratio is required, relative to lower SAR, to achieve the required mixed flow condition. This is reinforced by the effect of free stream Mach on transition pressure ratios presented in Figure 82. Data is presented only for approaching transition along the subsonic part of the performance characteristics. At higher free stream Mach numbers, with increased entrainment combined with reduced inlet recovery, significantly higher primary nozzle pressure ratios are required to effect transition from subsonic to supersonic mode.

Gross Thrust Coefficient

From the measured thrust minus drag performance, the mixer ejector nozzle gross thrust coefficient can be evaluated by adding all of the external drag as well as the ram drag contribution. Figure 83 depicts the various drag terms associated with the mixer ejector nozzle test configuration and it defines both thrust minus ram drag coefficient and the gross thrust coefficient. The external drag terms essentially consist of, skin friction drag on all surfaces of the mixer ejector nozzle, exposed to the free stream, nozzle flap pressure drag from flap external pressure distribution, nozzle base drag due to base pressure, and the ram drag associated with the secondary flow. The thrust minus ram drag coefficient is defined as the ratio of nozzle gross thrust minus ram drag to the ideal thrust of the fully expanded primary flow. The gross thrust coefficient is defined as the ratio of the nozzle gross thrust to the nozzle ideal thrust of the fully expanded primary flow. The skin friction drag over the external nozzle surfaces were estimated analytically. The flap static pressure distribution and the base pressures were arrived at based on test carried out exclusively to estimate the associated drag contributions. Due to limited test configurations and instrumentation the base pressure contribution to various actual test configurations was some what uncertain. The estimate of all of the drag contributions were performed, but are not presented here. The primary reason being, the thrust minus nozzle drag coefficient is the significant performance parameter for the overall systems. A knowledge of the thrust minus ram drag may facilitate extrapolation of the test data to actual ambient conditions under flight conditions for scaling of the performance parameters i.e. to include Reynold's number effects.

The nozzle gross thrust coefficient can also be arrived at based on a simple one dimensional approach illustrated in Figure 84. This approach is based on the fact, that under subsonic mode of operation, there is only one unique solution for the mixer ejector nozzle exit plane Mach number. The nozzle exit total temperature is estimated from energy balance between the primary and secondary. From continuity, the nozzle exit mass flow is estimated to be the sum of the primary and secondary flows. Then for a fully mixed flow at nozzle exit, from the nozzle exit area the exhaust jet velocity, Mach number and total pressure can be estimated. The exit static pressure is assumed to be ambient for unchoked exhaust jet conditions. For choked nozzle, the jet exit static pressure is assumed to be above ambient and the corresponding contribution to the gross thrust is included. For supersonic exit conditions, the solution is not unique and some additional assumptions need to be made to arrive at the nozzle exit velocities. For simplicity, the measured flap static pressure near the trailing edge was used as the nozzle exit static pressure.

The overall gross thrust coefficient estimates and the thrust minus ram drag coefficient along with the thrust minus nozzle drag coefficients are presented for the SAR 3.3, CER 1.22, MAR 0.85, aligned chute, long flap configuration is presented in Figure 85. The primary reason for choosing this test configuration is that the ejector nozzle stays subsonic over a larger range of nozzle pressure ratios as discussed in the previous section. All of these coefficients are same under static conditions as the external drag and ram drag contributions are zero. In reality there is some base drag, which was not accounted for due to lack of test data and any effect of induced forward velocity in the test section due to the ejector nozzle was also not included.

It is interesting to note the agreement between the simple 1D estimates of the gross thrust coefficient and the estimated test data under wind on conditions. The small disagreement at very low nozzle pressure ratios i.e. around 1.5 is to be expected as the mixed flow jet velocities are significantly lower. The agreement is also poor at very high nozzle pressure ratios, where the mixer ejector nozzle is in supersonic mode. The agreement between the simple 1D calculation and estimated test

data is remarkably good over a wide range of pressure ratios in subsonic mode. It is also interesting to note the very significant difference between the estimated 1D gross thrust coefficient and test data under static conditions. The primary reason is the error in calculated secondary flow entrainment due to lack of span–wise inlet measurements and the lack of base pressure correction. The significant contribution of the inlet ram drag is also evident at high free stream Mach numbers.

Conclusions and Recommendations

Conclusions

The two operating regions of the ejector – subsonic and supersonic modes – were identified. With converging flaps at Mixing Area Ratios (MAR) less than 1, the exhaust system acts as conventional nozzle in subsonic mode and as a diffuser in supersonic mode. A significant increase in nozzle performance is observed associated with the supersonic mode. The transition from subsonic to supersonic mode along increasing Nozzle Pressure Ratios (NPR) occurs at significantly higher pressure ratio than transition from supersonic to subsonic mode along decreasing NPR, resulting in hysterisis in thrust performance characteristics.

With diverging flaps at MAR greater than 1, the exhaust system acts as diffuser in the subsonic mode and as nozzle in the supersonic mode. The performance of the exhaust system is significantly lower than MAR less than 1, over the pressure ratios investigated in this test program.

In all supersonic modes, at all MARs significant shock presence is indicated by the flap static pressures. These shock structure moves down stream towards the exit of the nozzle with increasing primary nozzle pressure ratios.

Significant reduction in the thrust minus drag coefficient with external flow of about 5 points at a free stream Mach of 0.32 at NPR of 4.0 relative to static conditions is observed. The slope of the thrust minus drag coefficient with NPR for wind–on case is also steeper relative to the static case. Pumping increased with increasing free stream Mach Number. The actual increase in pumping with increased free stream Mach number is lower than the corresponding increase in secondary flow total pressure due to the inlet recovery.

The inlet recovery characteristics correlate well with free stream Mach number and secondary flow entrainment, independent of other geometric parameters such as Suppressor Area Ratio (SAR), Chute Expansion Ratio (CER), chute alignment and flap length. This may be due to the common inlet geometry used for all test configurations. Inlet recovery decreased significantly with increasing free stream Mach number and increased with increased secondary flow entrainment.

In general the convergent chutes with CER of 1.00 performed better than the convergent divergent chutes with CER of 1.22 for low NPRs and the convergent divergent chutes performed better than the convergent chutes at high NPRs. The cross over between the two occur in the NPR range of 3.5 to 4. The difference between the two thrust–drag coefficients at static conditions is nearly 4 to 5 point at NPR of 2.0 and the difference is about 1 to 2 point at NPR of 3.0. There is also a significant difference in pumping, especially at lower pressure ratios. The possible reasons for this difference at lower pressure ratios could be losses associated with the over–expansion and re–compression of the primary flow in the chutes.

The staggered chutes performed better than aligned chutes by 0.5 to 1 points over most of the pressure ratios tested. This improvement was limited to MAR less than 1 for the convergent chutes.

Flap length had no significant impact on pumping and thrust performance under static conditions at all MARs tested. Under wind on conditions, the long flap performed slightly better than the short flap, about 0.25 points in thrust minus drag coefficient at Mach 0.32, and nearly 1 point at Mach 0.7. The external skin friction drag is influenced favorably by short flap and the bottail angle and associated flap external pressure drag is favorable affected by the long flap. These are

also a strong function of MARs. These changes especially at the lower free stream Mach numbers seems to be insignificant. The only significant effect of flap length on performance is at 0.7 free–stream Mach and the long flap performs better than the short flap at the high free stream Mach in spite of the higher external skin friction losses, due to the reduction in the external boattail angle. It may be possible to optimize the nozzle performance for all reasonable flap lengths, if the lower flap length is desired from weight considerations.

The SAR of 3.3 with 28 percent higher secondary flow area than SAR of 2.8, pumps approximately 25 percent more at all NPRs. For MARs less than 1, the static thrust performance shows only a small improvement of about 1 point with increased SAR. The slight benefit in the observed static performance is not realized under under wind–on conditions, due to increased inlet ram drag and external form and friction drag associated with higher SAR.

The Mixing Area Ratio (MAR) had significant effect on performance. The nozzle performance or the thrust minus drag coefficient, essentially shows a peak at a MAR less than 1.0 for all pressure ratios tested. The pumping characteristics is nearly flat for all MARs higher than the MAR at which peak performance is obtained. The highest thrust minus drag performance observed at NPR of 3.5 is nearly 0.99 under static conditions, and 0.94 at Mach 0.32, for SAR 2.5 at a MAR of 0.9 in supersonic mode.

Transition occurs early at a MAR of 1 relative to a MAR of 0.85. For the SAR 3.3 suppressor, transition at a MAR of 0.85 occurs at a NPR of 5 and at a MAR of 1 it is at NPR of 2.7. Corresponding transition pressure ratios for SAR 2.5 is 4 and 2.55. At a MAR of 1, the transition pressure ratio is same along both increasing and decreasing NPR. The primary reason for higher transition pressure ratio required by the higher SAR is entrainment. Similarly, at higher free stream Mach numbers, with increased entrainment combined with reduced inlet recovery, significantly higher primary nozzle pressure ratios are required to effect transition from subsonic to supersonic mode. SAR 3.3 also has larger separation between the increasing and decreasing transition pressure ratios relative to SAR 2.5.

The agreement between a simple 1D calculation and estimated test data is remarkably good over a wide range of pressure ratios in subsonic mode under wind on conditions. There is a very significant difference between the estimated 1D gross thrust coefficient and test data under static conditions. The primary reason is the error in calculated secondary flow entrainment due to lack of span–wise inlet measurements and the lack of base pressure correction. The significant contribution of the inlet ram drag is also evident at high free stream Mach numbers.

Recommendation

- Evaluate the pumping characteristics, especially under static conditions through improved instrumentation.
- Evaluate the effect of Primary stream temperature in a hot model to further establish optimum pumping and performance characteristics with MAR.
- Evaluate the effect of CER, especially convergent divergent chutes ($1.0 \leq$ CER ≤ 1.22) on both aerodynamic and acoustic performance.
- Evaluate effect of chute alignment on aerodynamic and acoustic performance.

Appendix – Definition of Symbols

1D	One dimensional
2D	Two dimensional
2DCD	Two dimensional, convergent/divergent (exhaust nozzle configuration)
2DME	Two dimensional, mixer/ejector (exhaust nozzle configuration)
3D	Three dimensional
A	Cross-sectional area, in^2
A_9	Exhaust nozzle exit area, $2 \times h_9 \times w_9$
A_{mix}	Total mixed-flow area, $A_{p8} + A_{s8} = 2 \times h_{mix} \times w_9 - 2n \times (h_{mix} - h_8) \times w_{p8}$
A_{p8}	Primary nozzle throat area, $(h_8 - h_{gap}) \times w_{p8} \times 2n + 2 \times h_{gap} \times w_9$
A_{p89}	Suppressor exit plane area, $(h_{mix} - h_{gap}) \times w_{s8} \times 2n$
A_{s8}	Secondary flow area at throat plane, $(h_{mix} - h_{gap}) \times w_{s8} \times 2n$
CD	Convergent/divergent
C_{D8}	Primary nozzle flow coefficient: ratio of actual mass flow to the ideal mass flow
CER	Chute expansion ratio: ratio of the primary flow area at the suppressor exit to the primary throat area, A_{p89} / A_{p8}
CFD	Computational fluid dynamics
C_{f-Dnoz}	Thrust minus nozzle drag coefficient: ratio of measured nozzle thrust minus drag to the primary nozzle ideal thrust, $(F-D_{noz}) / F_i$
C_{f_g}	Nozzle thrust coefficient or coefficient of gross thrust: ratio of measured exit gross thrust to ideal gross thrust
D	Total drag, lbf
D_{noz}	Nozzle drag
F	Thrust, lbf
F–D	Measured thrust minus drag corrected for balance tares
$F–D_{noz}$	Measured thrust minus nozzle drag
F_i	Primary nozzle ideal thrust based on measured weight flow rate, $W_p \times V_j$
F_N	Net thrust, $F - D$
GEAE	GE Aircraft Engines
h	Height (usually half height), inches
h_8	Chute height from centerline at throat plane
h_9	Half height of nozzle from centerline to flap trailing edge (exit)
h_{ex}	Half height at ejector exit

h_{gap}	Half height from nozzle centerline to suppressor chute foot
h_{mix}	Chute height from nozzle centerline at mixing plane
HSCT	High Speed Civil Transport
L	Length, in
L_{ej}	Ejector length (divergent flap)
M	Mach number (free-stream unless otherwise designated)
M_0	Free-stream Mach number, calculated
MAR	Mixing area ratio: ratio of mixer exit to inlet area, A_9 / A_{mix}
MFTF	Mixed-flow turbofan
MPA	Model preparation area
n	Number of chutes in each half of suppressor
NPR	Primary nozzle pressure ratio: calculated as P_{tp} / P_0
NPR_C	Critical primary nozzle pressure ratio
P	Static pressure, psia
P_T	Total pressure, psia
P_{T0}	Free-stream total pressure, measured
P_{Tp}	Primary nozzle inlet total pressure, measured
P_{Ts}	Secondary inlet total pressure, measured
SAR	Suppressor area ratio: ratio of mixed-flow area to primary nozzle throat, A_{mix} / A_{p8}
T	Static temperature, °R
T_0	Free-stream static temperature, calculated
T_8	Nozzle throat static temperature
TOGW	Takeoff gross weight, lbm
T_T	Total temperature, °R
T_{T0}	Free-stream total temperature, measured
T_{T8}	Total temperature at nozzle throat (primary jet)
T_{Tp}	Primary nozzle inlet total temperature, measured
T_{Ts}	Secondary nozzle inlet total temperature
V	Flow velocity, ft/s
V_0	Free-stream velocity (simulated flight speed)
VCE	Variable-cycle engine
V_j	Primary nozzle ideal jet velocity, ft/s, calculated based on *NPR* and T_{T8}
W	Fluid flow, lbm/s

w	Width, in
w_9	Exhaust system width from sidewall to sidewall
W_s	Secondary inlet flow, calculated
W_T	Total nozzle flow rate: $W_p + W_s$
W_p	Primary nozzle flow
W_{pi}	Primary nozzle ideal flow, calculated
γ	Ratio of specific heat at constant pressure to specific heat at constant volume
ω	Pumping ratio: ratio of secondary to primary flow rates, W_s / W_p
$\omega \sqrt{\tau}$	Corrected pumping ratio, $(W_s / W_p) \sqrt{(T_{Ts} / T_{Tp})}$

Plane (Engine Station) Designations and Other Subscripts

0	Free stream
2	Fan inlet
7	Exhaust nozzle inlet
8	Nozzle throat
9	Nozzle exit
89	Suppressor exit
∞	Ambient: static air conditions outside the engine
ej	Ejector
f	Flap
noz	Nozzle
mix	Mixing plane
p	Primary chute
S	Static
s	Secondary chute
T	Total

References

1. Majjigi, R.K. et al., "Low Noise Exhaust Nozzle Technology Development," Final Contract Report Prepared by GEAE for Contract NAS3–25415, November 1996.
2. Majjigi, R.K. et al., "Low Noise Exhaust Nozzle Technology Development – Preliminary Design Report and Test Plan Review," Contract Report Prepared by GEAE for Contract NAS3–25415, January 1993.
3. Staff of the Propulsion Aerodynamic Branch, "A User's Guide to the Langley 16–Foot Transonic Wind Tunnel Complex," NASA TM102750, September 1990.
4. Braden, R.P., Nagaraja, K.S., and Von Ohain, H.J.P., "Proceedings: Ejector Workshop for Aerospace Applications," AFWL–TR–82–3059, Wright–Patterson Air Force Base, June 1982.

Table 1. Preliminary Design Point Cycle Summary
NRA – 2D Mixer Ejector Exhaust System

GE21/F14 Study L1M; M=2.4 Cruise, 700 Lbs/sec Size

Altitude	= 689 ft	PC	= 68
M	= 0.322	FN	= 50,000 Lbs
Tambient	= 534.2^0R	NPR	= 4.0
Pambient	= 14.334 psia	T7	= 2040^0R
ERAM1A	= 0.97	W7	= 708.6 pps
T2	= 545.3^0R	A8	= 1086 in^2
P2	= 14.939 psia	AE8	= 1064 in^2

Table 2. Mixer Ejector Nozzle Phase I Test Configurations

CONFIGURATION VARIABLES							MAR			
CHUTE	SAR	A_{p8} sq. in.	CER	Alignment	Wedge	FLAP Length in.	0.80	1.00	1.20	1.40
1000	2.80	9.31	1.22	ALIGNED		7.44			W	W
1000	2.80	9.31	1.22	ALIGNED		11.10	W	W	W	W
1000	3.17	7.69	1.22	ALIGNED	YES	11.10		W	W	W
2000	2.80	9.31	1.38	ALIGNED		7.44			W	W
2000	2.80	9.31	1.38	ALIGNED		11.10			W	W
2000	3.17	7.69	1.38	ALIGNED	YES	11.10		W	W	W
3000	3.30	8.04	1.22	ALIGNED		7.44			W	W
3000	3.30	8.04	1.22	ALIGNED		11.10			W	W
3000	3.88	6.42	1.22	ALIGNED	YES	11.10		W	W	W
4000	3.30	8.04	1.38	ALIGNED		7.44			W	W
4000	3.30	8.04	1.38	ALIGNED		11.10			W	W
4000	3.88	6.42	1.38	ALIGNED	YES	11.10		W	W	W

W – Tested Statically & Wind–on @ 0.32, 0.40, 0.55 & 0.70 Mach Numbers
Wedge – Tested with two different wedges one long and one short

Table 3. Mixer Ejector Nozzle Phase II Test Configurations

Configuration Variables						MAR						
CHUTE	SAR	A_{p8} Sq. in.	CER	Alignment	Flap Length in.	0.80	0.85	0.90	0.95	0.975	1.00	1.20
1000	2.80	9.31	1.22	ALIGNED	11.10	SW	SW	SW	SW	SW	SW	SW
3000	3.30	8.04	1.22	ALIGNED	11.10	S	S	S	S	S	S	S
4000	3.30	8.04	1.38	ALIGNED	11.10		S	S	S	S	S	
5000	2.80	9.31	1.22	STAGGER	11.10	W	SW	SW	SW		SW	
5000	2.80	9.31	1.22	STAGGER	7.44	W	SW	SW	SW		SW	
6000	2.80	9.31	1.00	ALIGNED	11.10	W	SW	SW	SW	W	SW	
7000	2.80	9.31	1.00	STAGGER	11.10	W	SW	SW	SW		SW	
7000	2.80	9.31	1.00	STAGGER	7.44	W	SW	SW	SW		SW	
9000	2.50	10.51	1.00	STAGGER	11.10		W	W	W		W	
9000	2.50	10.51	1.00	STAGGER	7.44		W	W	W		W	

S – Tested statically out side the tunnel
W – Tested Statically & Wind–on @ 0.32, 0.40, 0.55 & 0.70 Mach Numbers

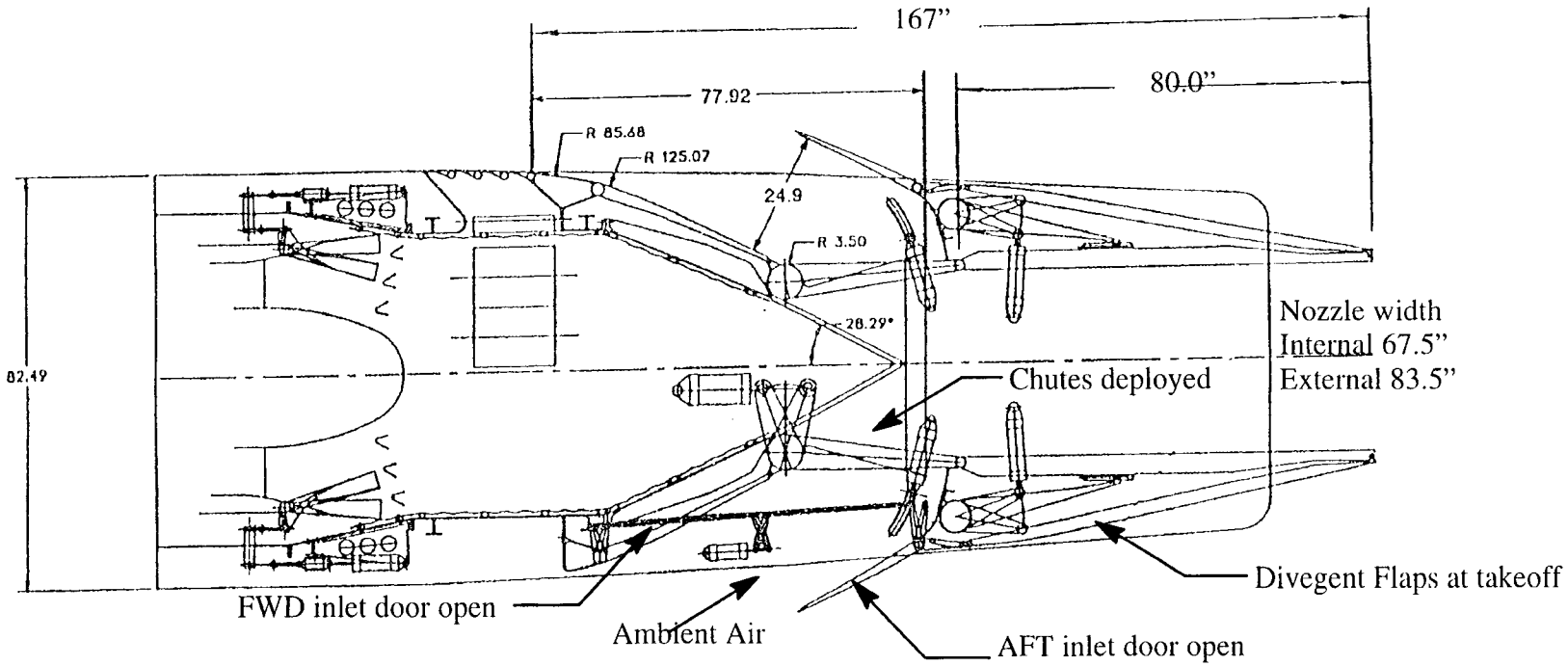

Figure 1. Typical cross section of the 2D Mixer–Ejector nozzle at takeoff.

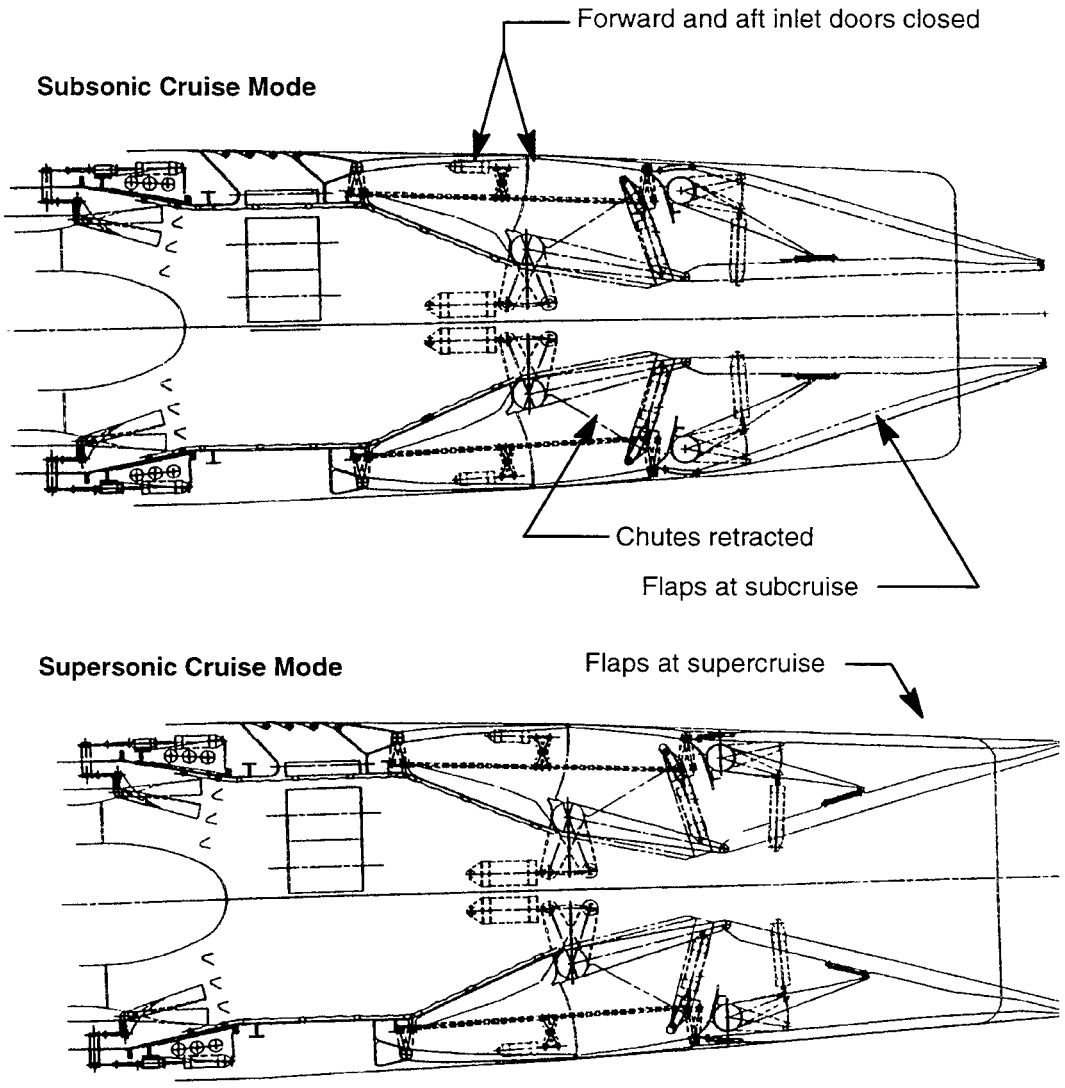

Figure 2. Two-Dimensional mixer-ejector nozzle in cruise mode configurations

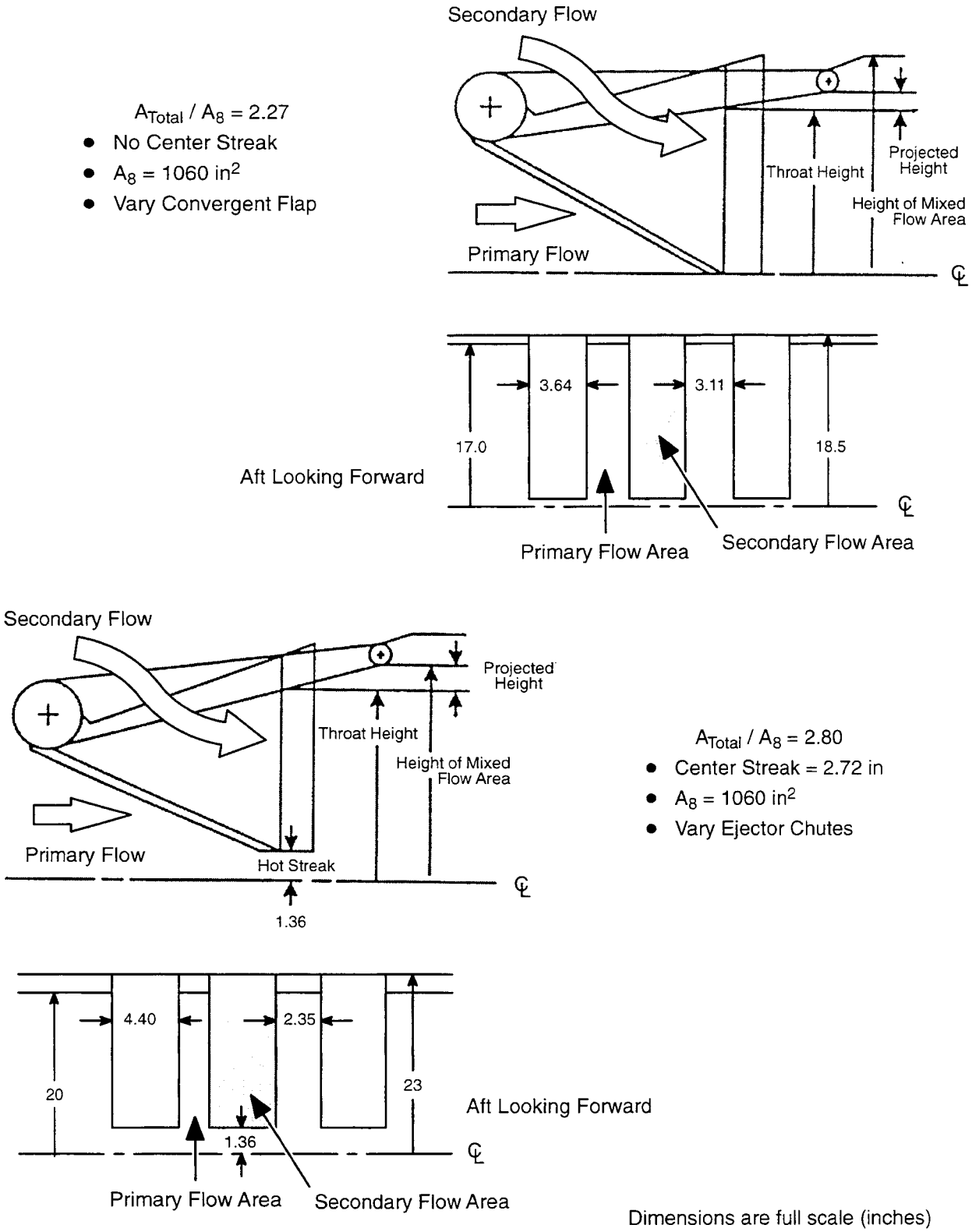

Figure 3. Preliminary design concepts for variable throat area at cutback

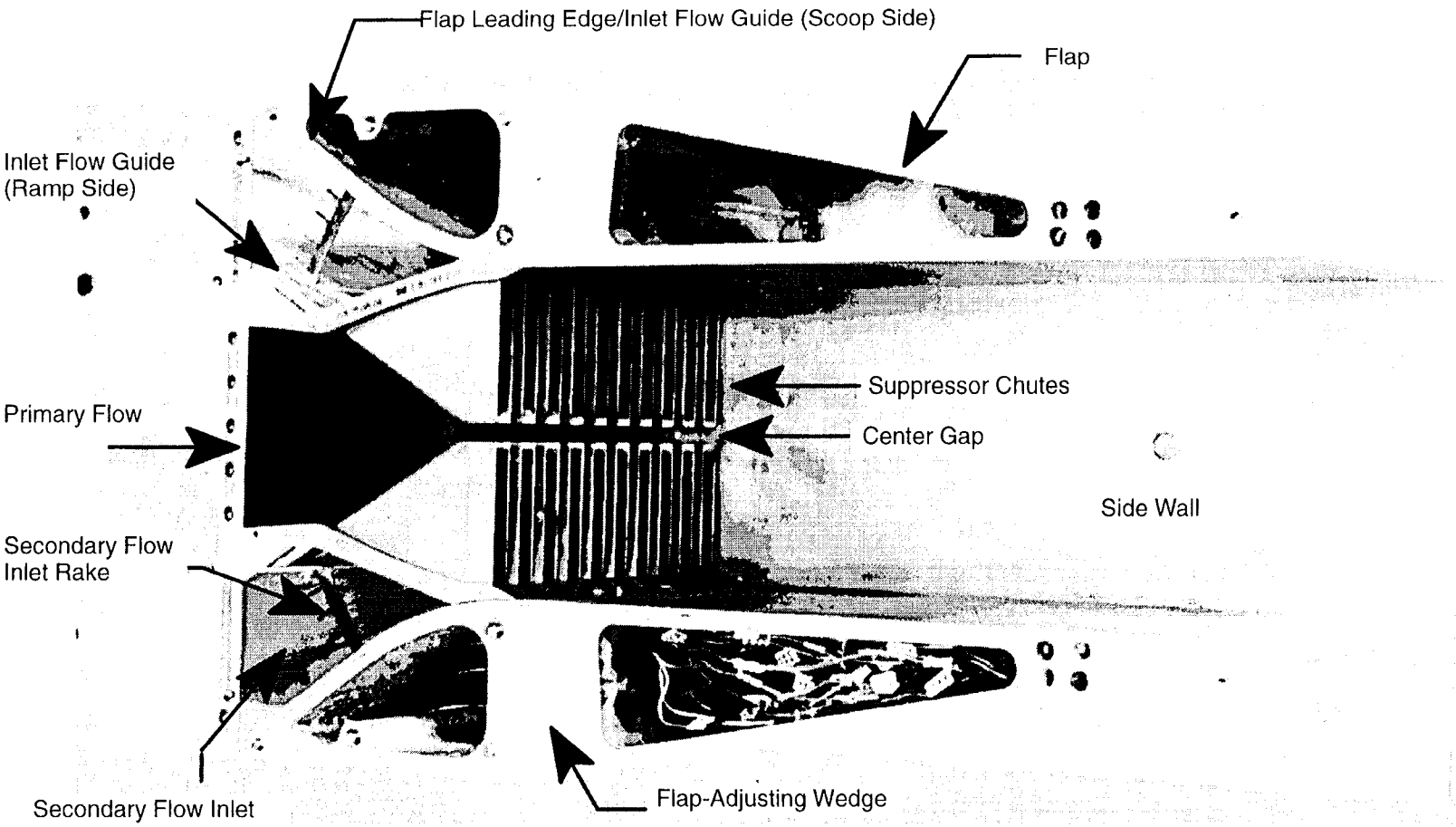

Figure 4. Mixer ejector nozzle scale model with one side wall removed

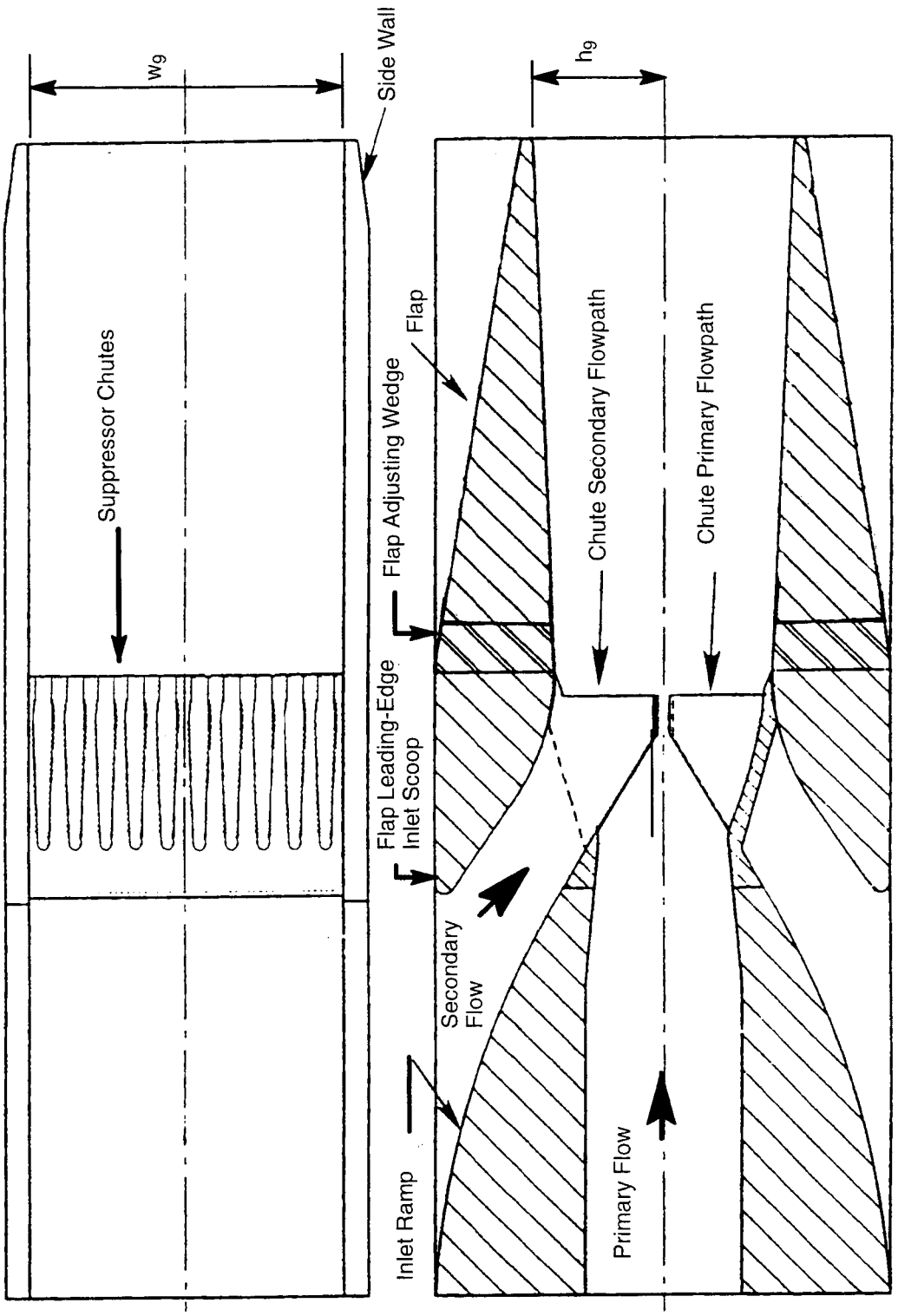

Figure 5. Schematic of exhaust sytem scale model

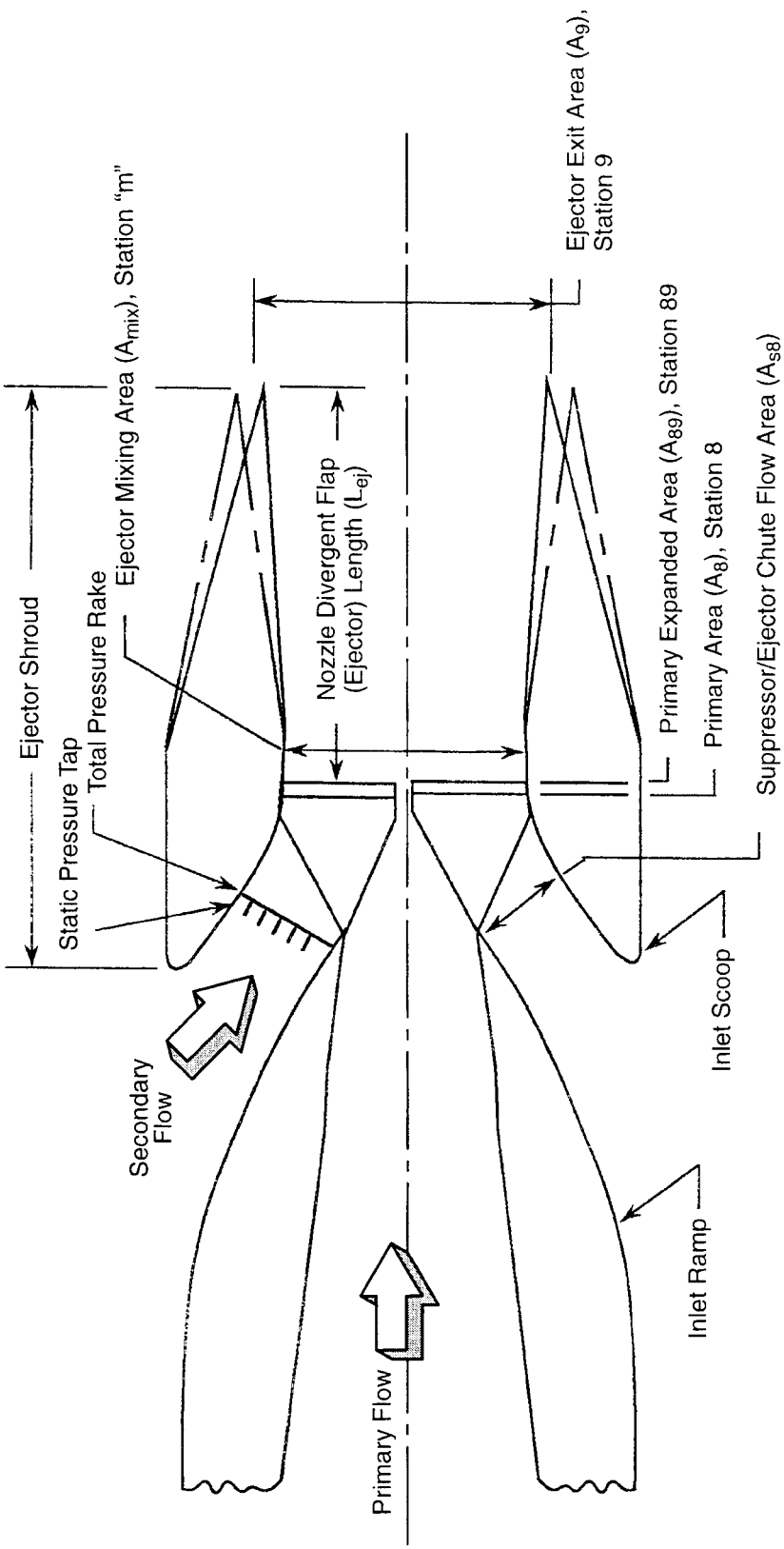

Figure 6. Exhaust system key dimensions

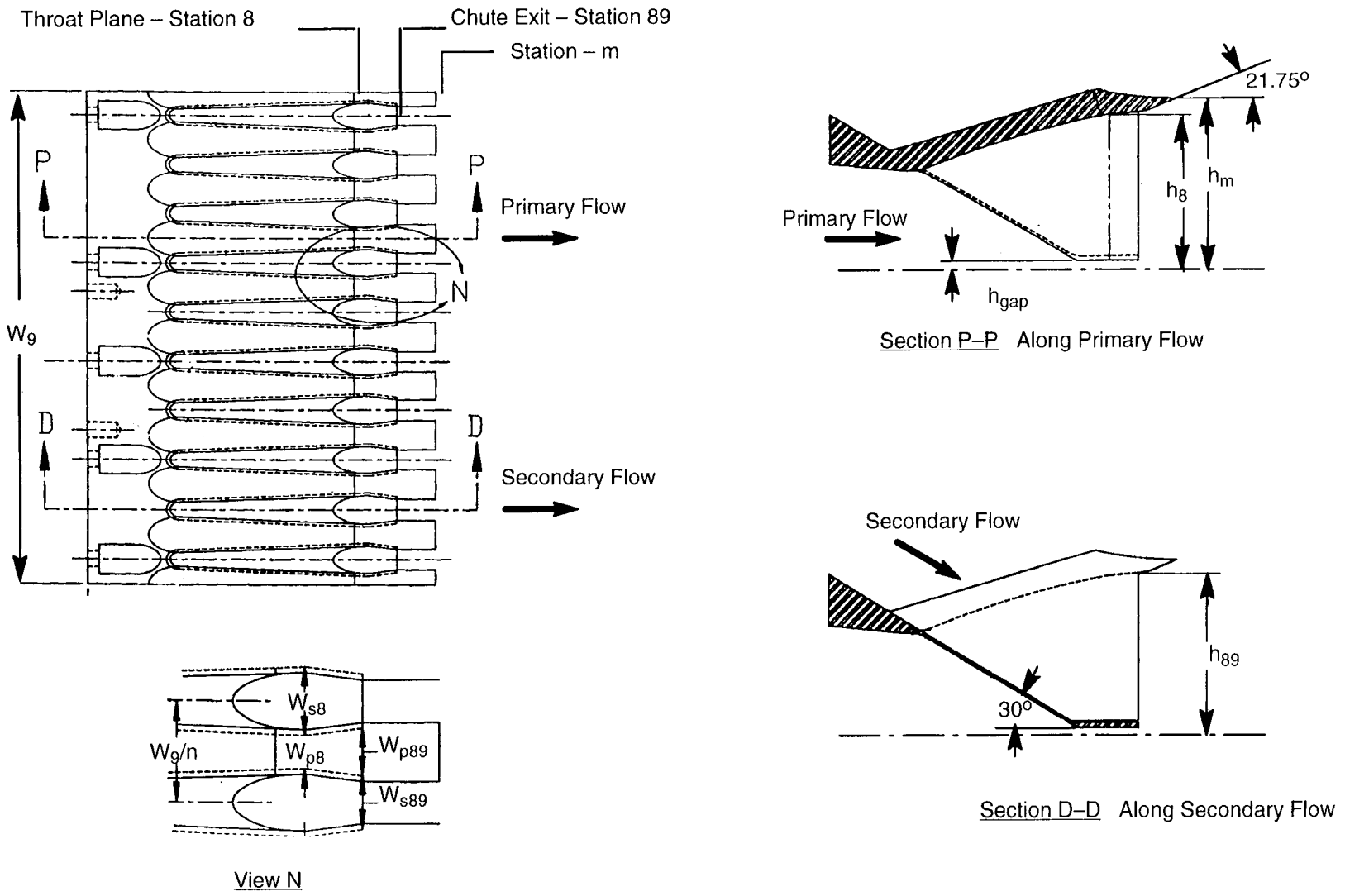

Figure 7. Basic key dimensions of the multichute suppressor

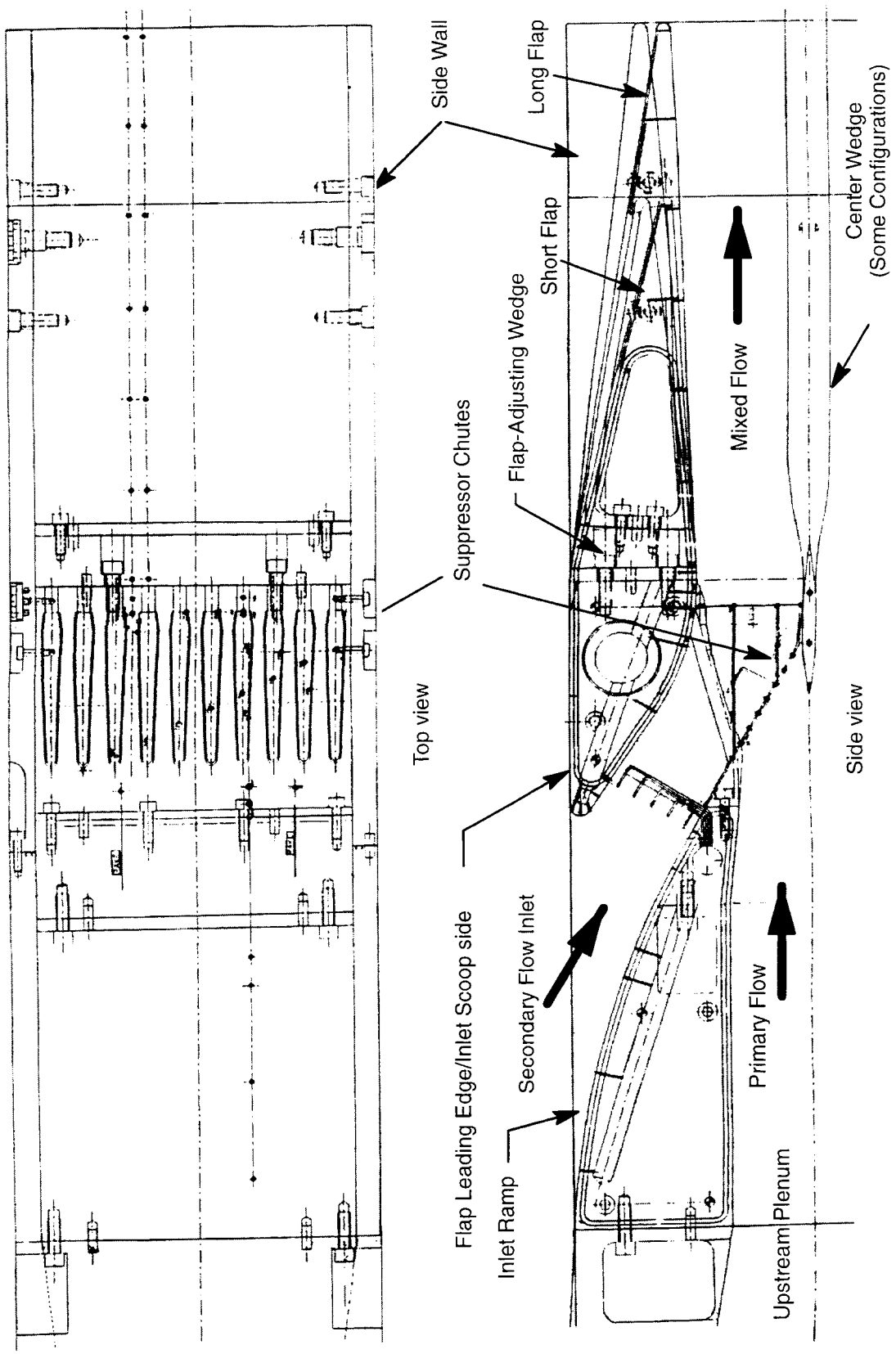

Figure 8. Scale model of 2DME nozzle

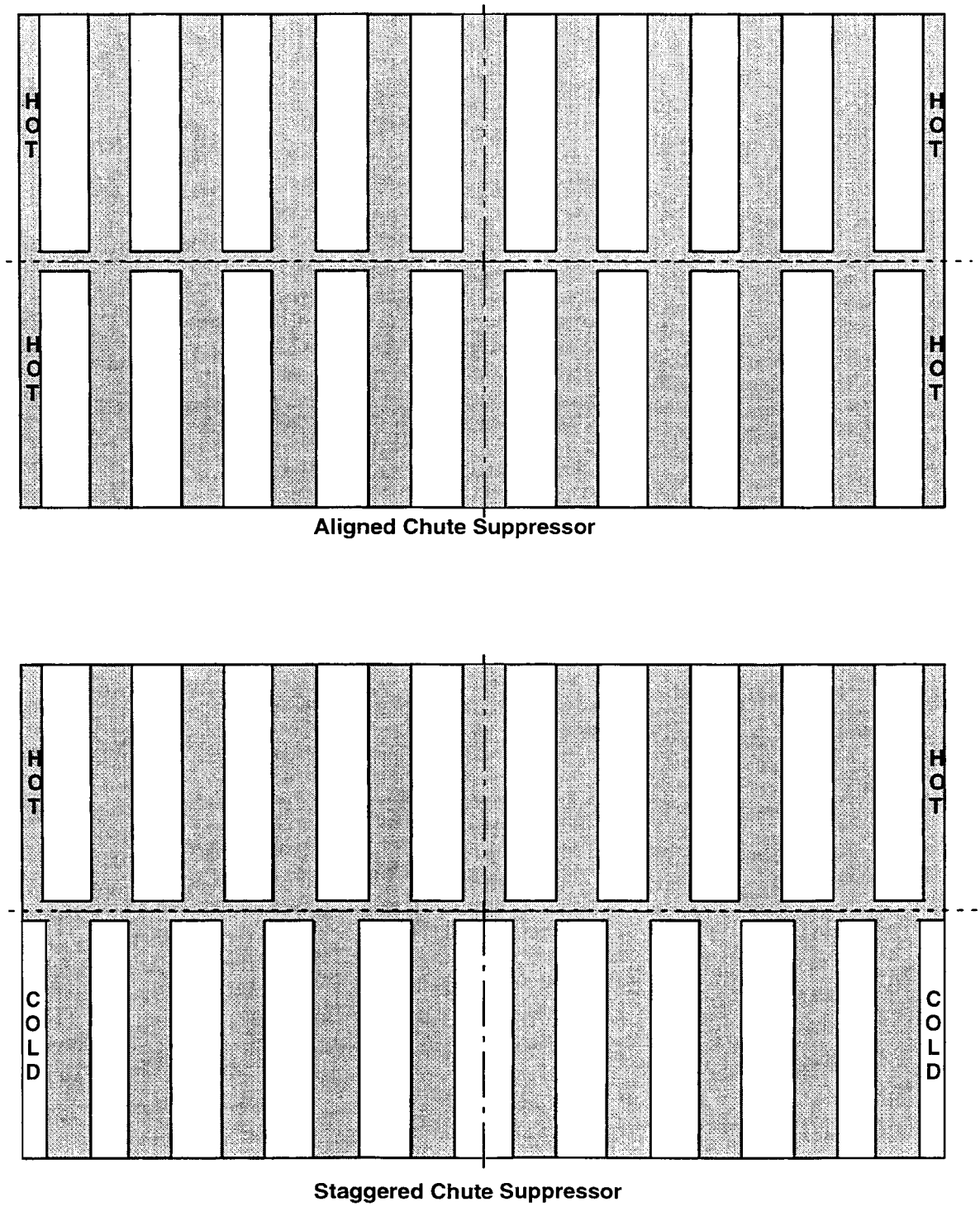

Figure 9. Schematic of the aligned and staggered chute suppressor exit view

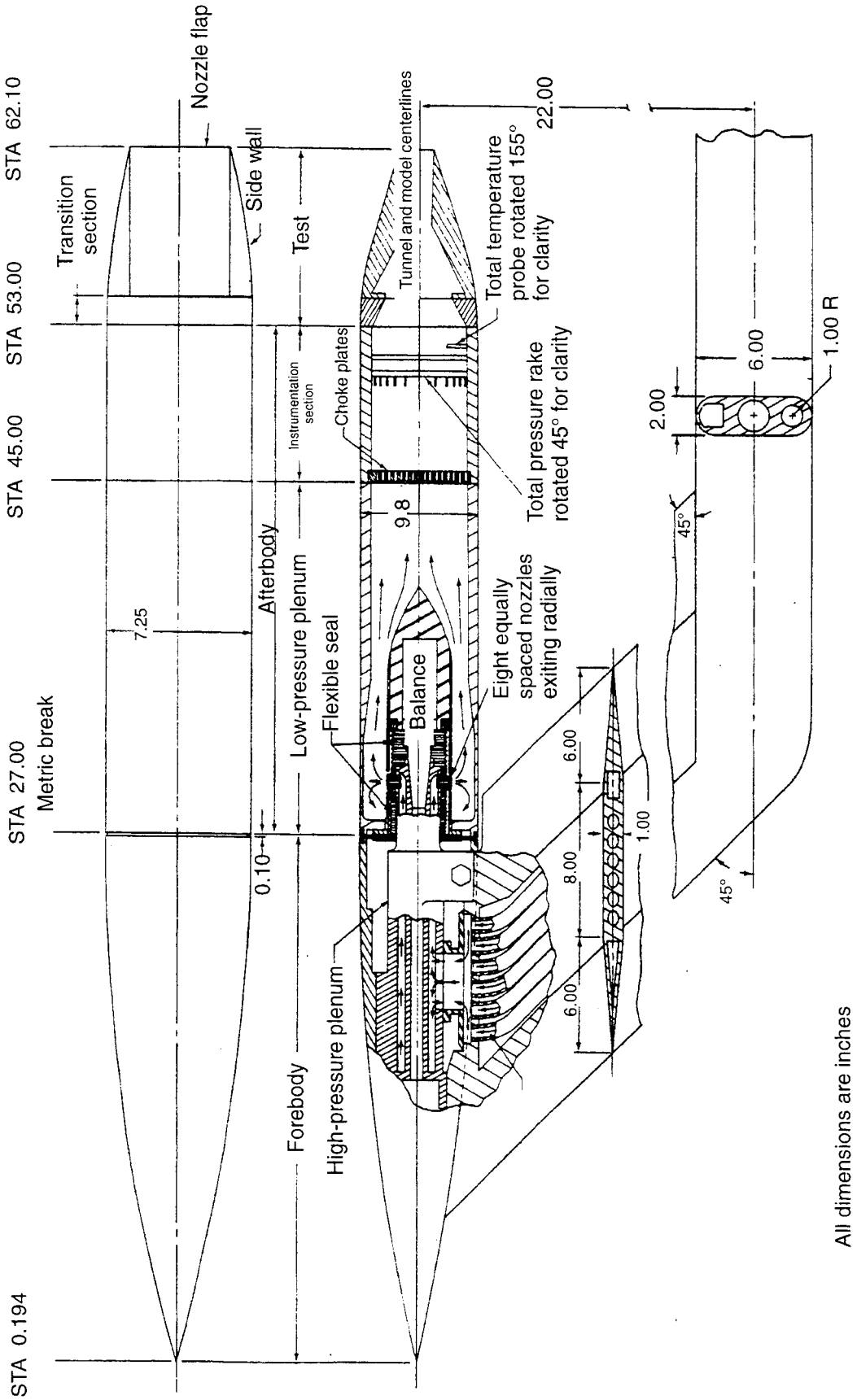

Figure 10. Sketch of nonaxisymmetric, single-engine propulsion simulator

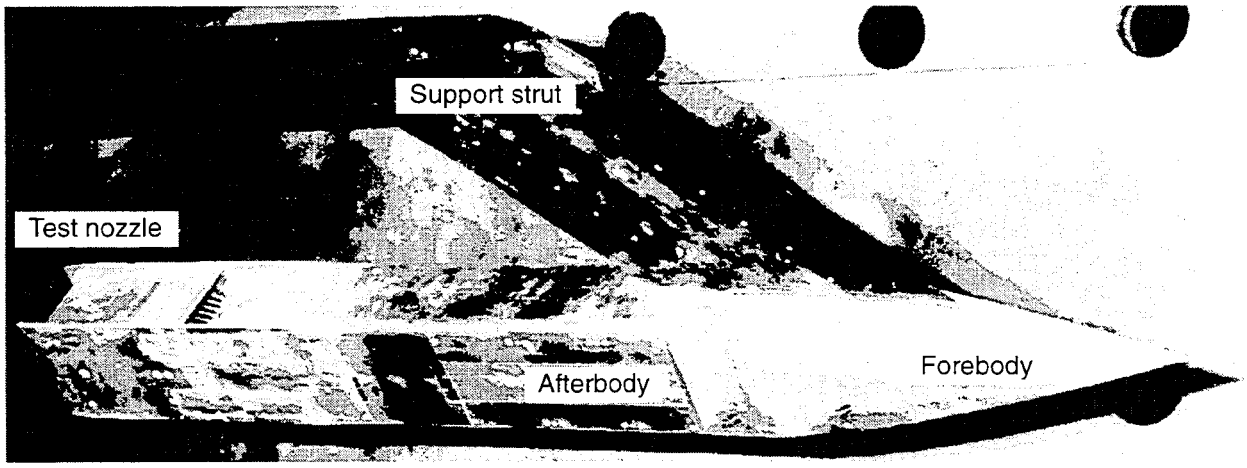

Figure 11. View of the 2DME nozzle scale-model installation

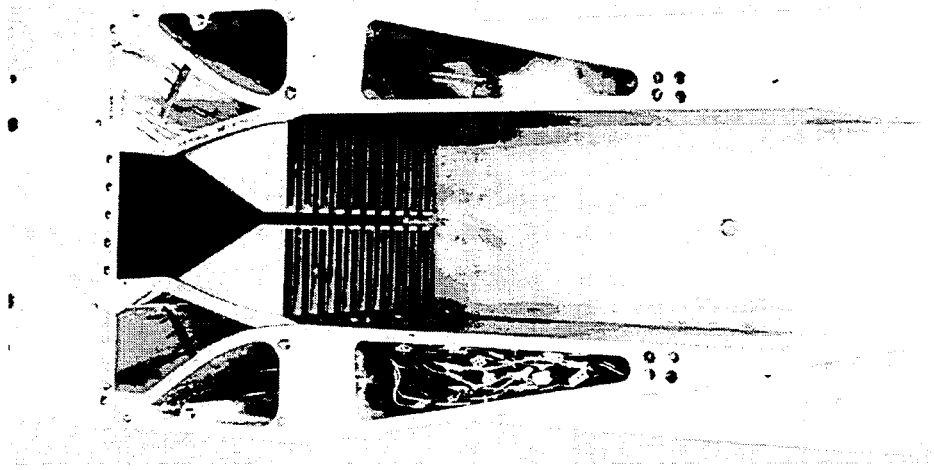

Figure 12. View of 2DME scale-model with long flap, MAR = 1.0 (sidewall removed)

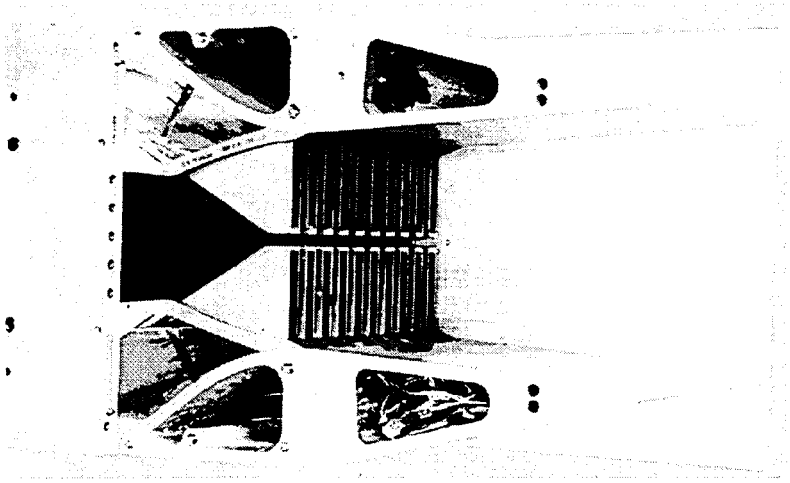

Figure 13. View of 2DME scale-model with short flap, MAR = 1.2 (sidewall removed)

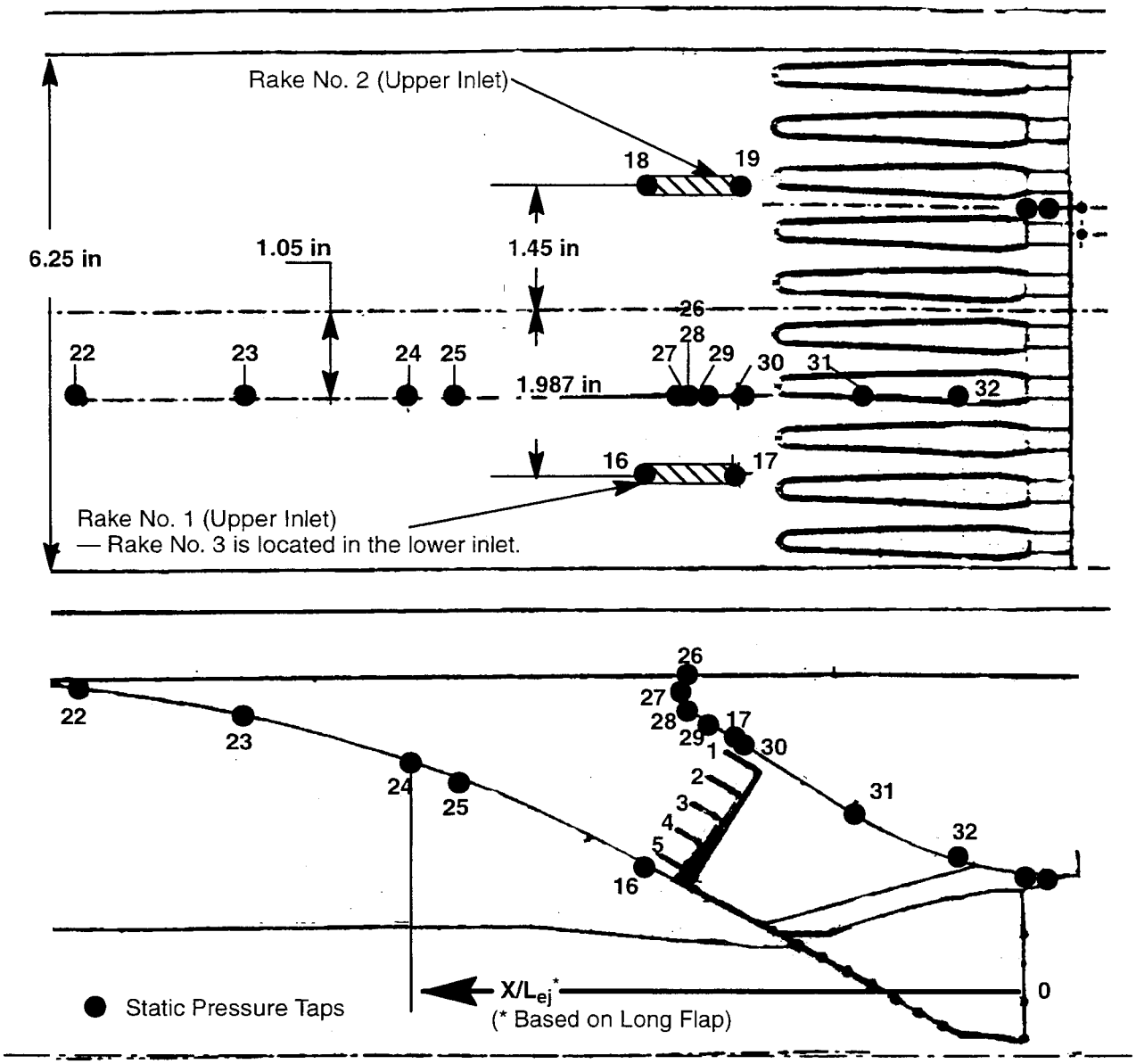

Rake Wall Statics

Tap	X/L_{ej}
16	–0.387
17	–0.308
18	–0.387
19	–0.308
20	–0.387
21	–0.308

Ramp Wall Statics

Tap	X/L_{ej}
22	–0.997
23	–0.827
24	–0.656
25	–0.508

Scoop/Flap LE Wall Statics

Tap	X/L_{ej}
26	–0.358
27	–0.367
28	–0.358
29	–0.335
30	–0.305
31	–0.188
32	–0.072

Figure 14. Scale-model 2DME exhaust system secondary flow inlet instrumentation.

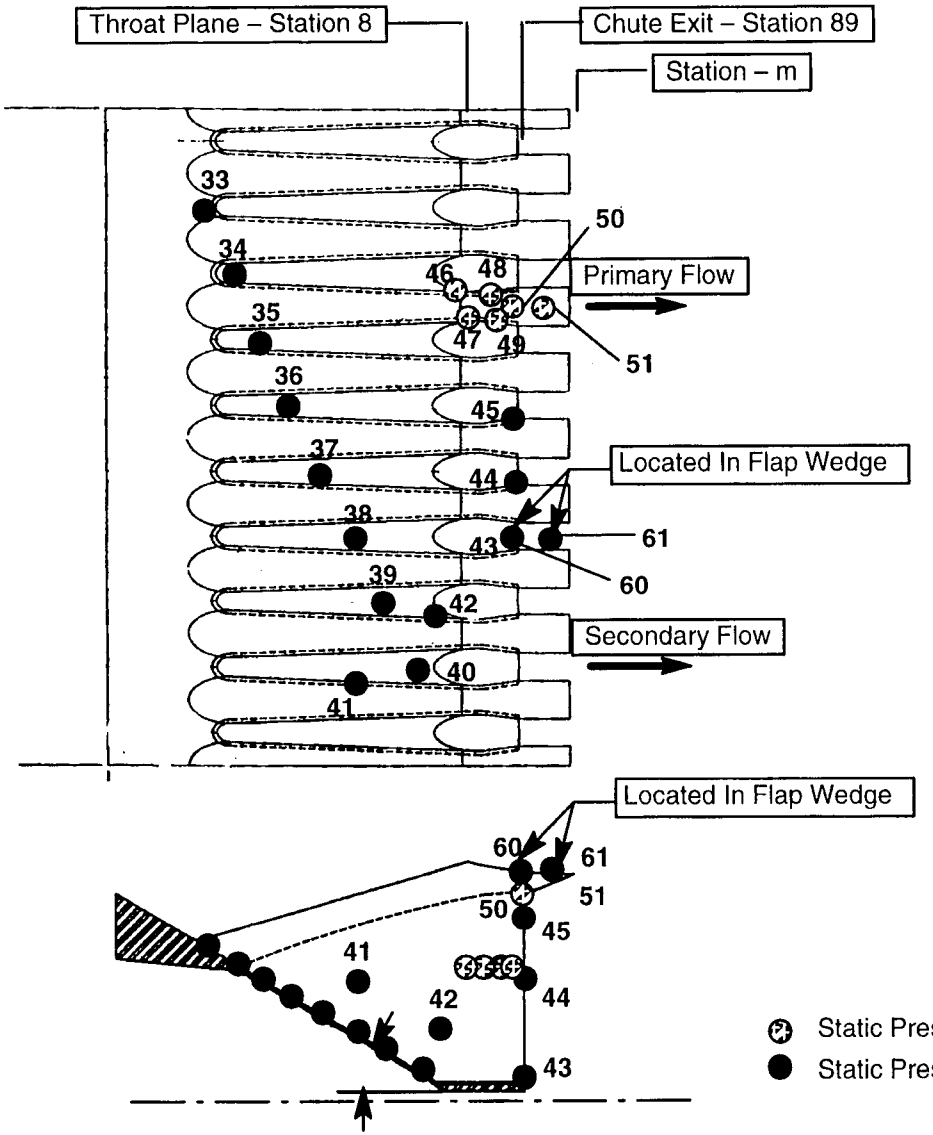

Secondary Aligned Statics

Tap	X (in)
33	–0.270
34	–0.245
35	–0.218
36	–0.192
37	–0.167
38	–0.140
39	–0.114
40	–0.088
41	–0.135
42	–0.071
43	0.00
44	0.00
45	0.00
60	0.00
61	0.02

Primary Aligned Statics

Tap	X (in)
46	–0.033
47	–0.024
48	–0.014
49	–0.004
50	0.00
51	0.02

Figure 15. Suppressor chute static pressure instrumentation

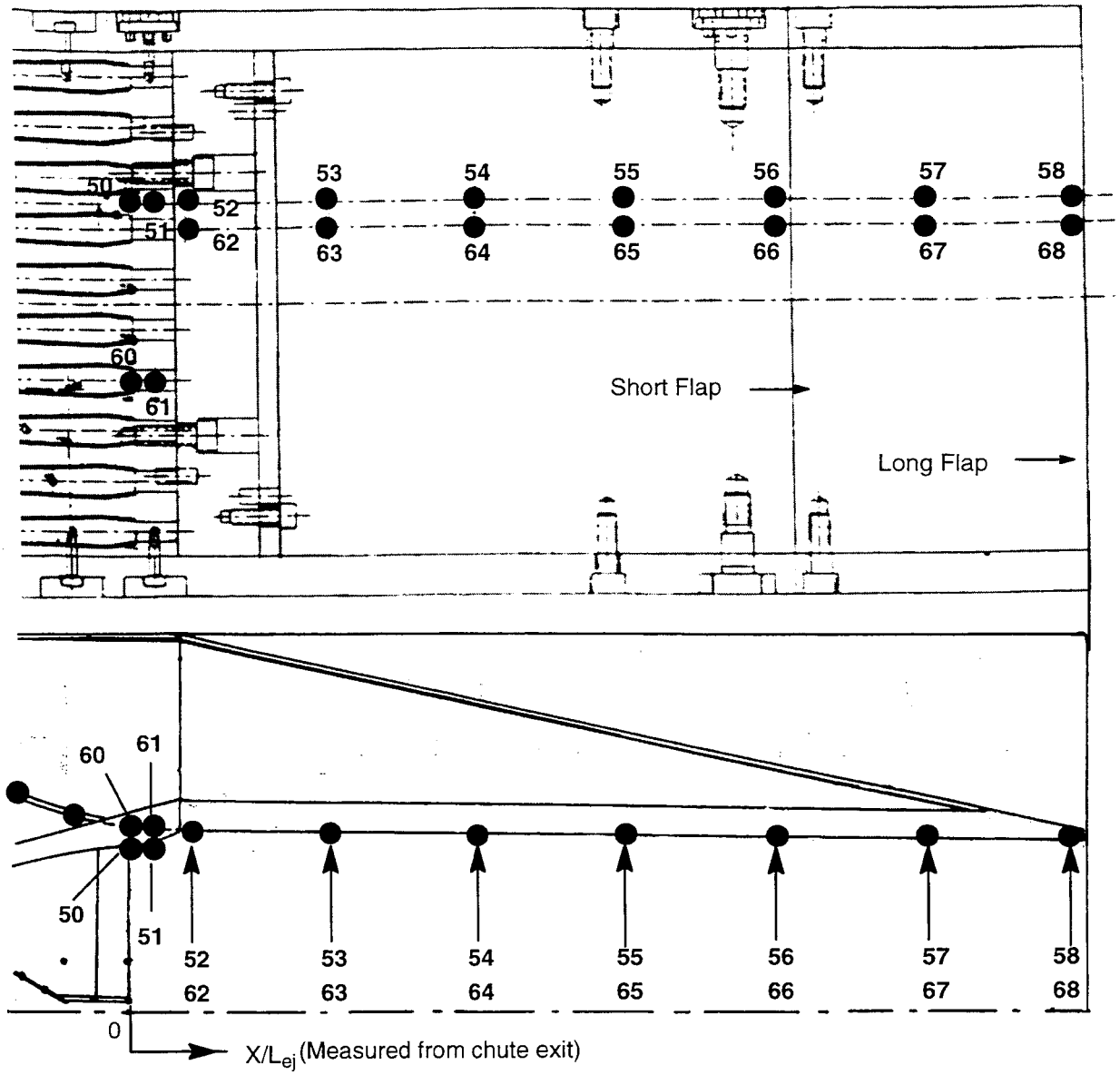

Figure 16. Flap static pressure instrumentation

Flap Static Pressure Locations

Primary Aligned Static Taps	50	51	52	53	54	55	56	57	58
Secondary Aligned Taps	60	61	62	63	64	65	66	67	68
Axial Position X/L_{ej}	0	0.020	0.058	0.213	0.368	0.524	0.679	0.894	0.989

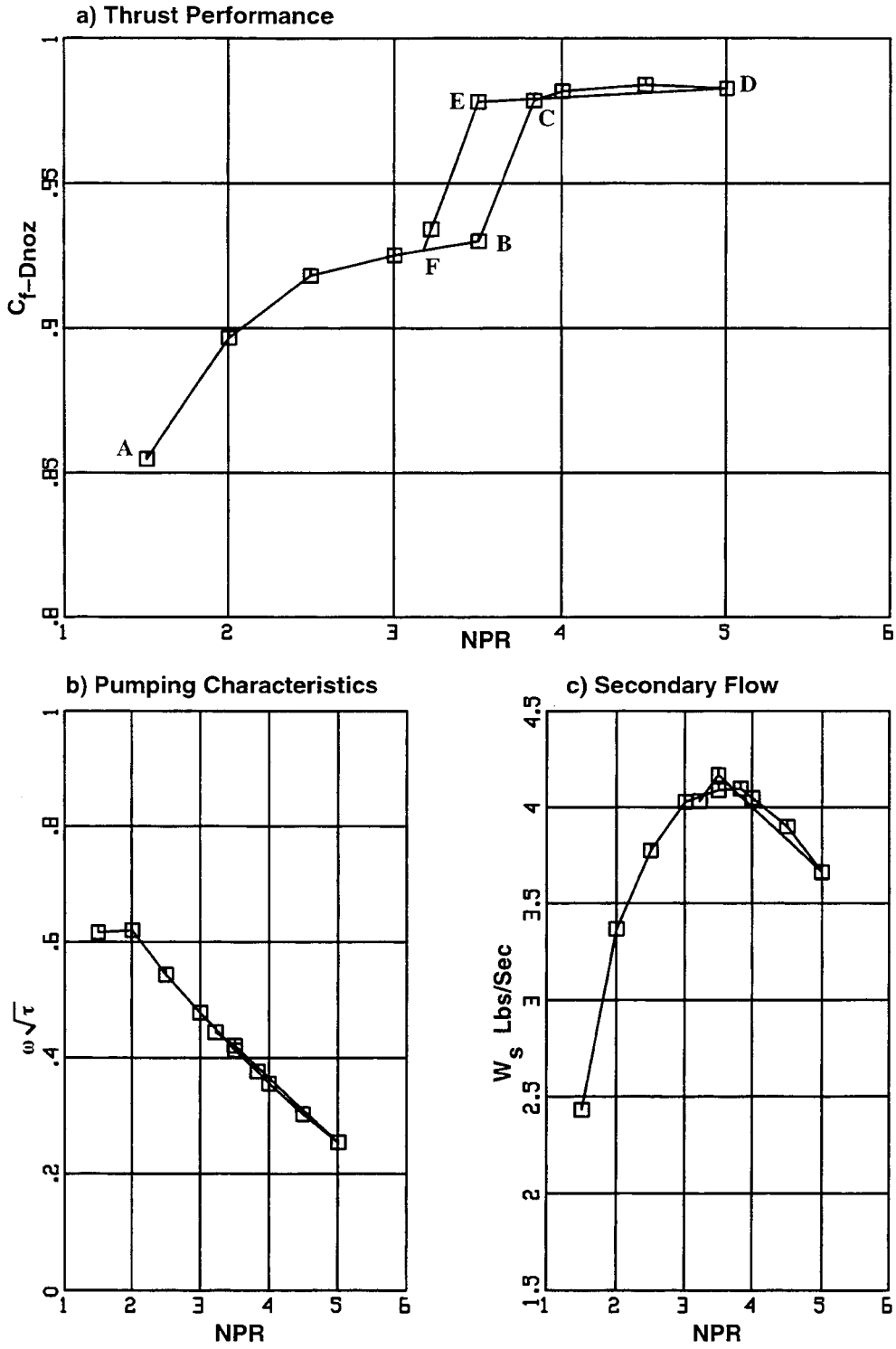

Figure 17. Typical static performance at MAR less than 1
SAR =3.3, CER=1.22, MAR=0.9 Aligned Chutes, Long Flap Configuration.

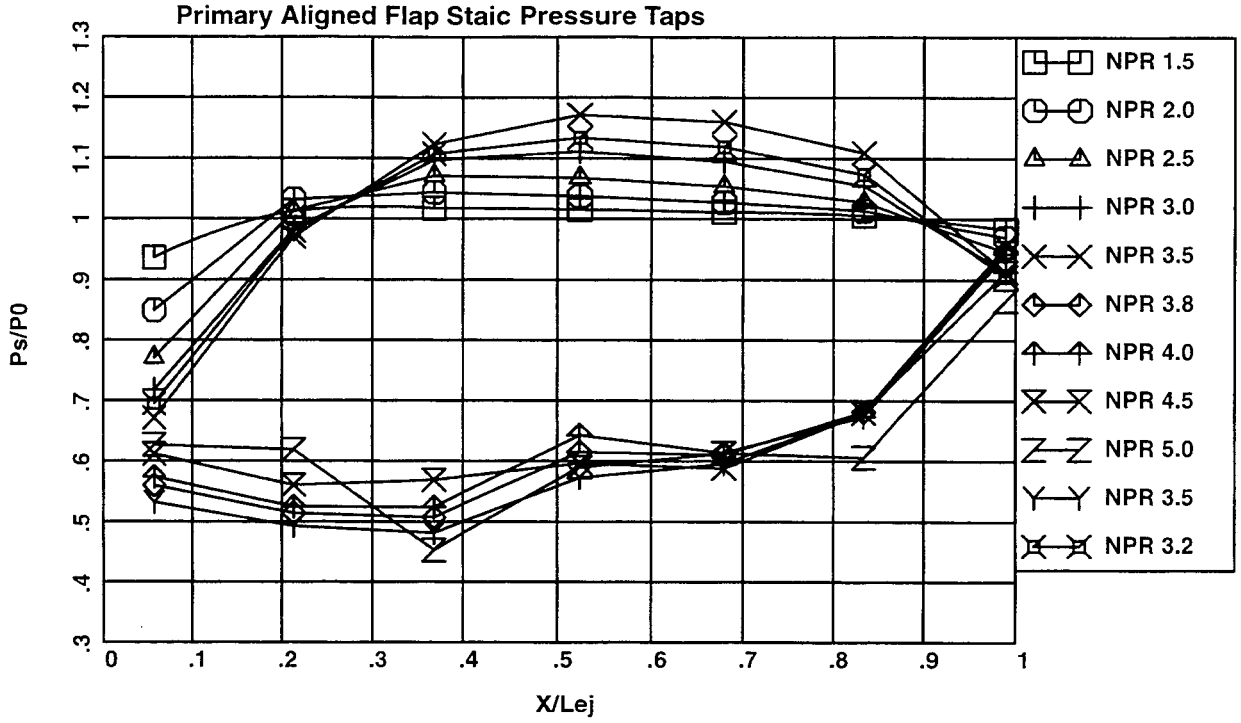

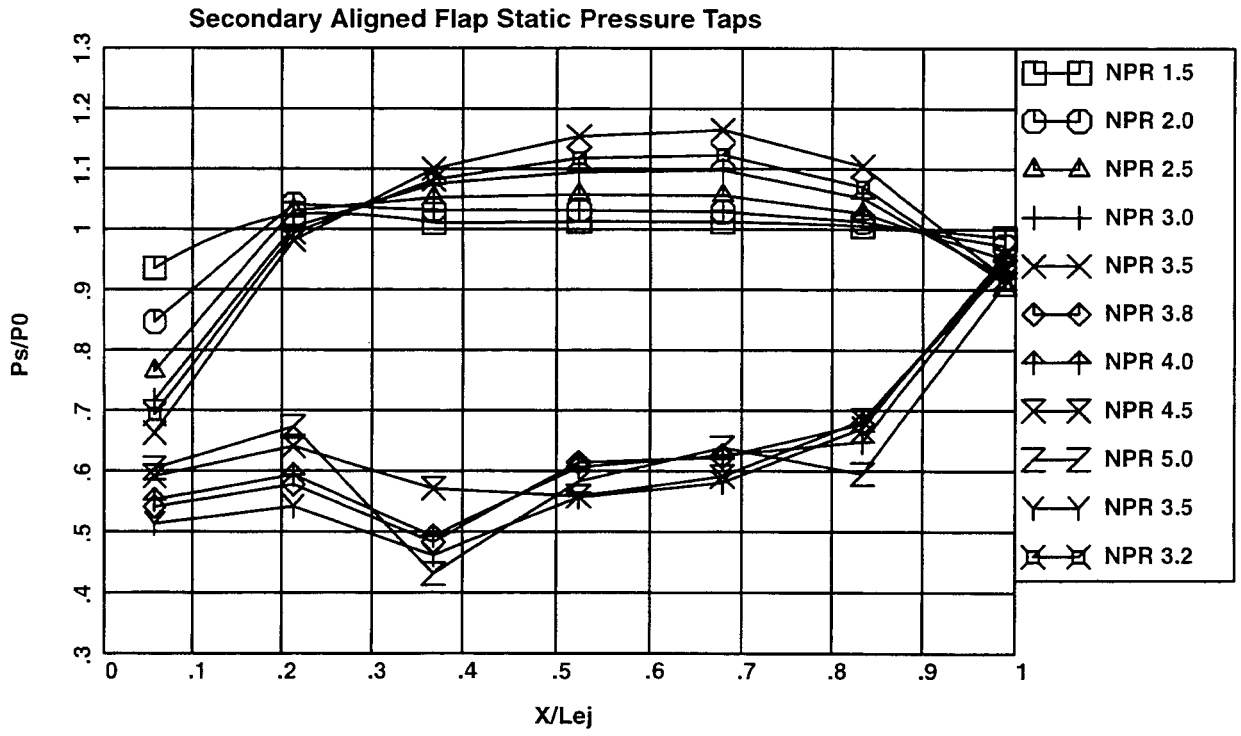

Figure 18. Flap static pressure distribution at various NPRs.
SAR 3.3, MAR 0.9, CER 1.22, Aligned Chutee, Long flap configuration at M_0=0.

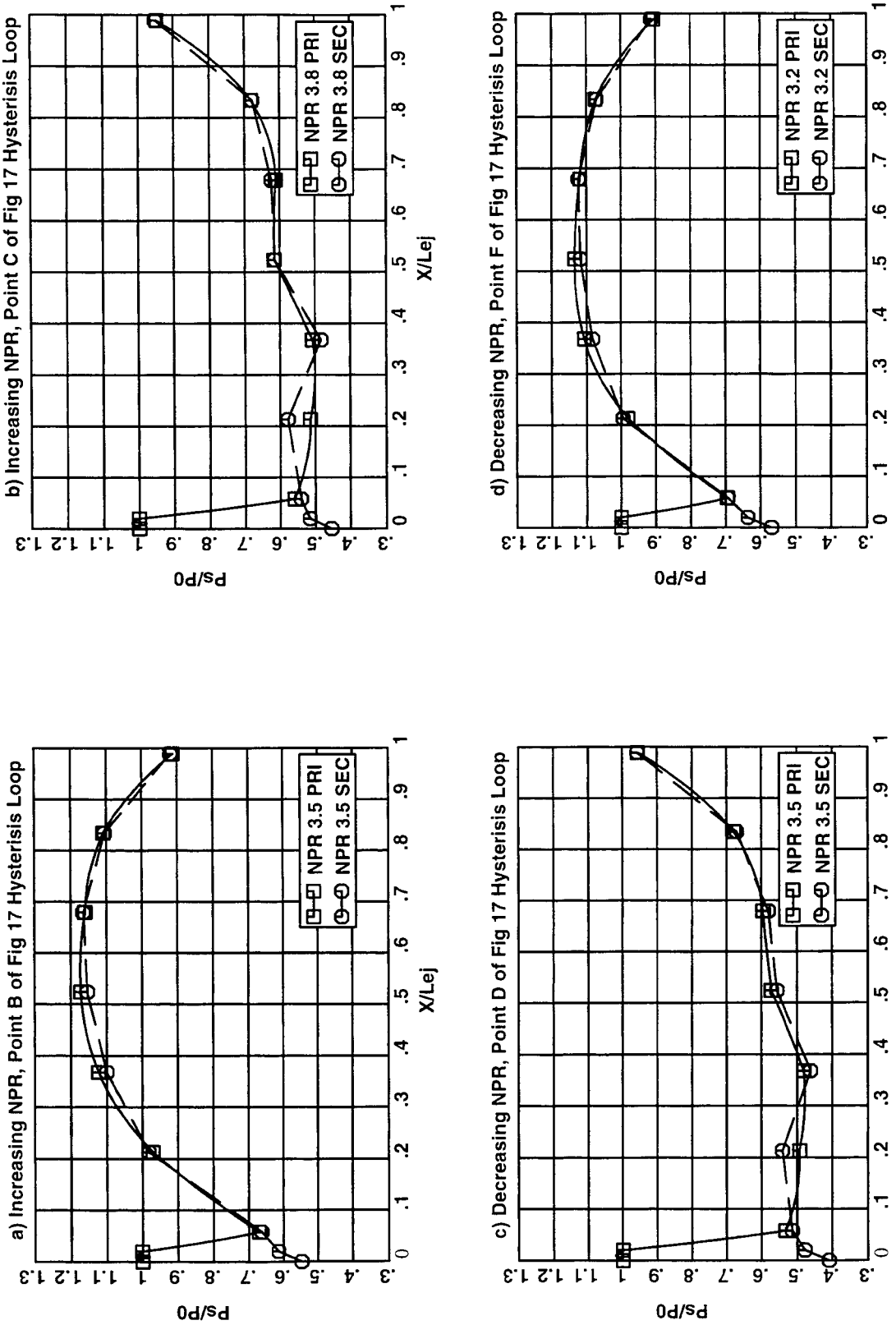

Figure 19. Comparison of primary & secondary aligned flap static pressures at selected test conditions SAR 3.3, MAR 0.9, CER 1.22, Aligned Chutes, Long Flap Configuration at M_0=0.

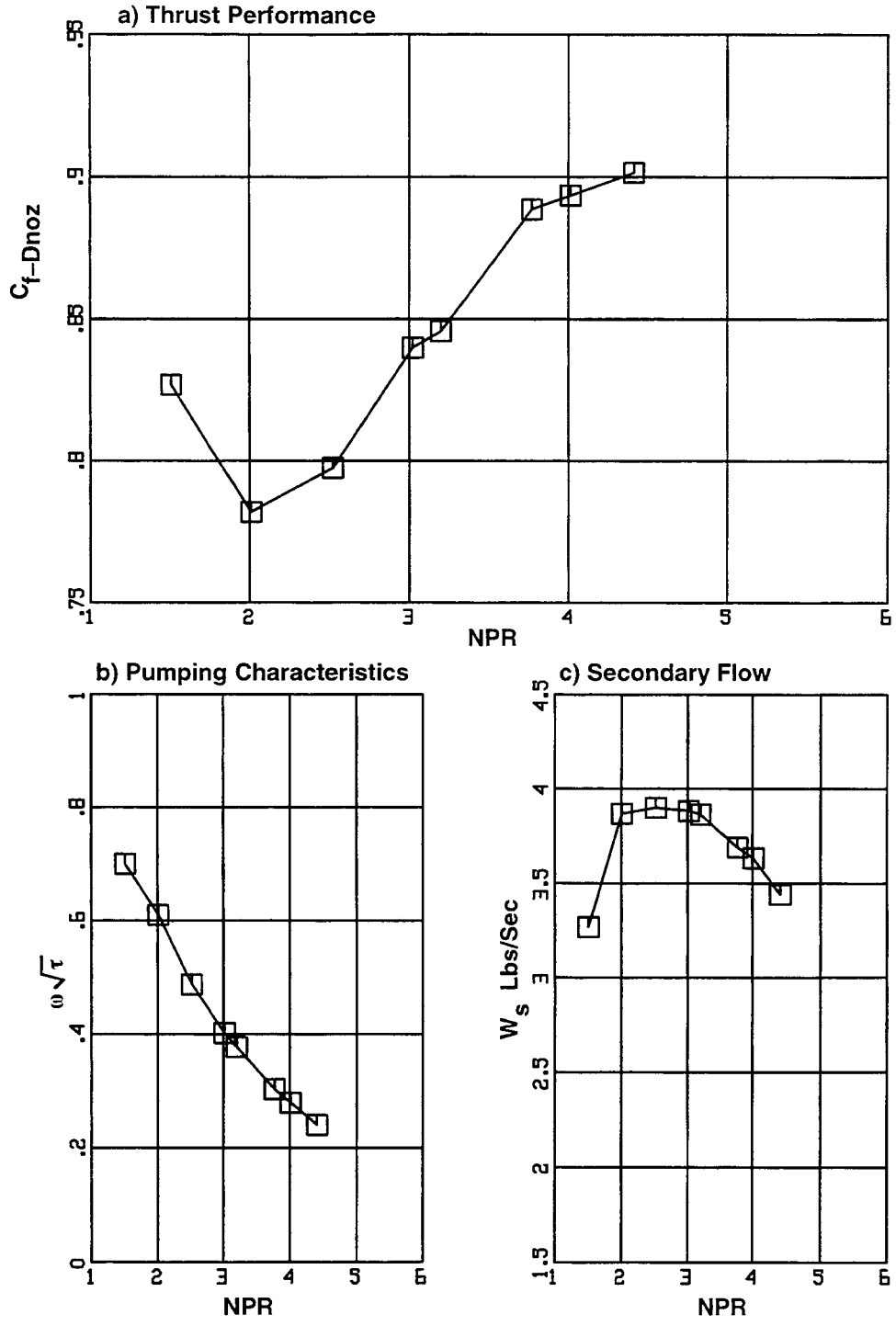

Figure 20. Typical static performance at MAR greater than 1 SAR 2.8, MAR 1.2, CER 1.22, Aligned chute, Long flap Configuration.

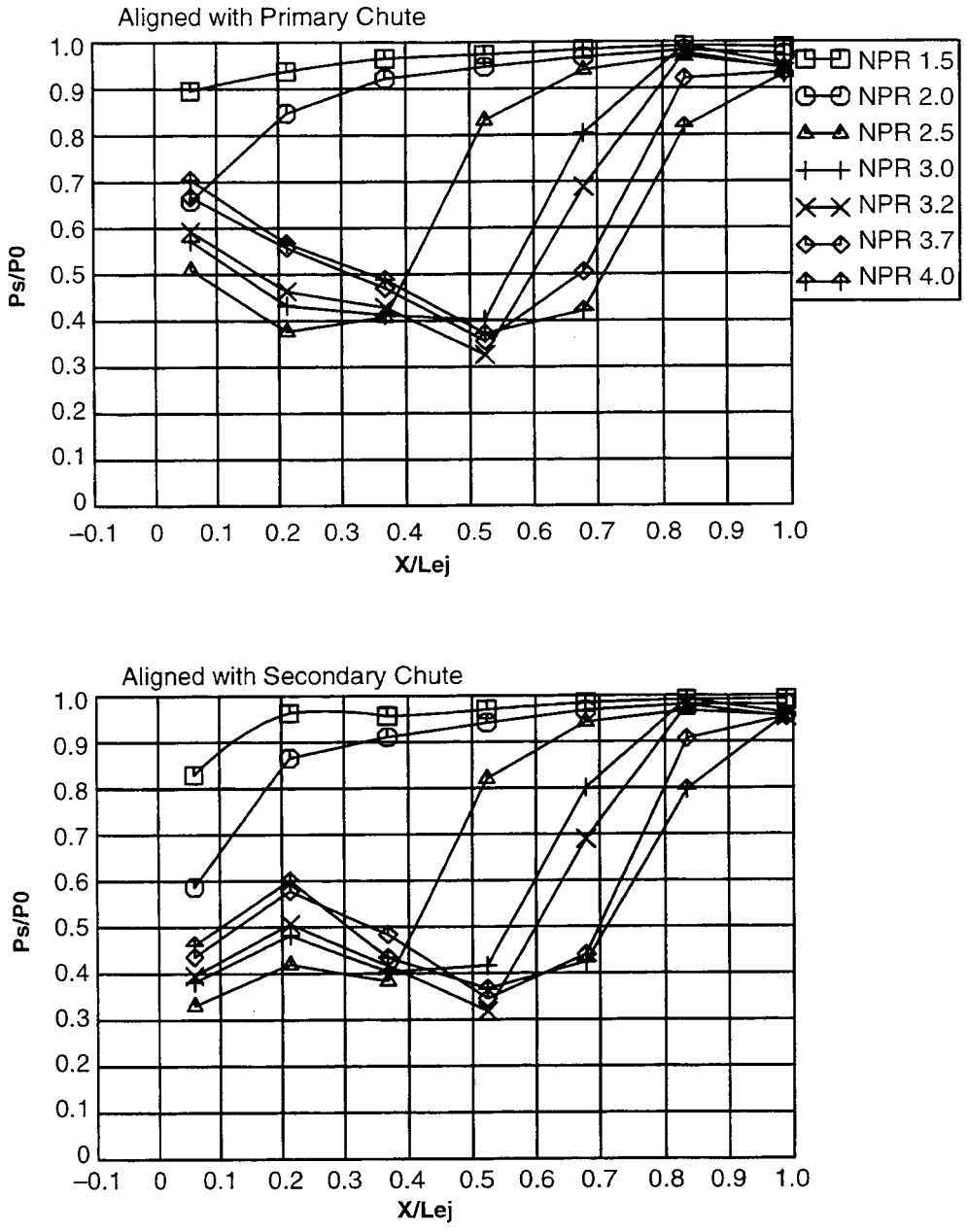

Figure 21. Flap static pressure distribution at various NPR's SAR 2.8, MAR 1.2, CER 1.22, Aligned Chuts, Long flap configuration at M_0=0

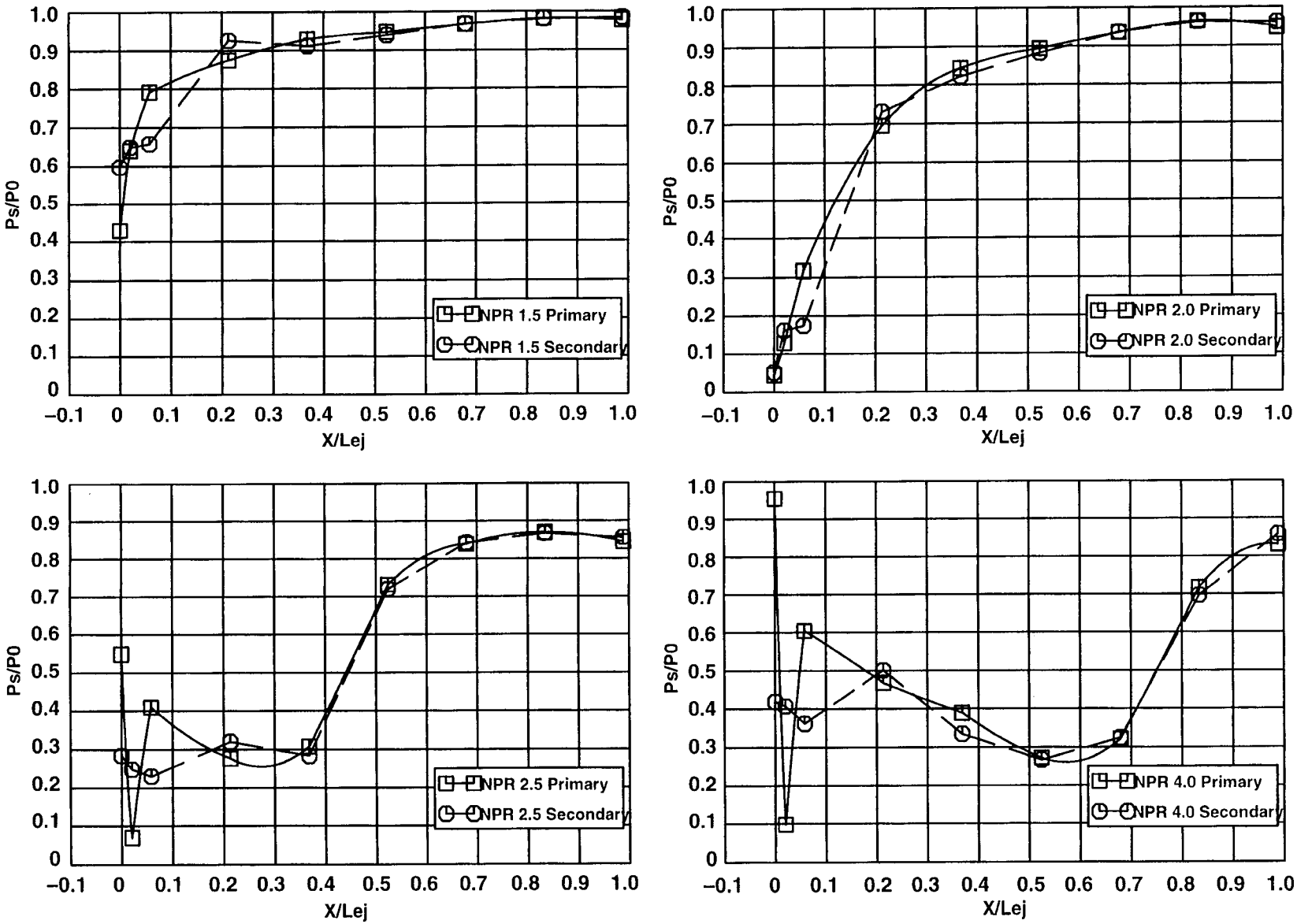

Figure 22. Comparison of primary and secondary aligned flap static pressures at various NPRs SAR 2.8, MAR 1.2, CER 1.22, Aligned chute, Long flap configuration at M_0=0.

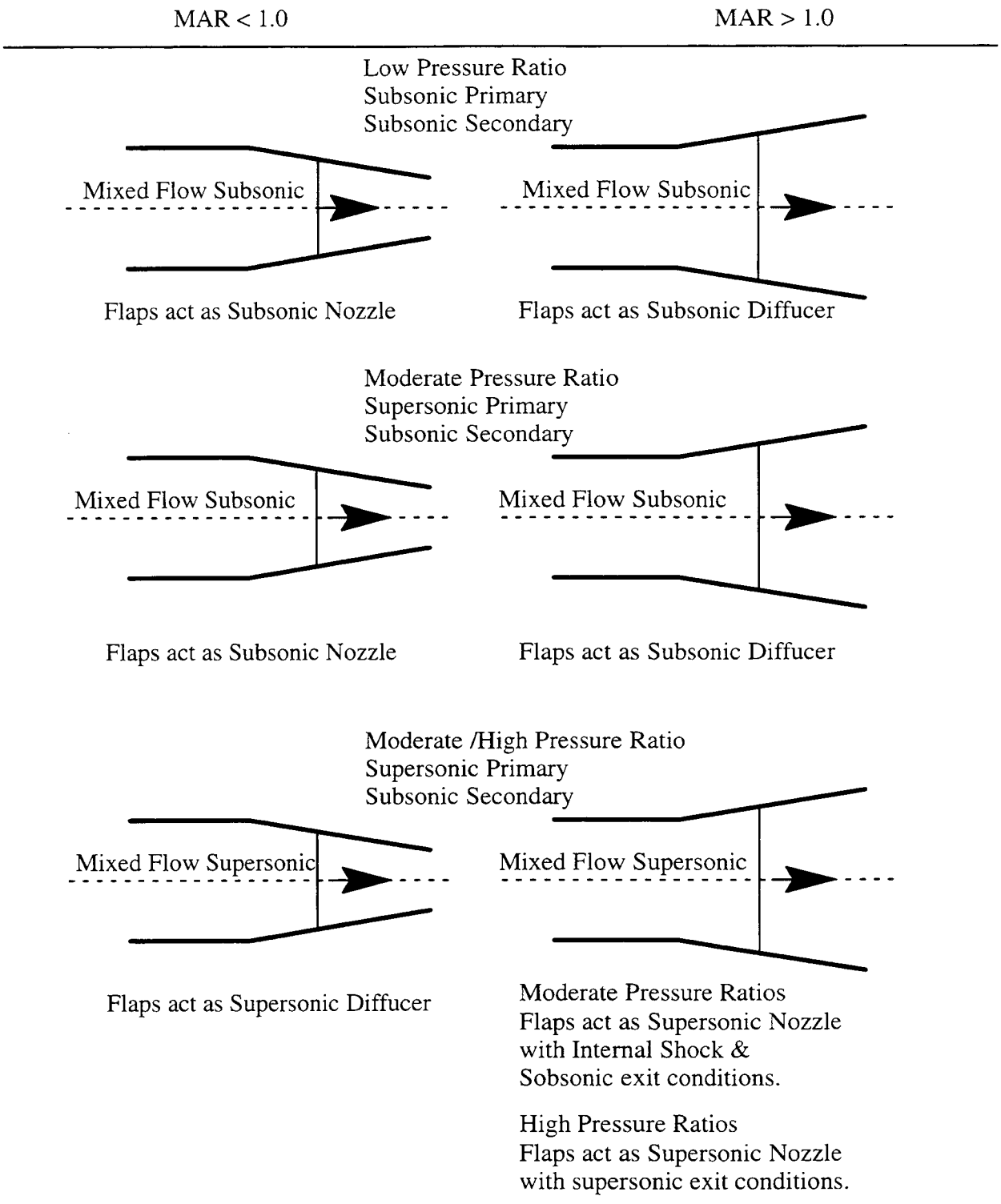

Figure 23. Schematic of the various operting conditions Of the Mixer Ejector Nozzle.

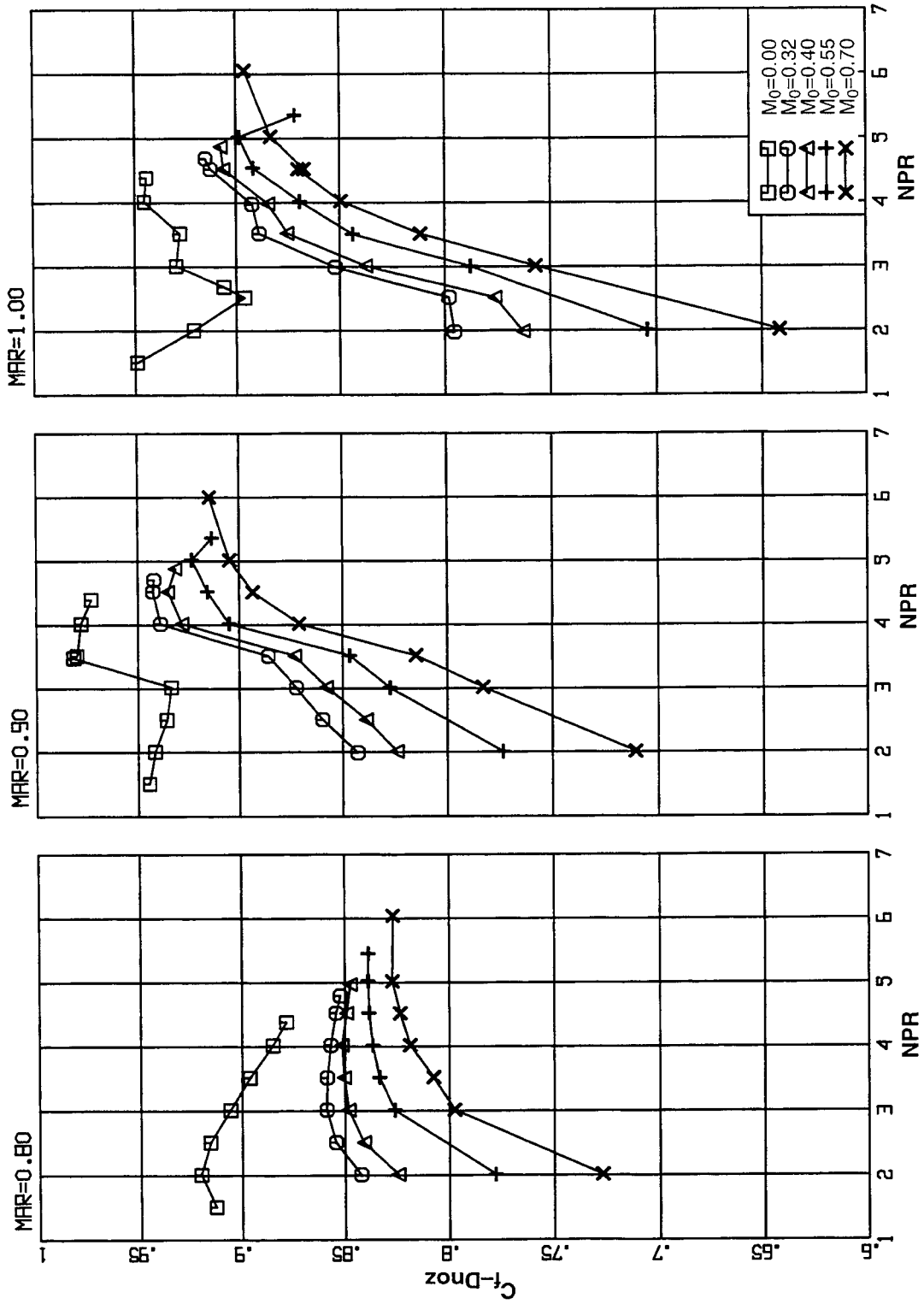

Figure 24. Effect of free stream Mach on thrust performance at selected MARs SAR 2.8, CER 1.00, Aligned Chutes, Long Flap Configuration.

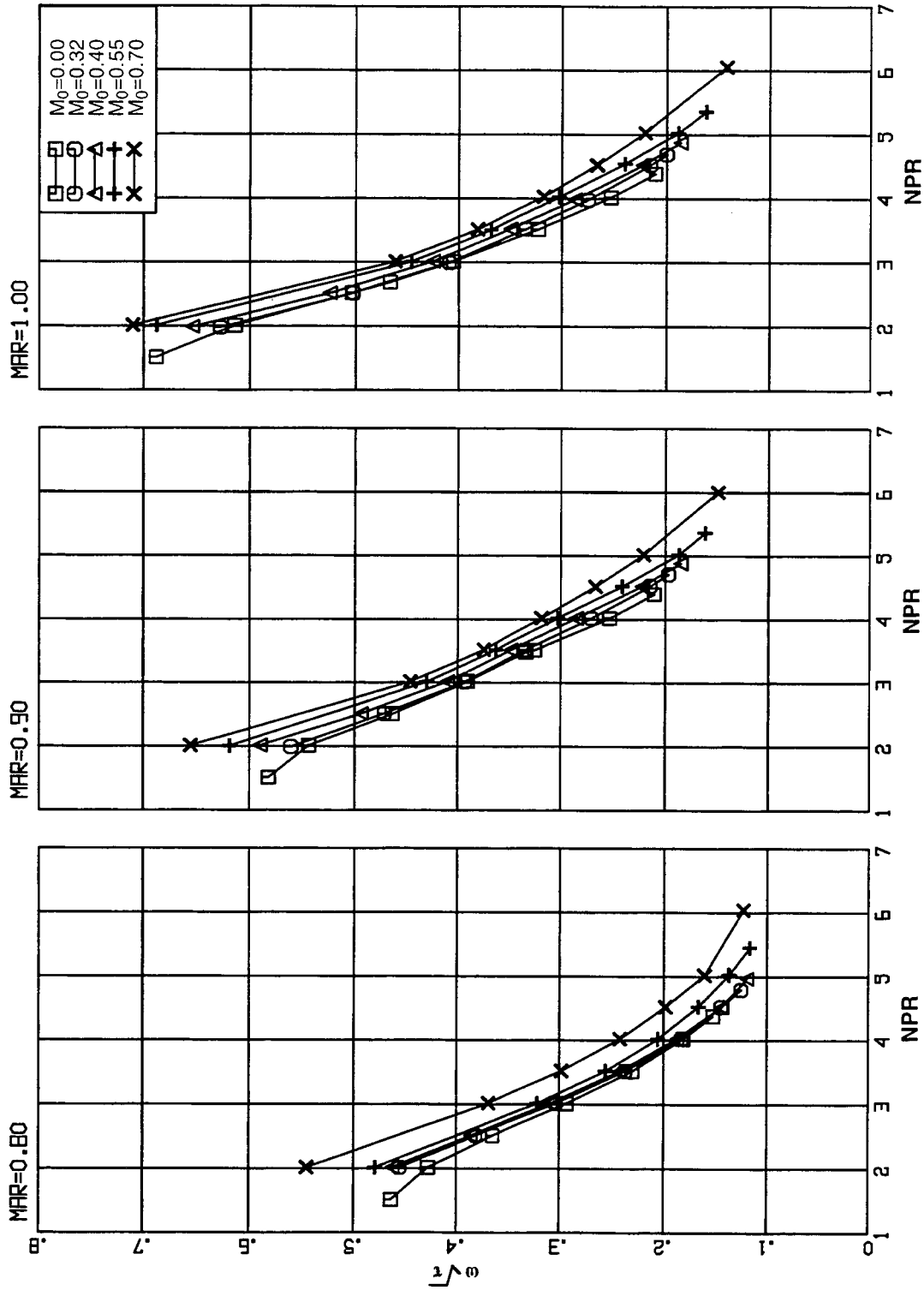

Figure 25. Effect of free stream Mach on pumping characteristics at selected MARs. SAR 2.8, CER 1.00, Aligned Chutes, Long Flap Configuration.

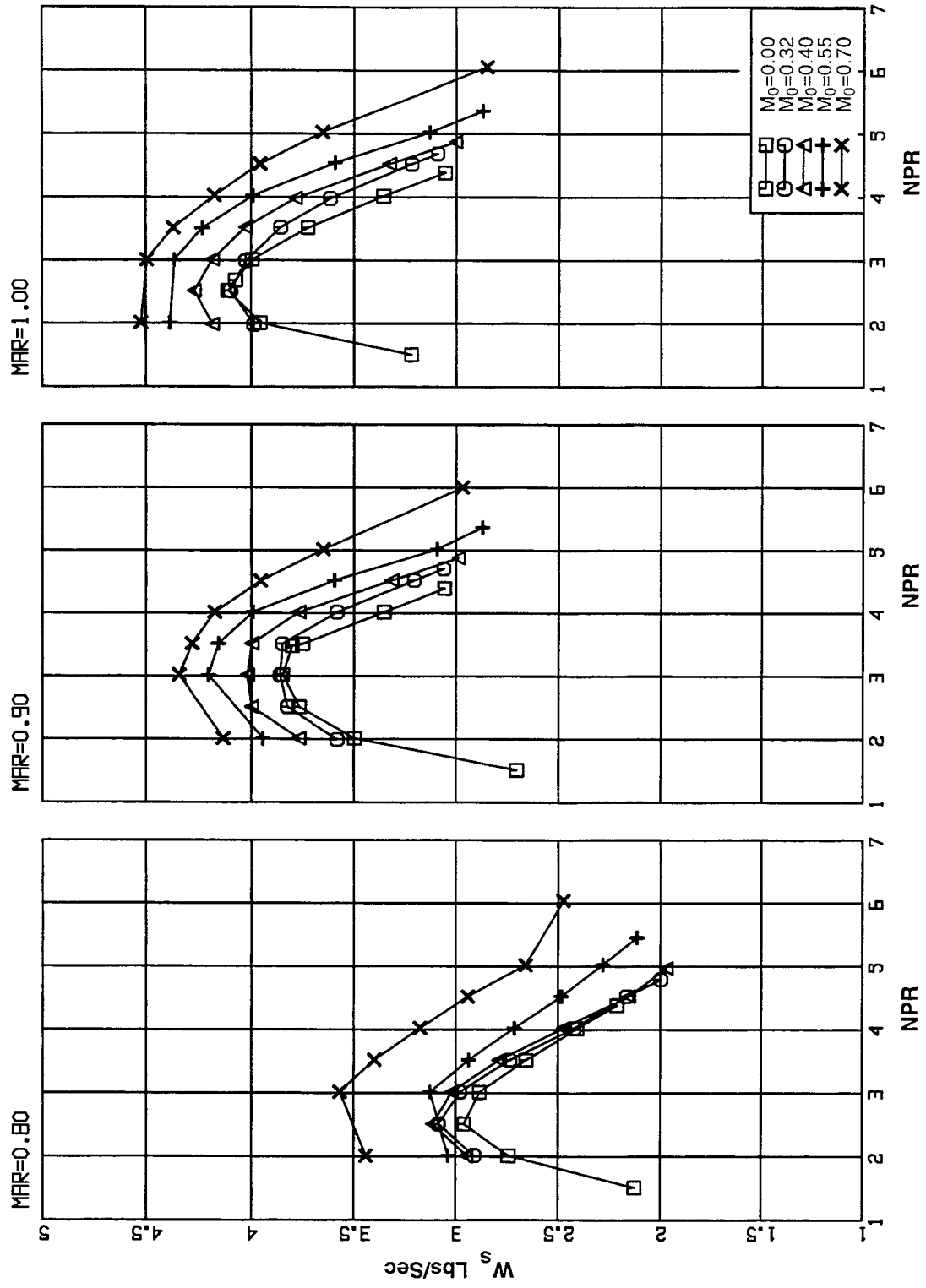

Figure 26. Effect of free stream Mach on Secondary flow at selected MARs. SAR 2.8, CER 1.00, Aligned Chutes, Long Flap Configuration.

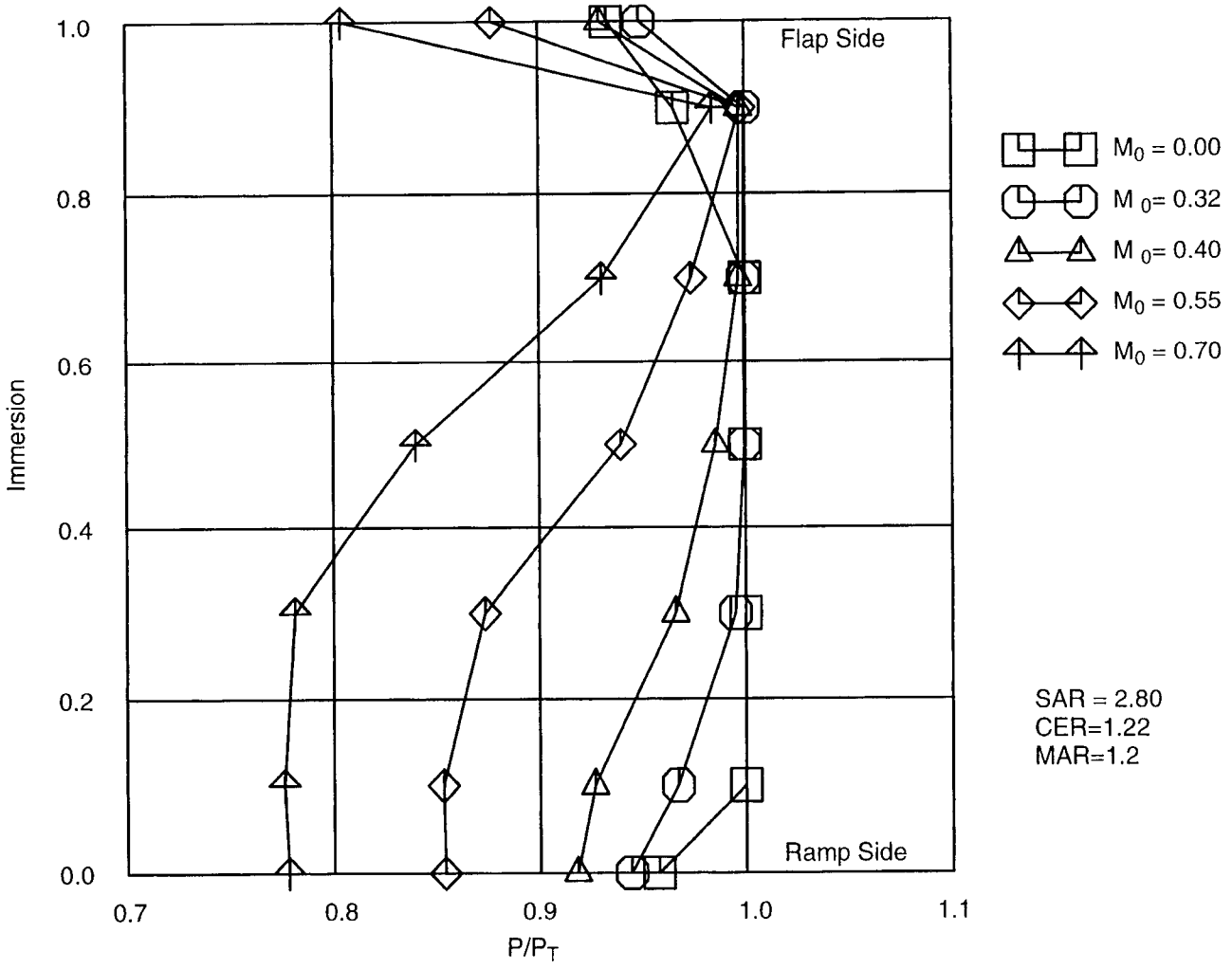

Figure 27. Typical Ejector inlet rake pressure profiles at various free stream Mach.

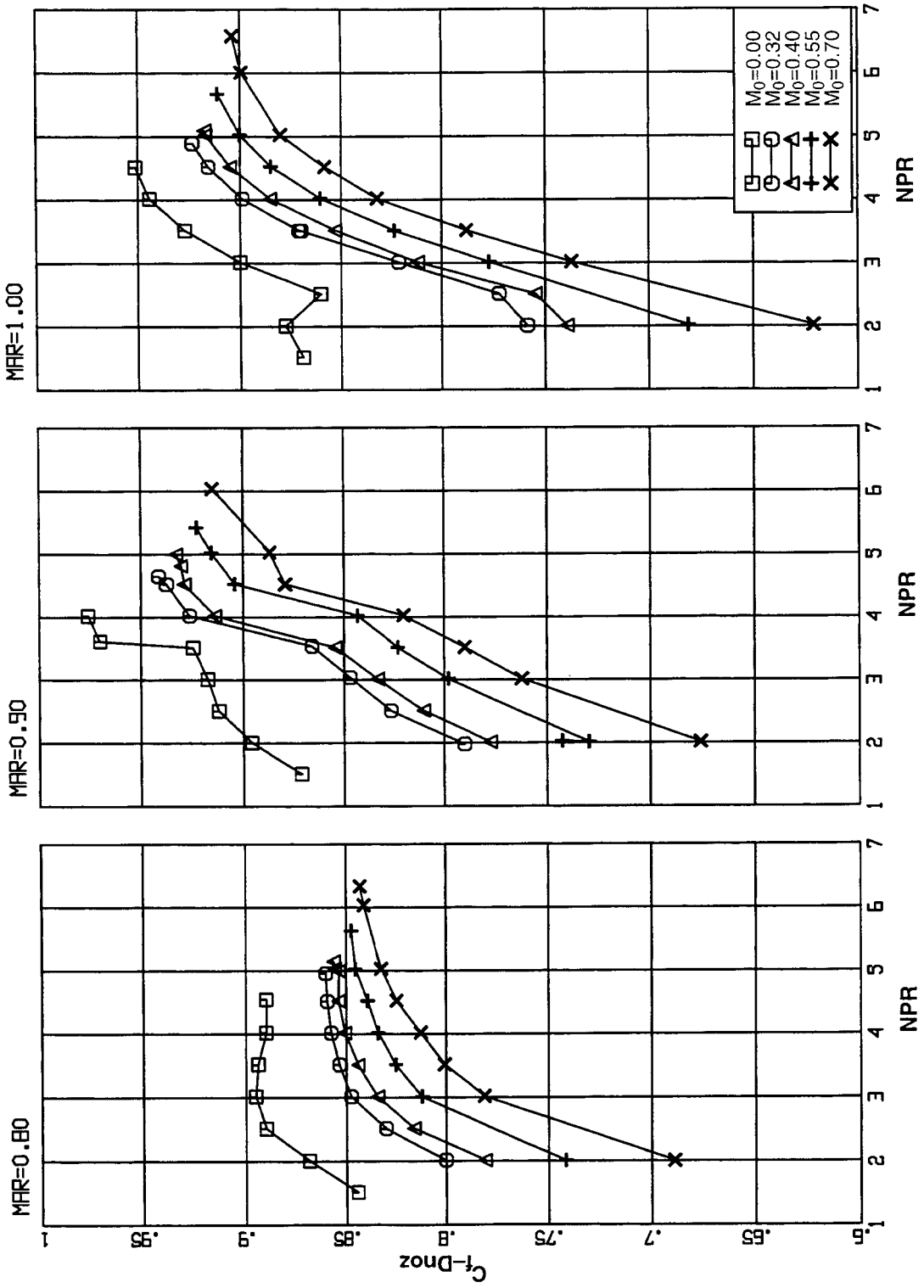

Figure 28. Effect of free stream Mach on thrust performance at selected MARs SAR 2.8, CER 1.22, Aligned Chutes, Long Flap Configuration.

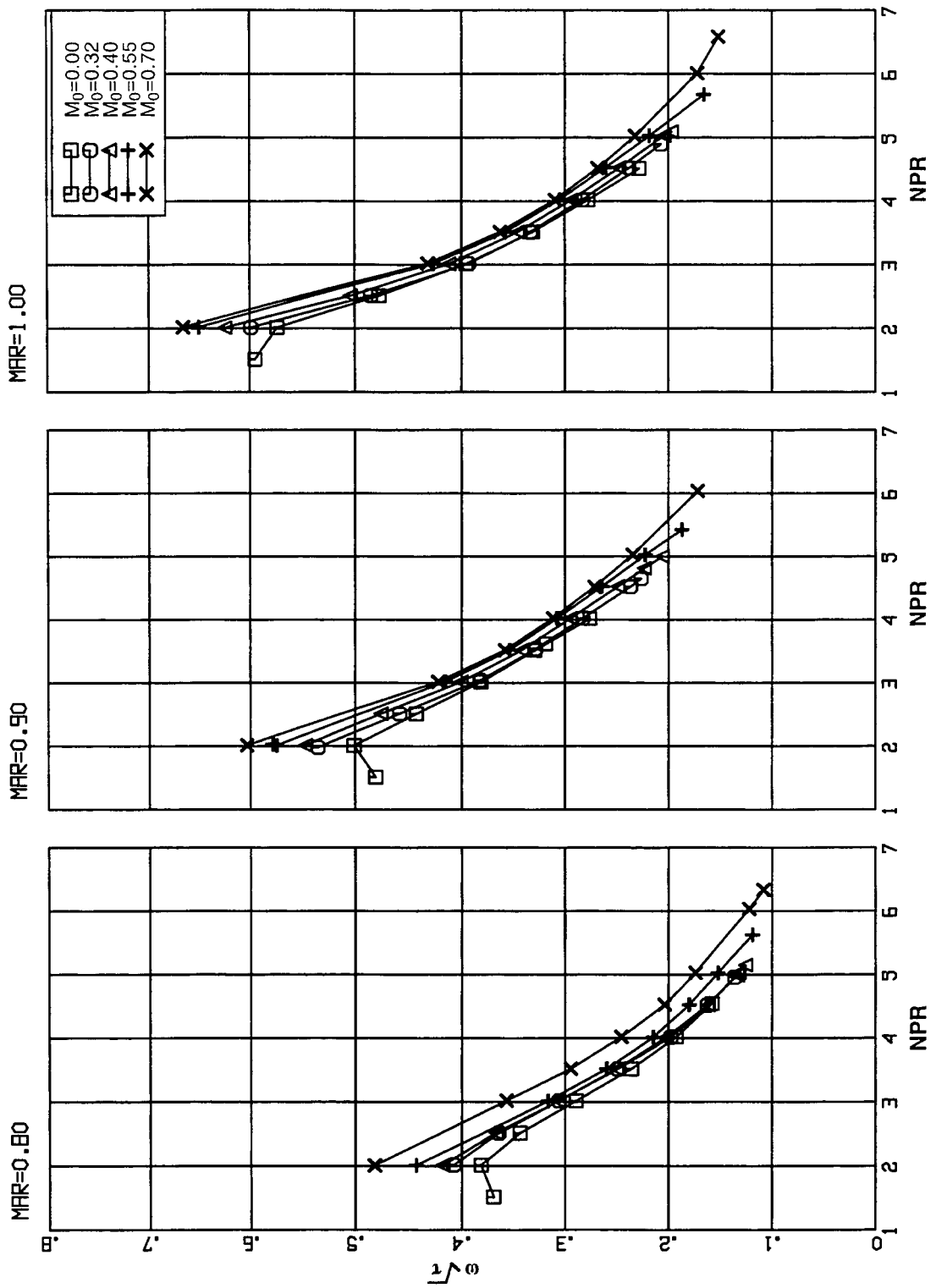

Figure 29. Effect of free stream Mach on pumping characteristics at selected MARs. SAR 2.8, CER 1.22, Aligned Chutes, Long Flap Configuration.

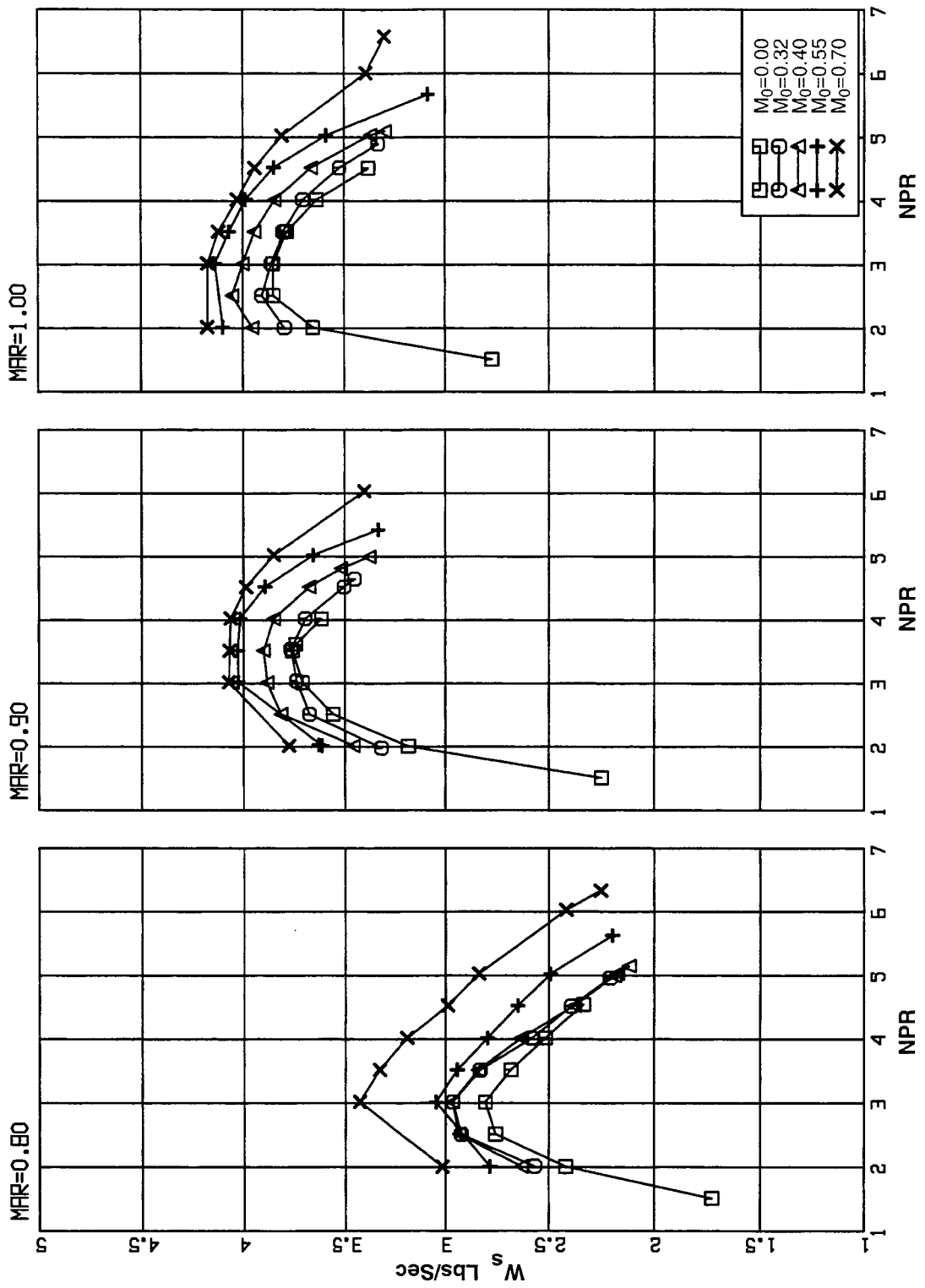

Figure 30. Effect of free stream Mach on Secondary flow at selected MARs. SAR 2.8, CER 1.22, Aligned Chutes, Long Flap Configuration.

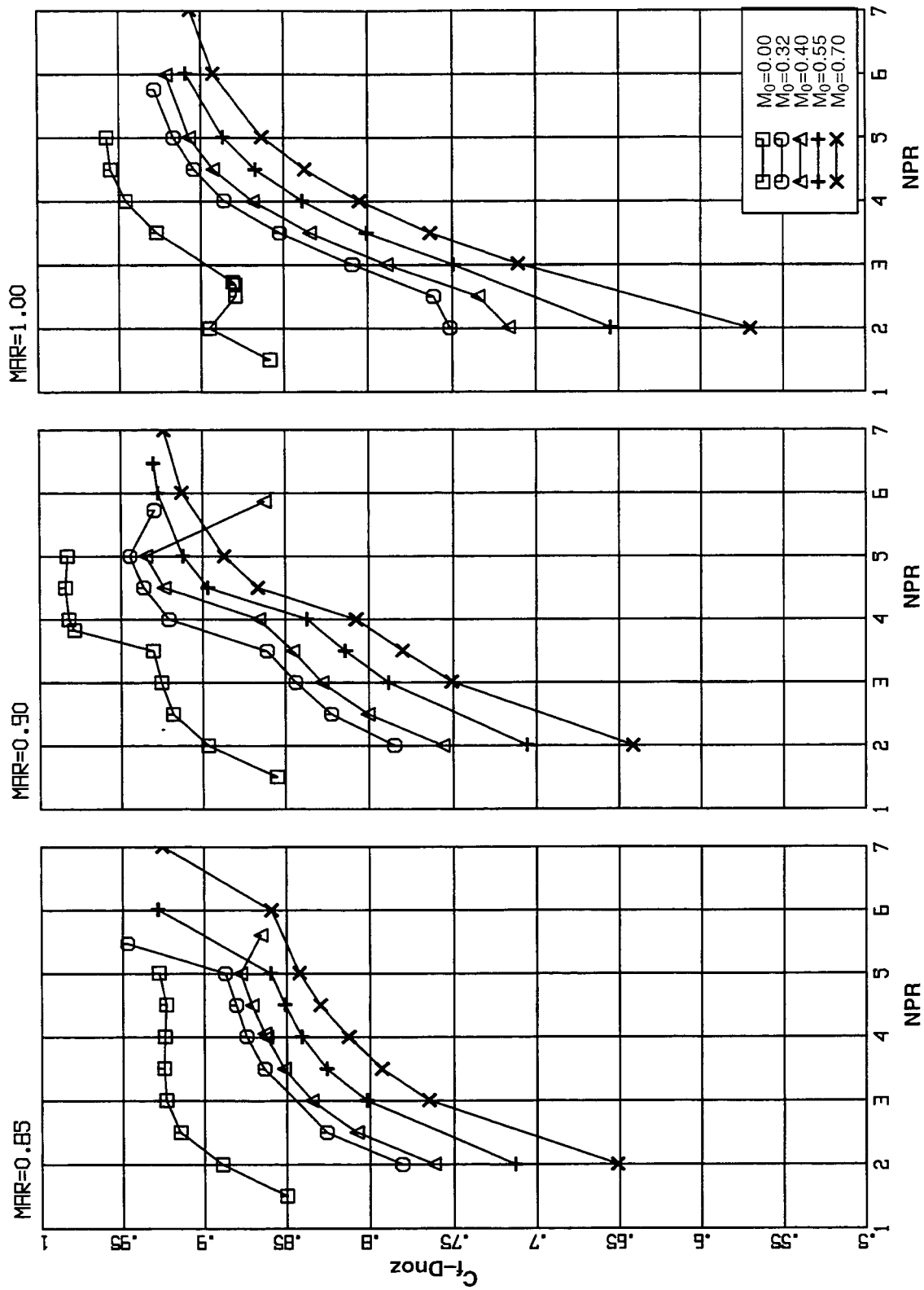

Figure 31. Effect of free stream Mach on thrust performance at selected MARs SAR 3.3, CER 1.22, Aligned Chutes, Long Flap Configuration.

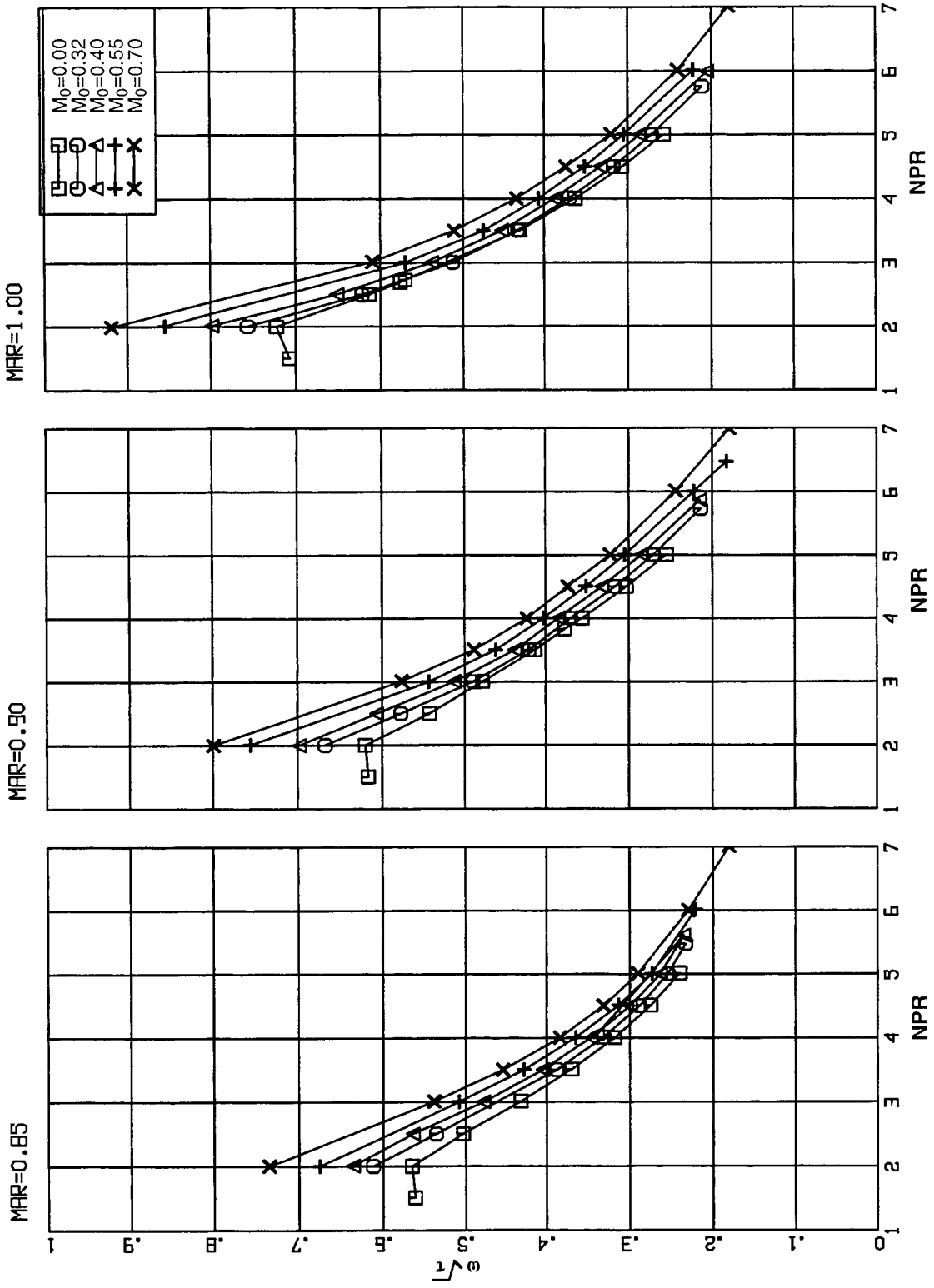

Figure 32. Effect of free stream Mach on pumping characteristics at selected MARs. SAR 3.3, CER 1.22, Aligned Chutes, Long Flap Configuration.

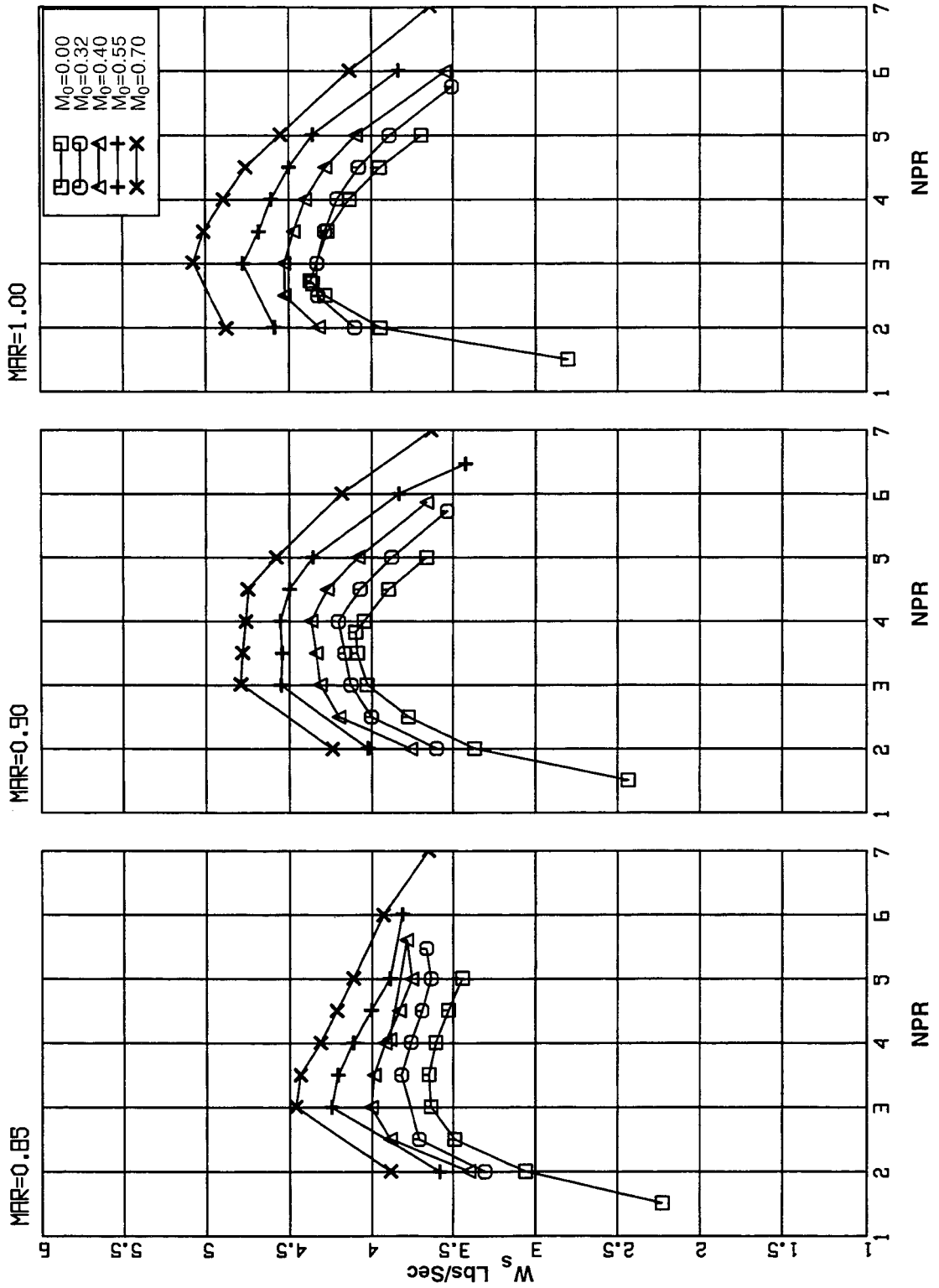

Figure 33. Effect of free stream Mach on Secondary flow at selected MARs. SAR 3.3, CER 1.22, Aligned Chutes, Long Flap Configuration.

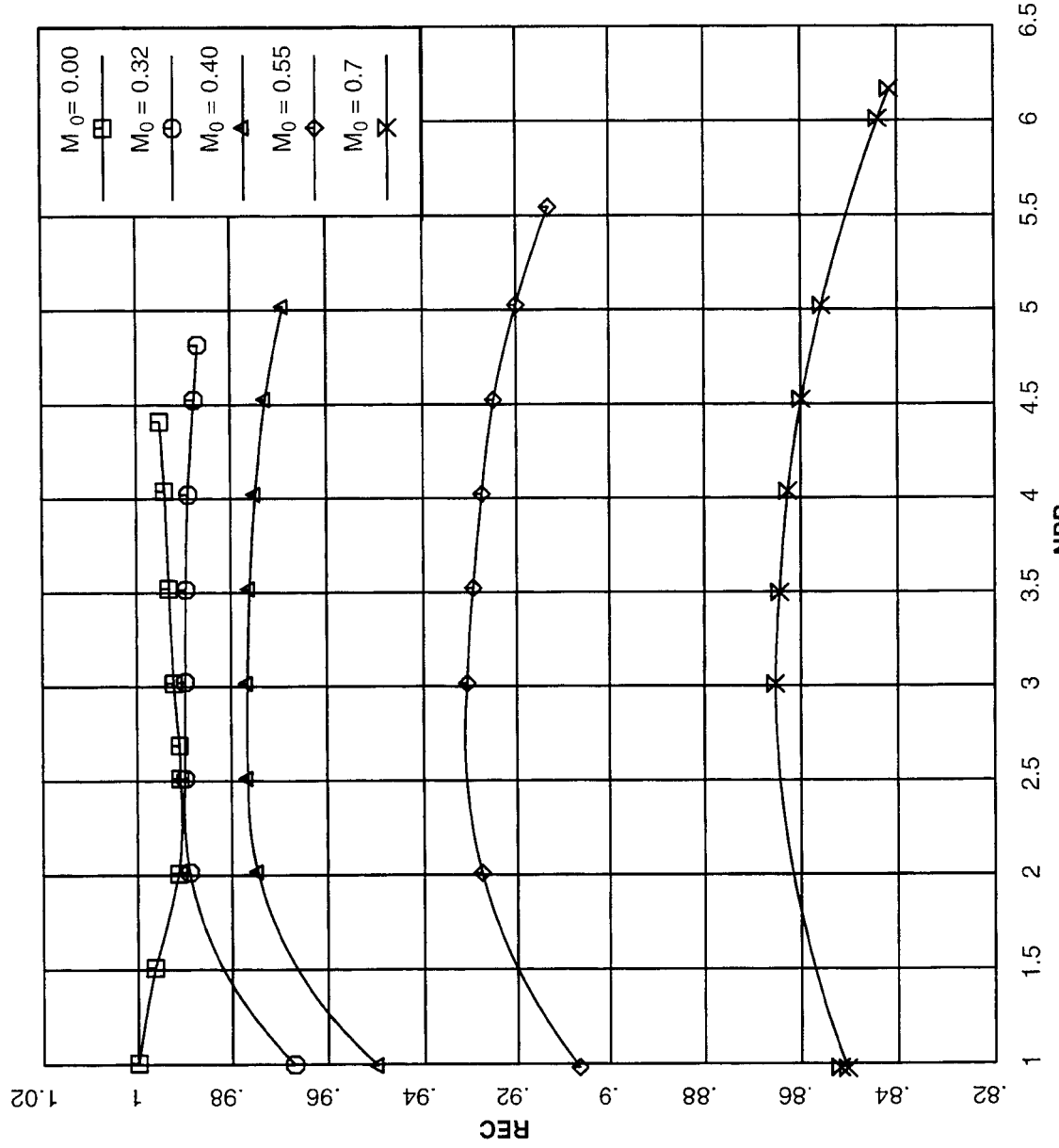

Figure 34. Estimated ejctor inlet recovery as a function of nozzle presure ratio. SAR 2.8, CER 1.22, MAR 0.95, Long flap, Aligned chute configuration at various free stream conditions.

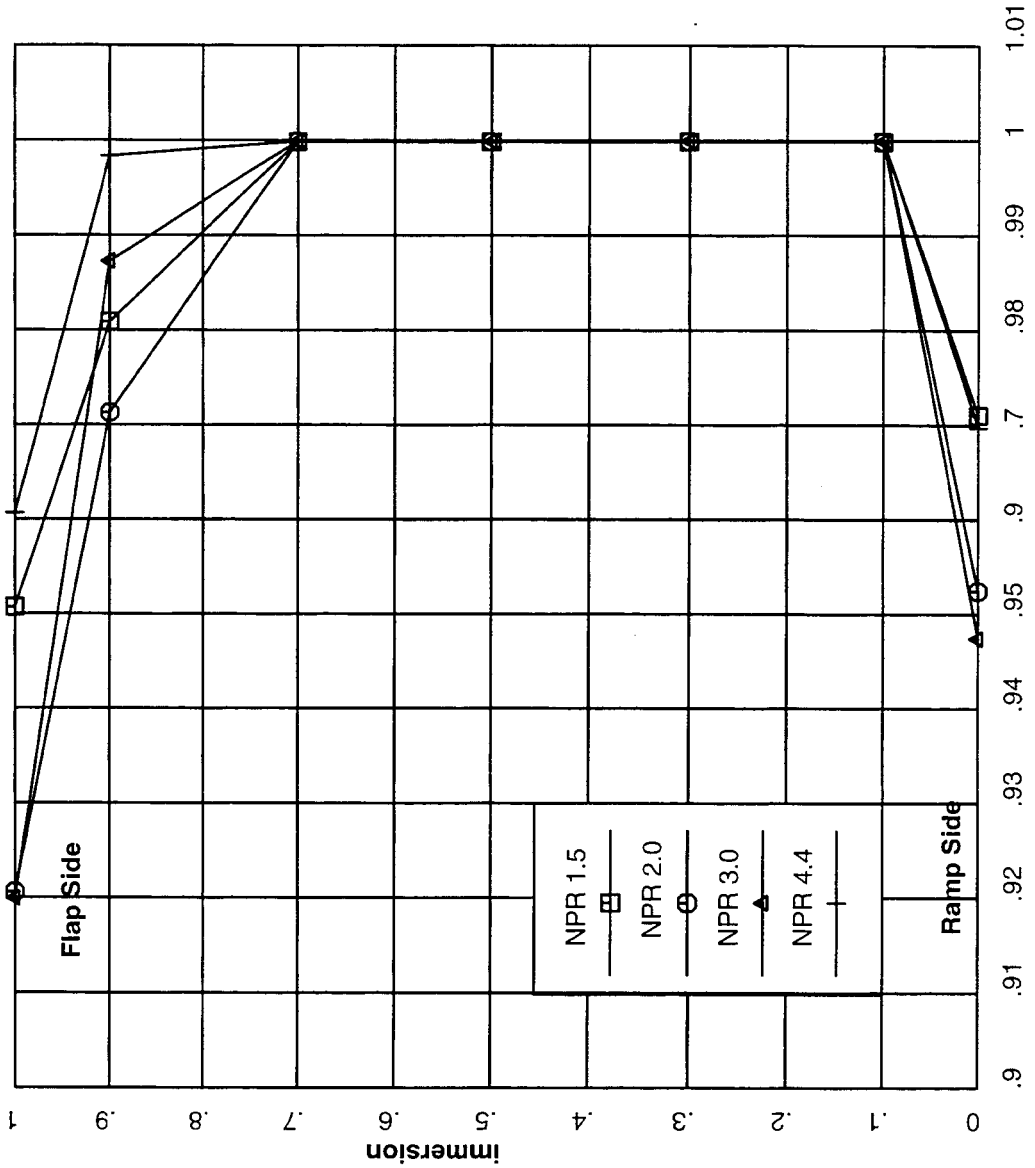

Figure 35. Inlet total pressure profile at selected nozzle pressure ratios under static conditions. SAR 2.8, CER 1.22, MAR 0.95, Aligned Chute, Long Flap Configuration.

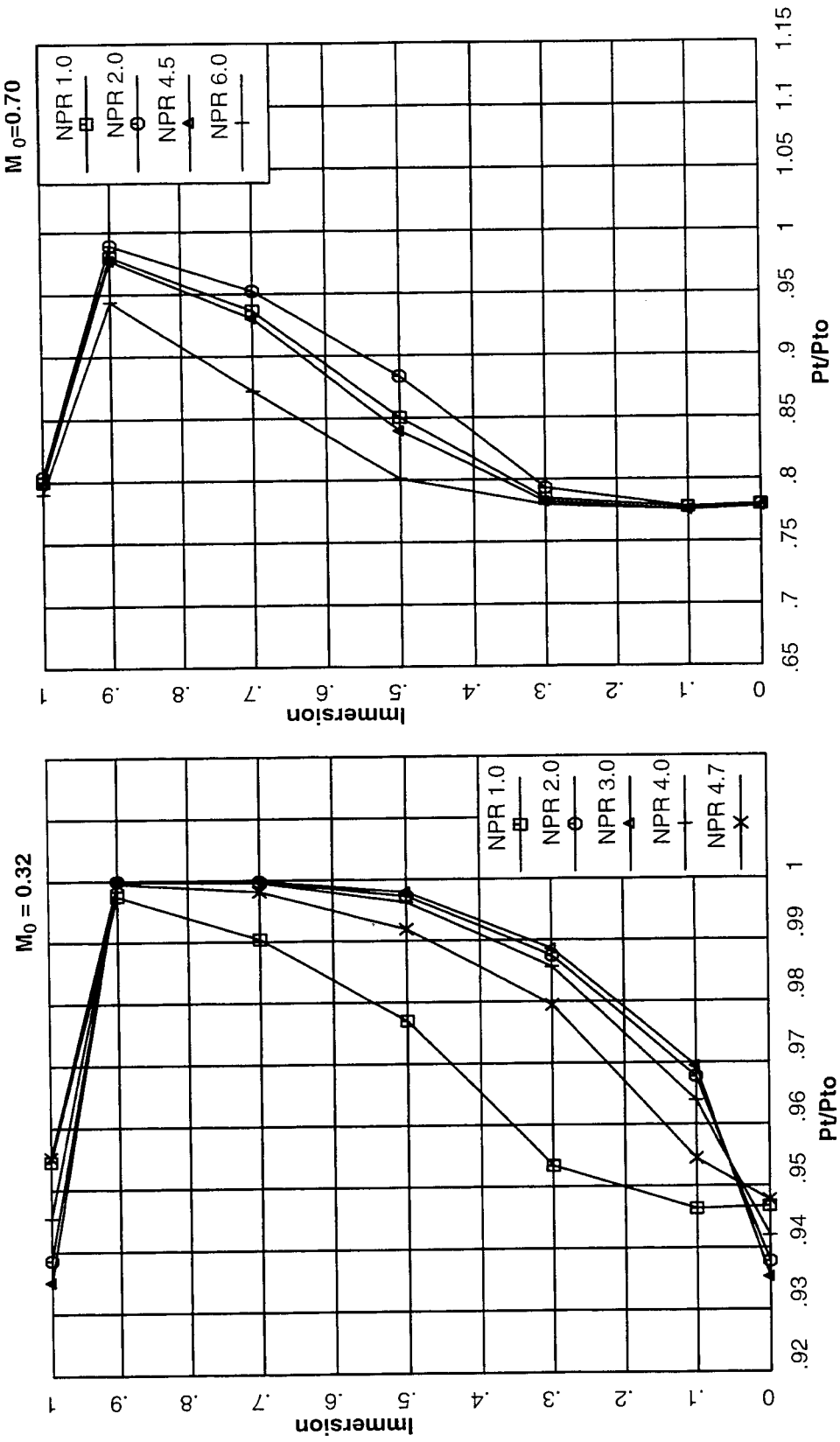

Figure 36. Inlet total pressure profile at selected nozzle pressure ratiios and free stream Mach Number SAR 2.8, CER 1.22, MAR 0.95, Aligned Chute, Long Flap Configuration.

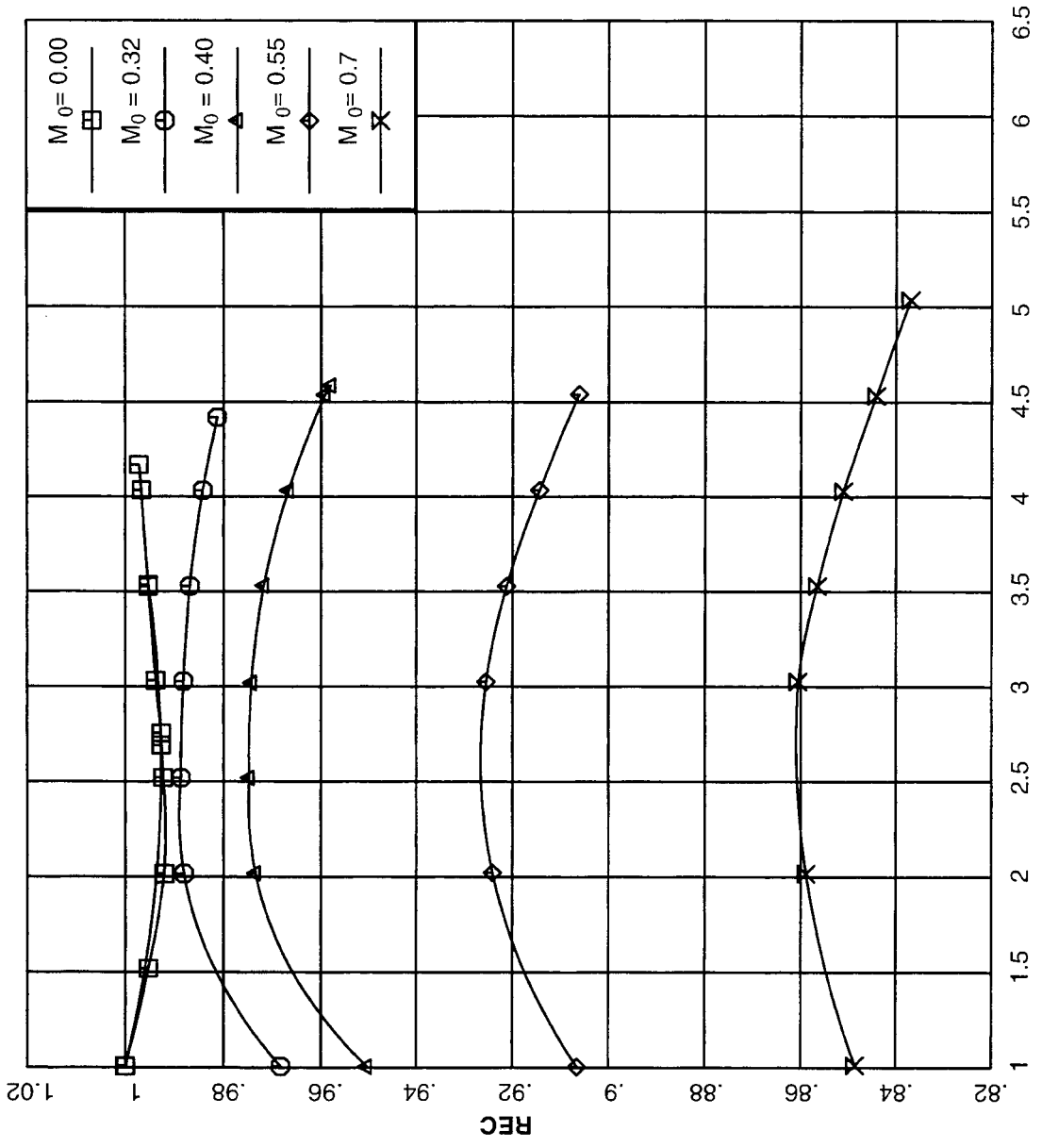

Figure 37. Estimated ejctor inlet recovery as a function of nozzle presure ratio. SAR 2.5, CER 1.00, MAR 0.95 Long flap, Aligned chute configuration at various free stream conditions.

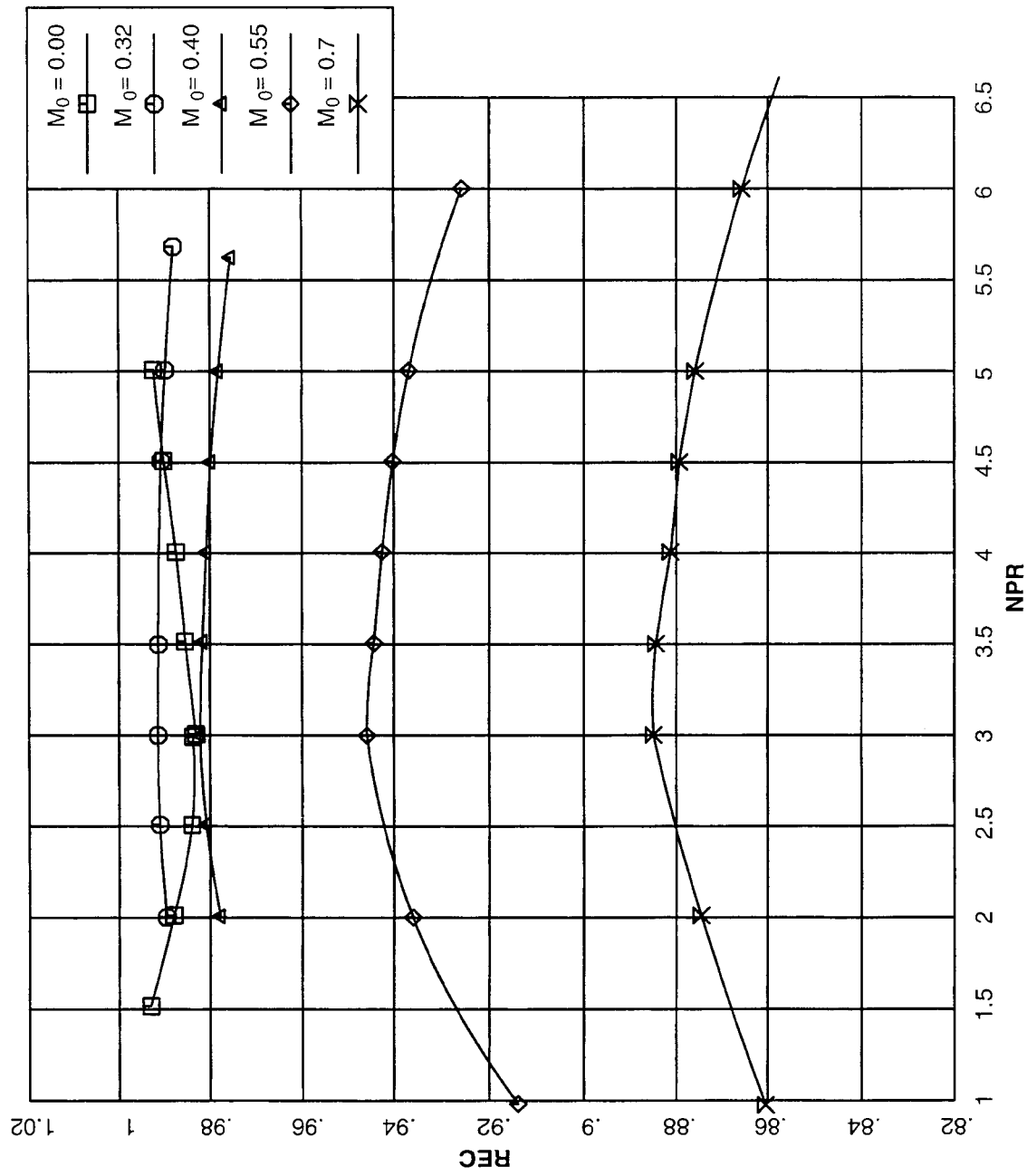

Figure 38. Estimated ejctor inlet recovery as a function of nozzle presure ratio. SAR 3.3, CER 1.22, MAR 0.95 Long flap, Aligned chute configuration at various free stream conditions.

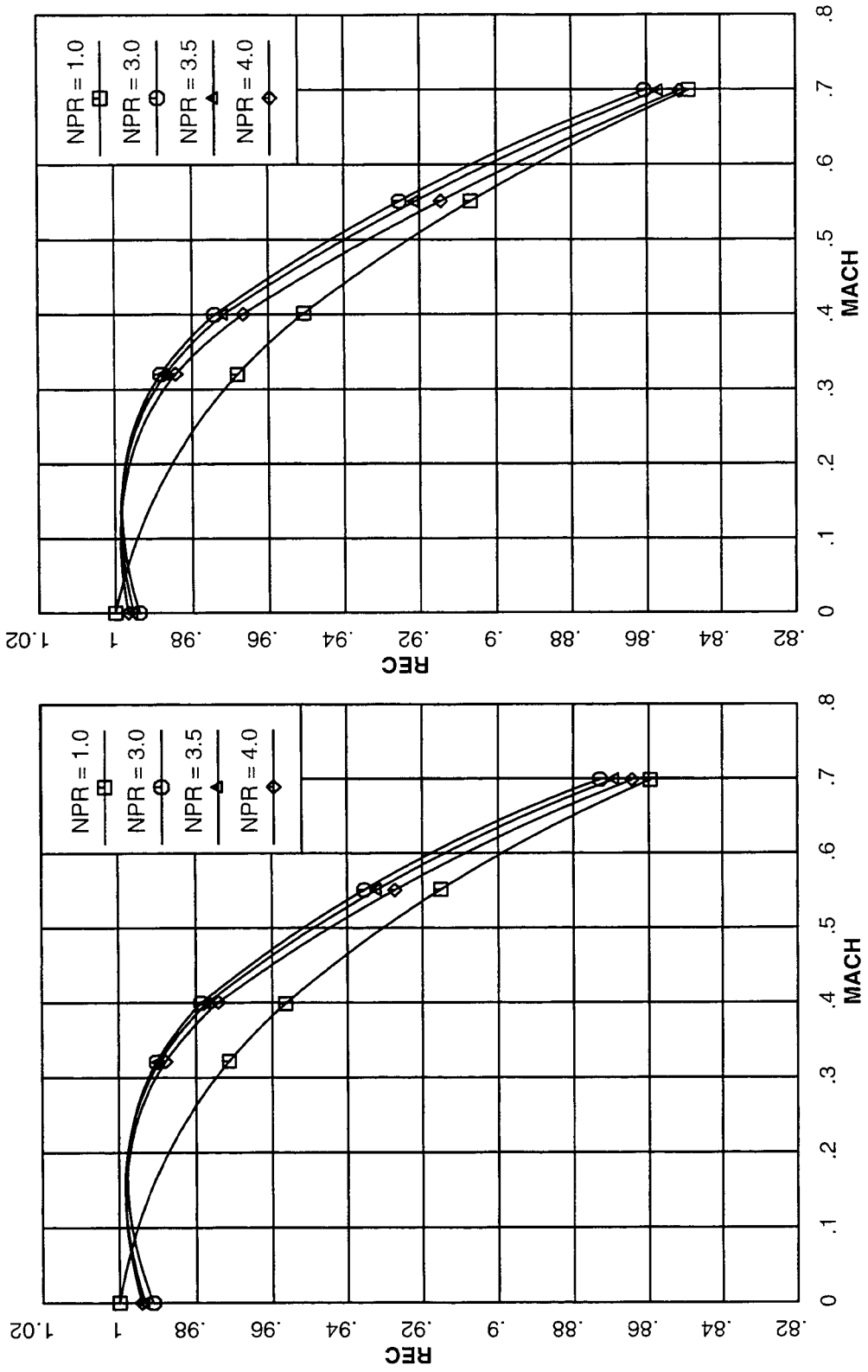

Figure 39. Effect of free stream condition on ejctor inlet recovery.
SAR 2.8, CER 1.00, MAR 0.95 Long flap, Aligned chute configuration at selected nozzle presure ratios.

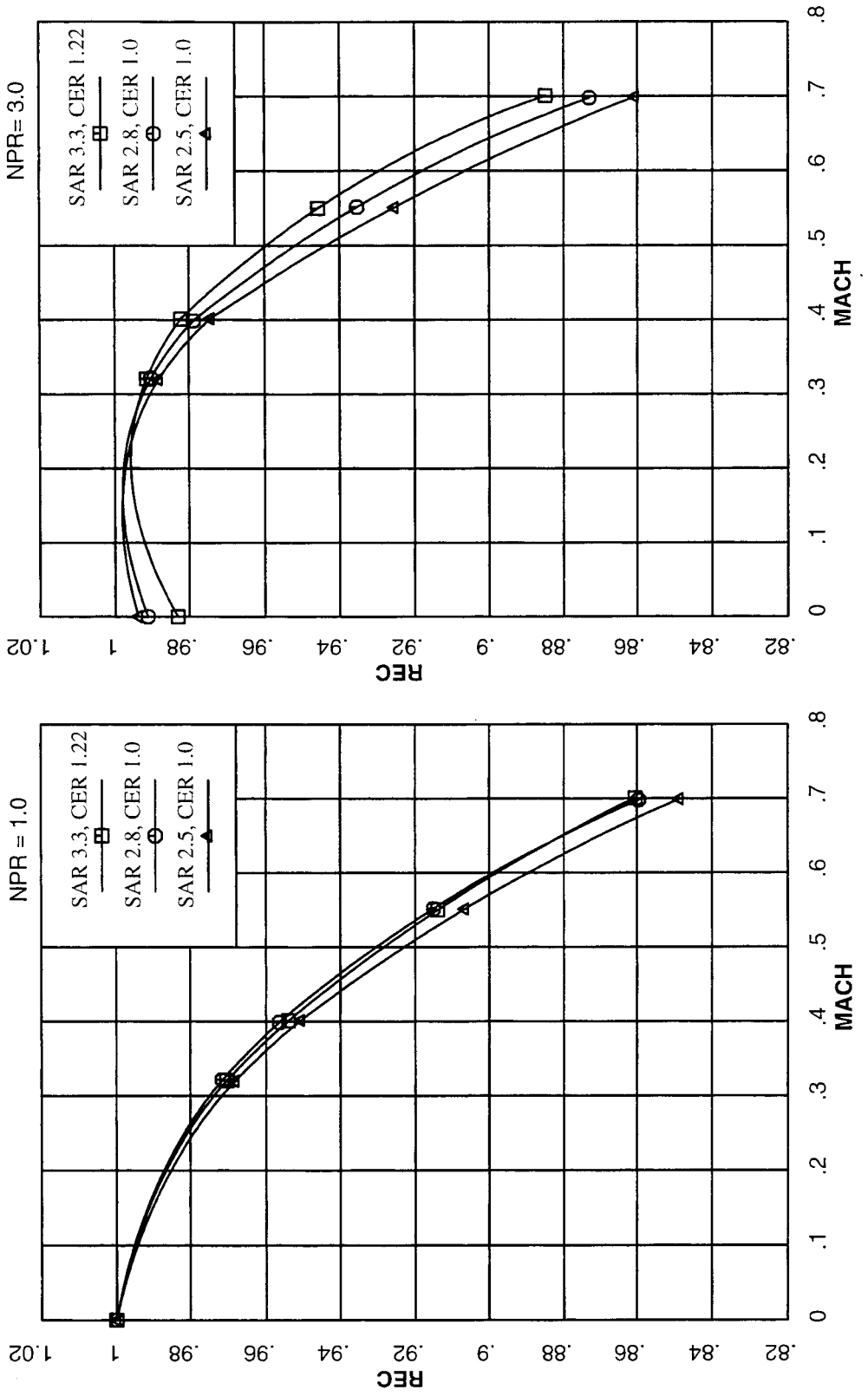

Figure 40. Effect of free stream condition on ejctor inlet recovery. MAR 0.95 Long flap, Aligned chute configuration at selected nozzle presure ratios.

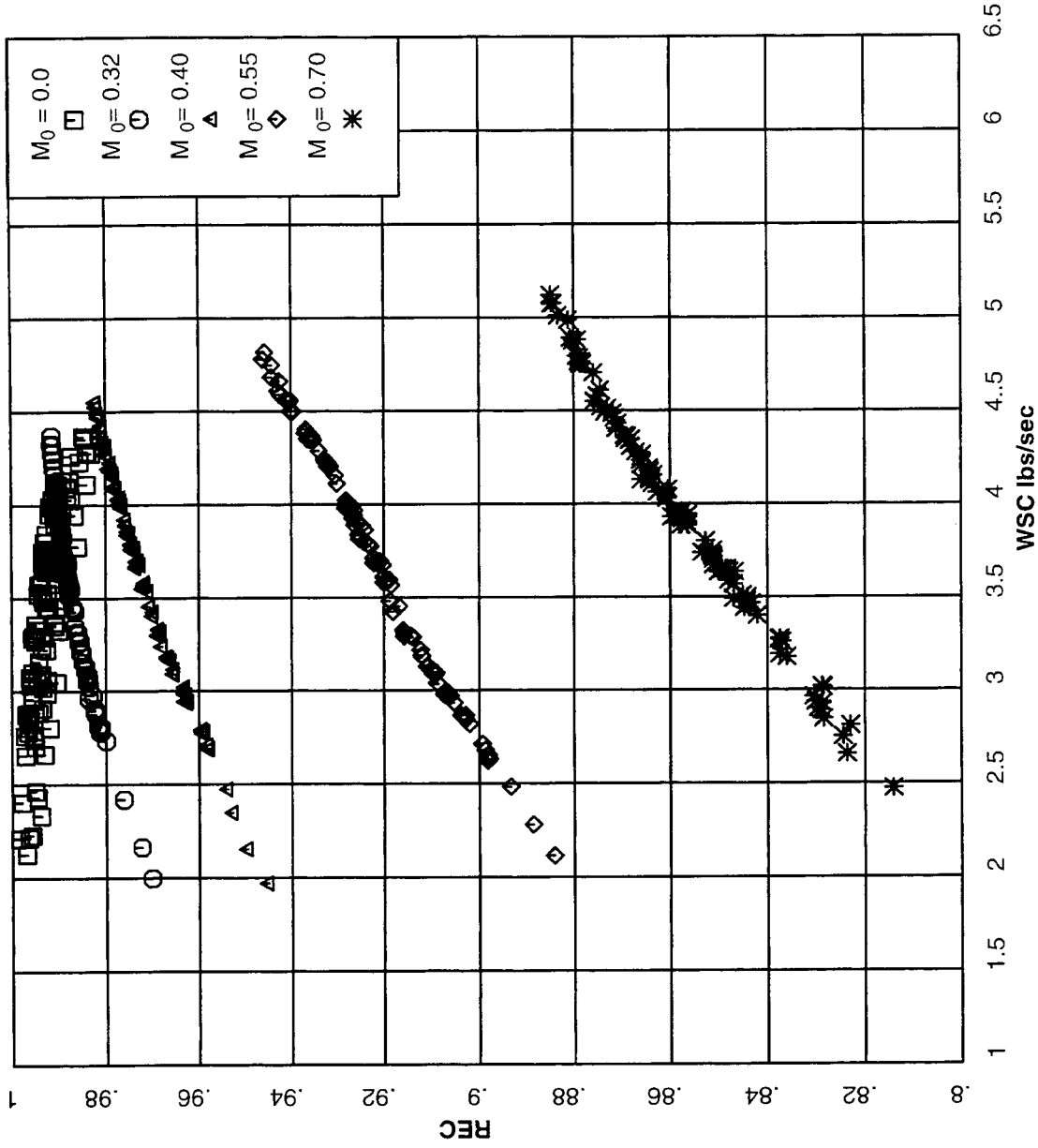

Figure 41. Effect of Free Stream Mach Number and secondary flow on inlet recovery

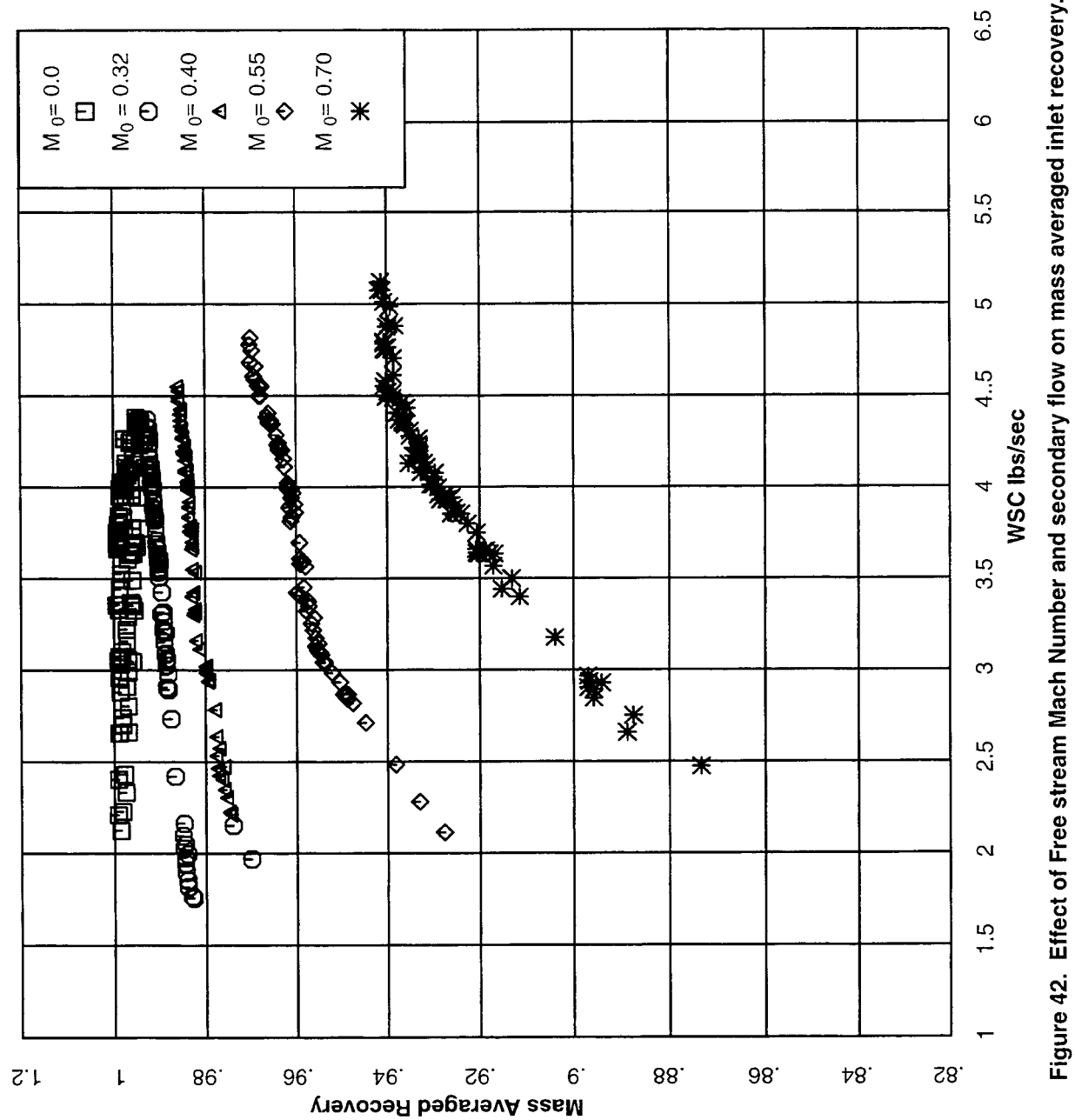

Figure 42. Effect of Free stream Mach Number and secondary flow on mass averaged inlet recovery.

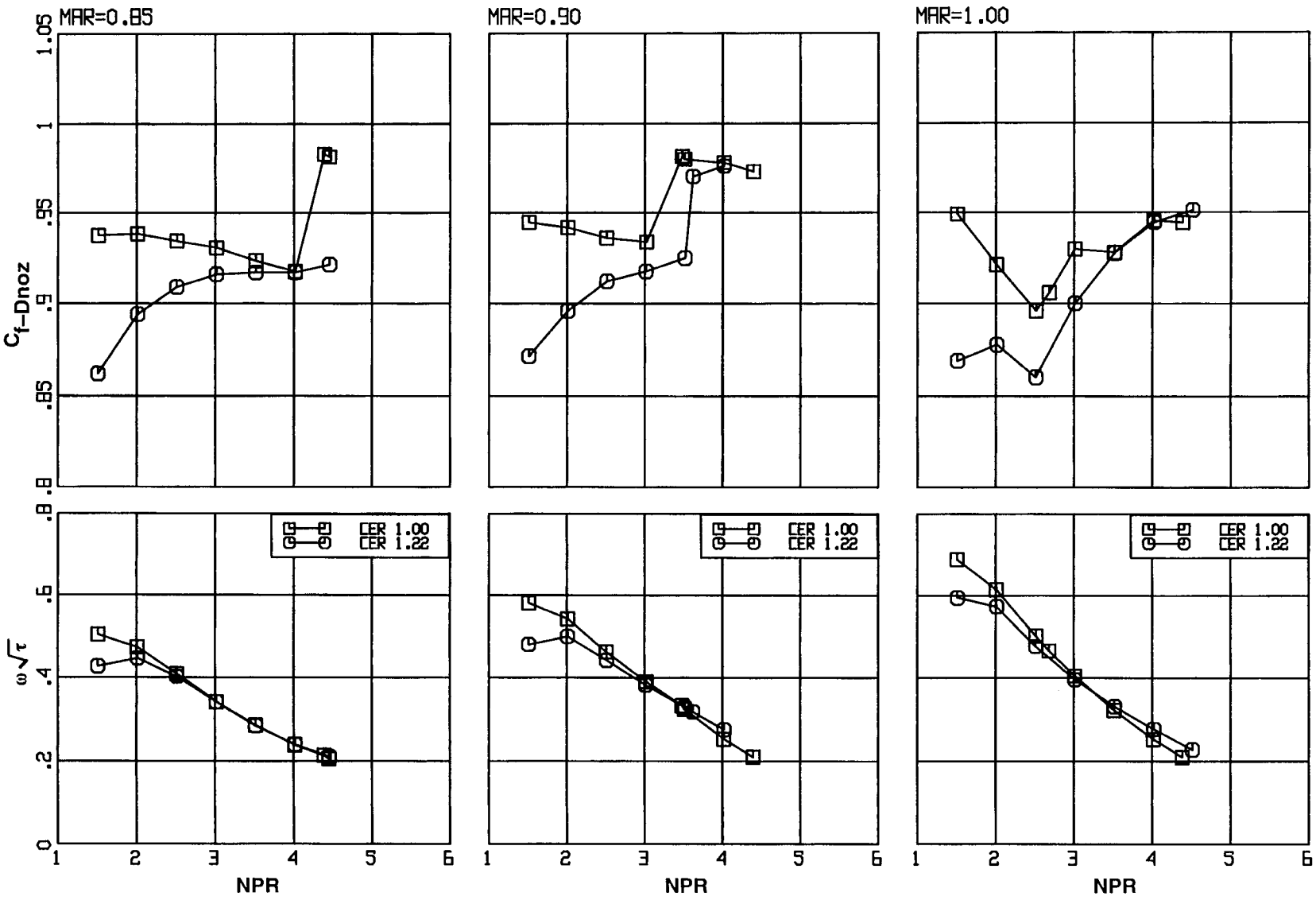

Figure 43. Effect of chute expansion ratio on ejector nozzle performance. SAR 2.8, Aligned chutes, Long Flap configuration at M_0=0.0

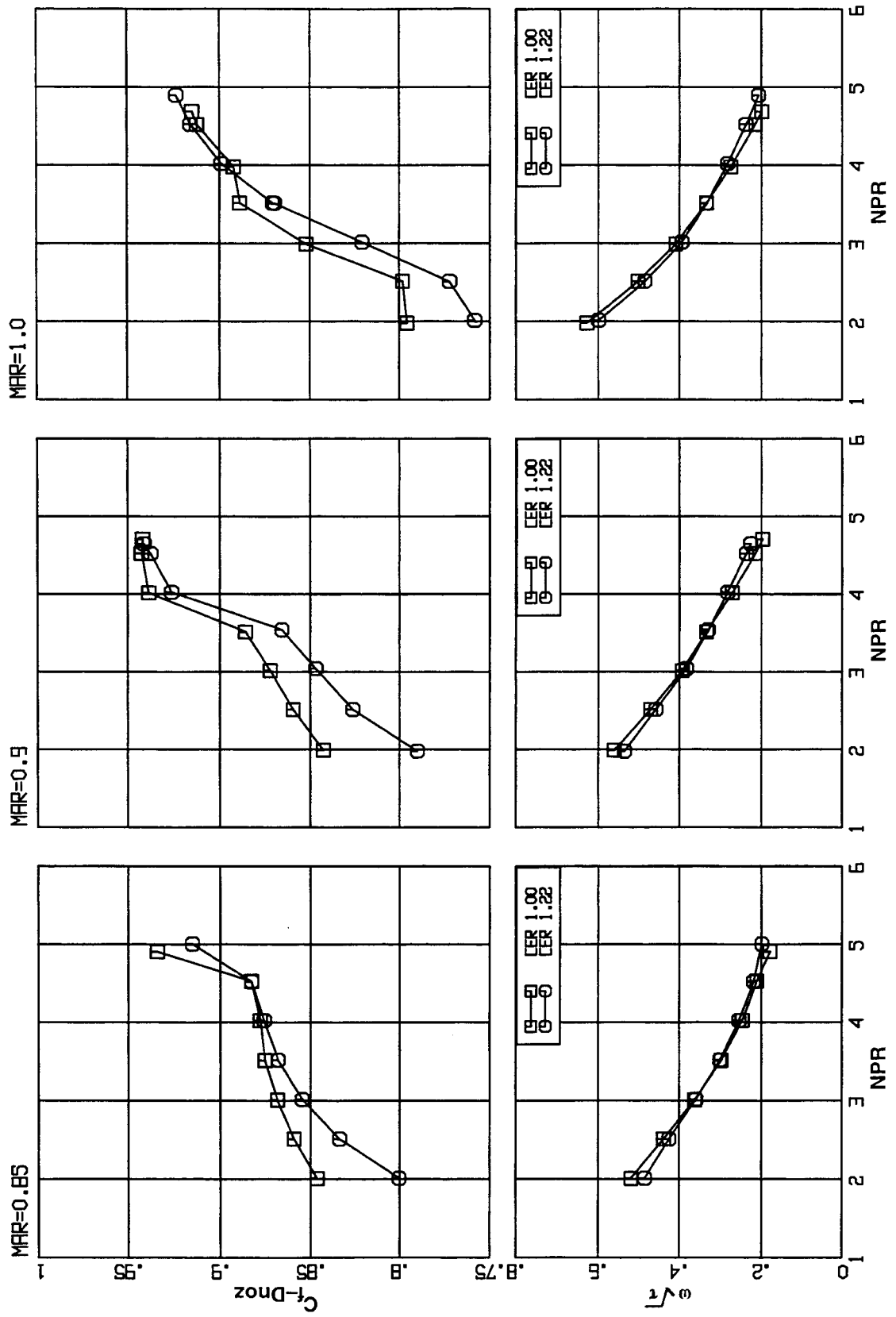

Figure 44. Effect of chute expansion ratio on ejector nozzle performance. SAR 2.8, Aligned chutes, Long Flap configuration at M_0=0.32

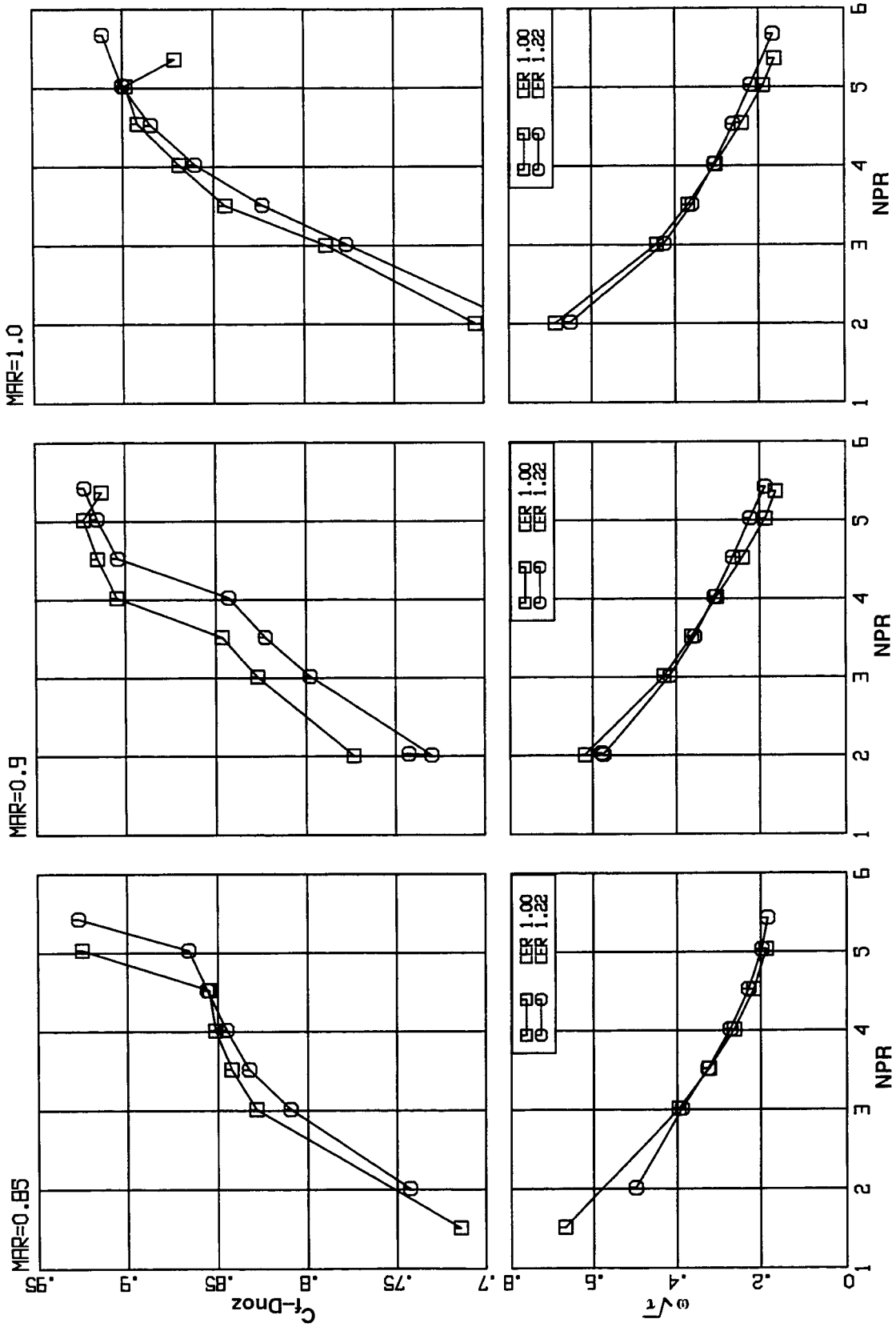

Figure 45. Effect of chute expansion ratio on ejector nozzle performance. SAR 2.8, Aligned chutes, Long Flap configuration at M_0=0.55

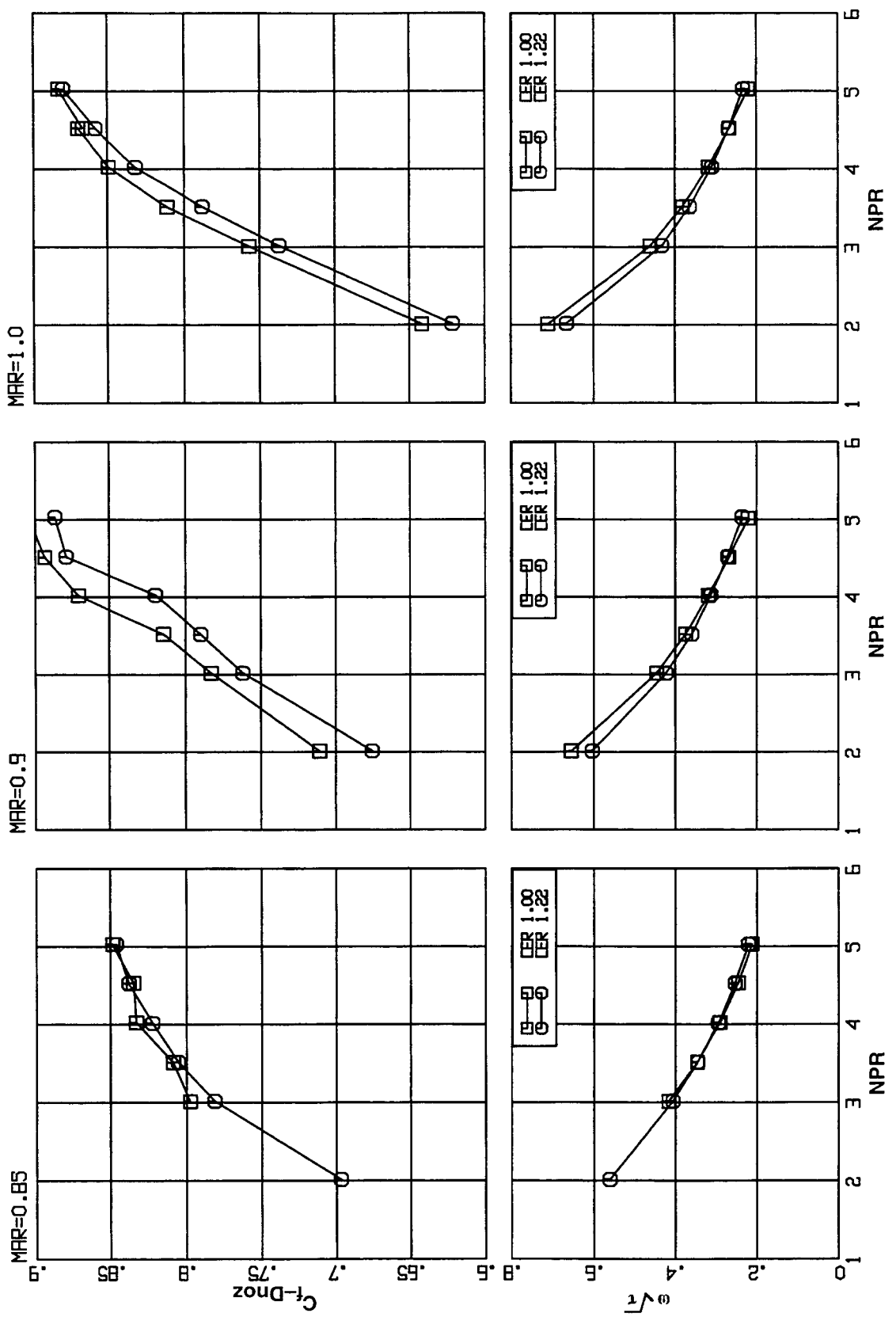

Figure 46. Effect of chute expansion ratio on ejector nozzle performance. SAR 2.8, Aligned chutes, Long Flap configuration at M_0=0.70

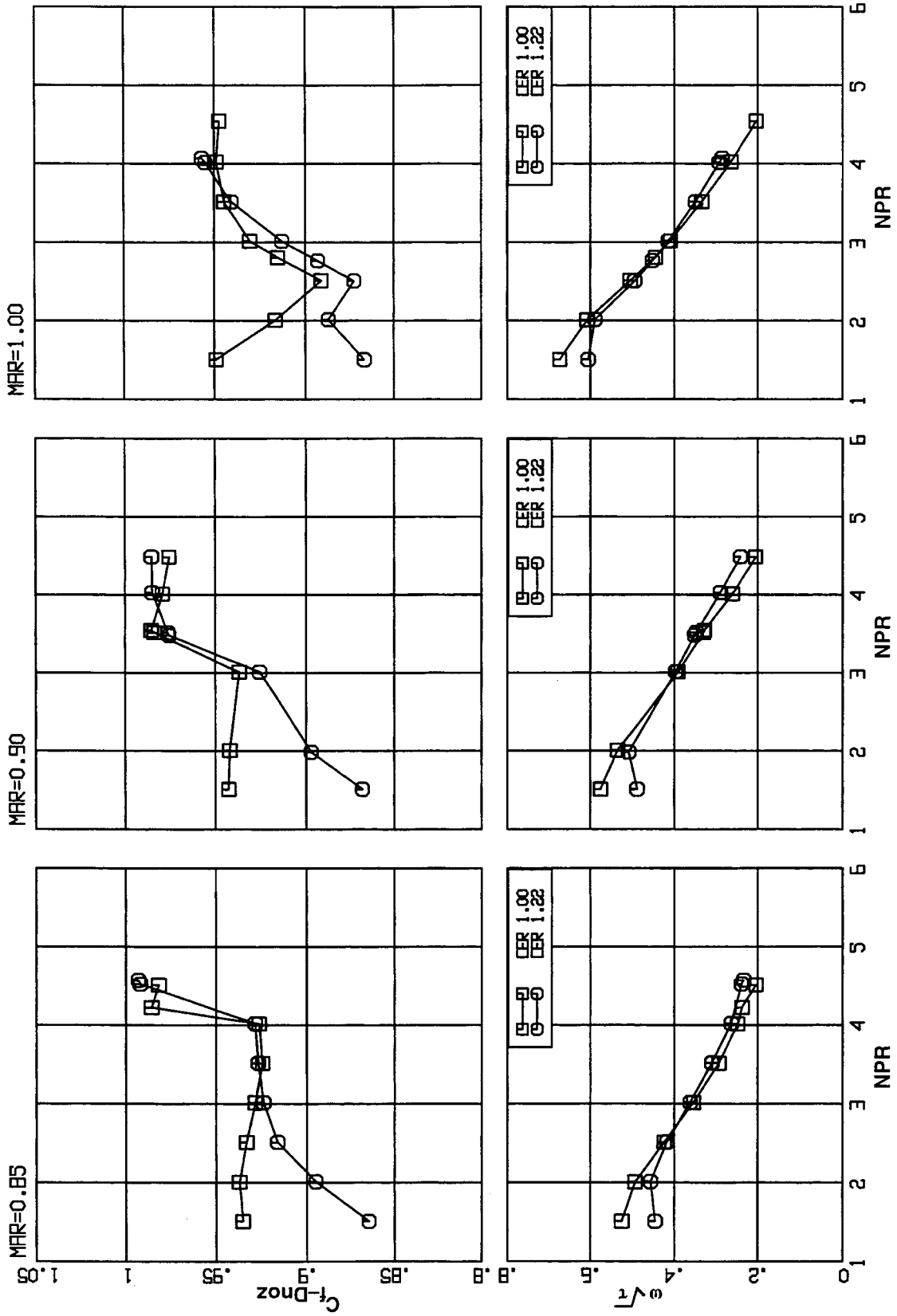

Figure 47. Effect of chute expansion ratio on ejector nozzle performance. SAR 2.8, Staggered chutes, Long Flap configuration at M_0=0.00

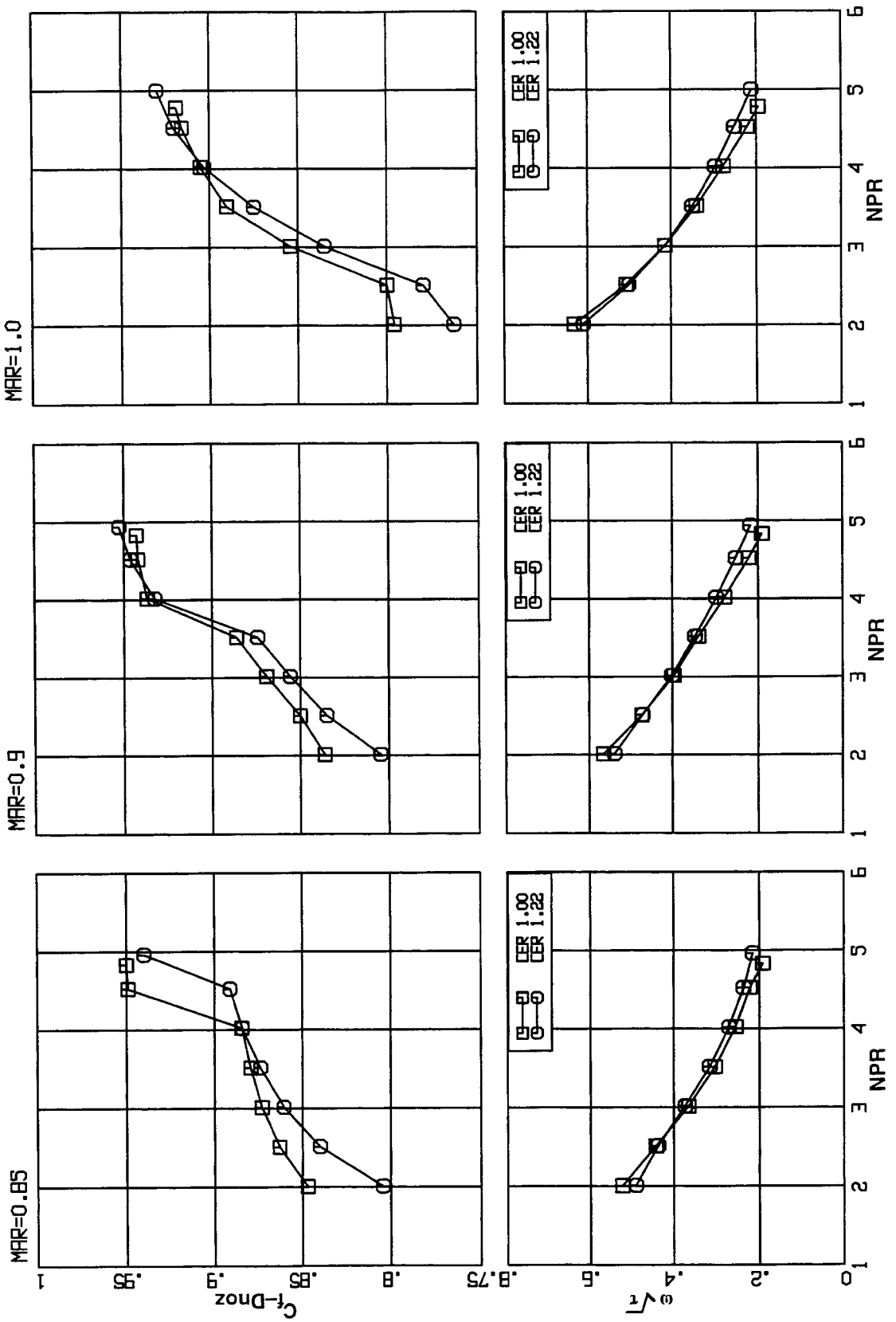

Figure 48. Effect of chute expansion ratio on ejector nozzle performance. SAR 2.8, Staggered chutes, Long Flap configuration at M_0=0.32

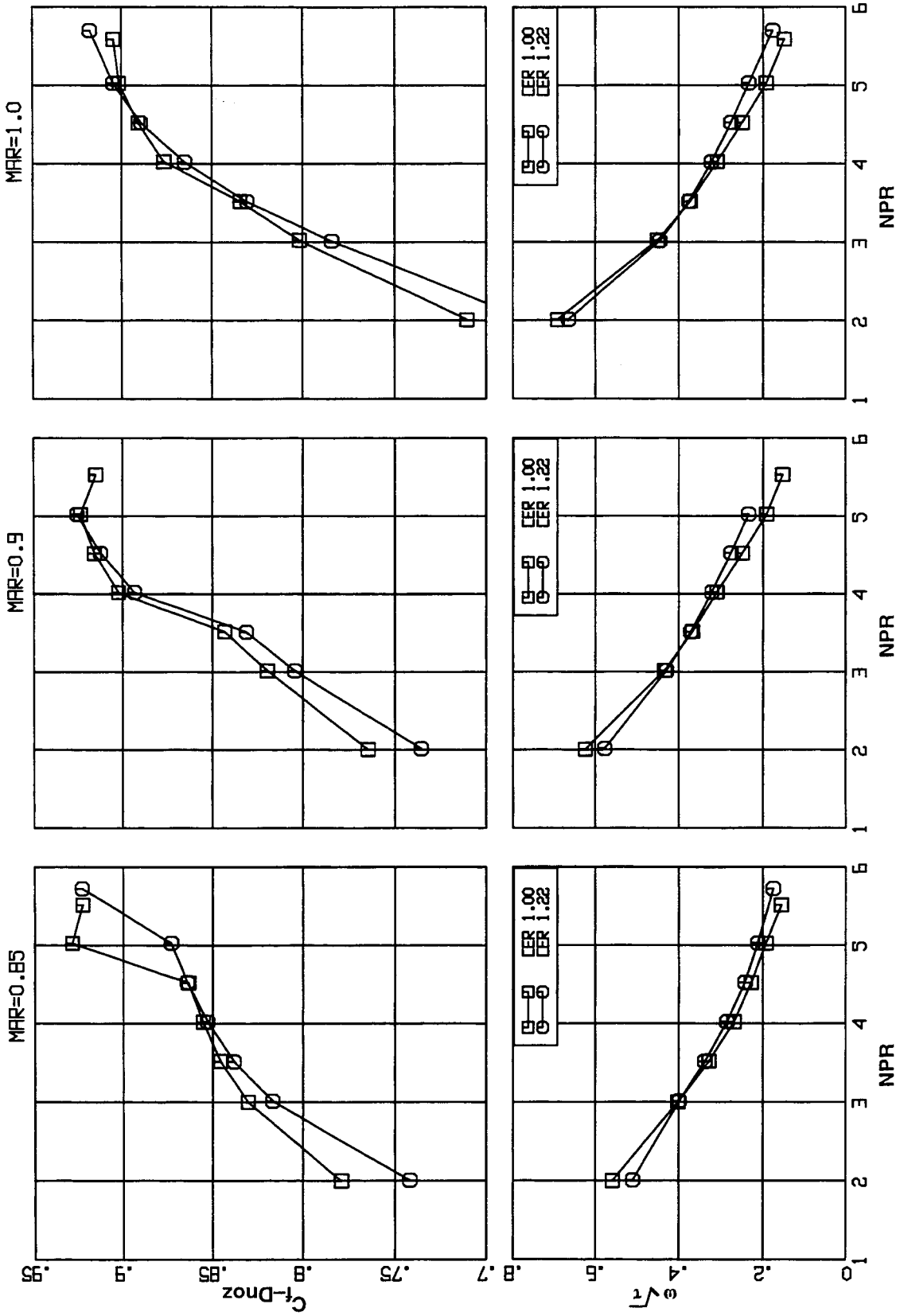

Figure 49. Effect of chute expansion ratio on ejector nozzle performance. SAR 2.8, Staggered chutes, Long Flap configuration at M_0=0.55

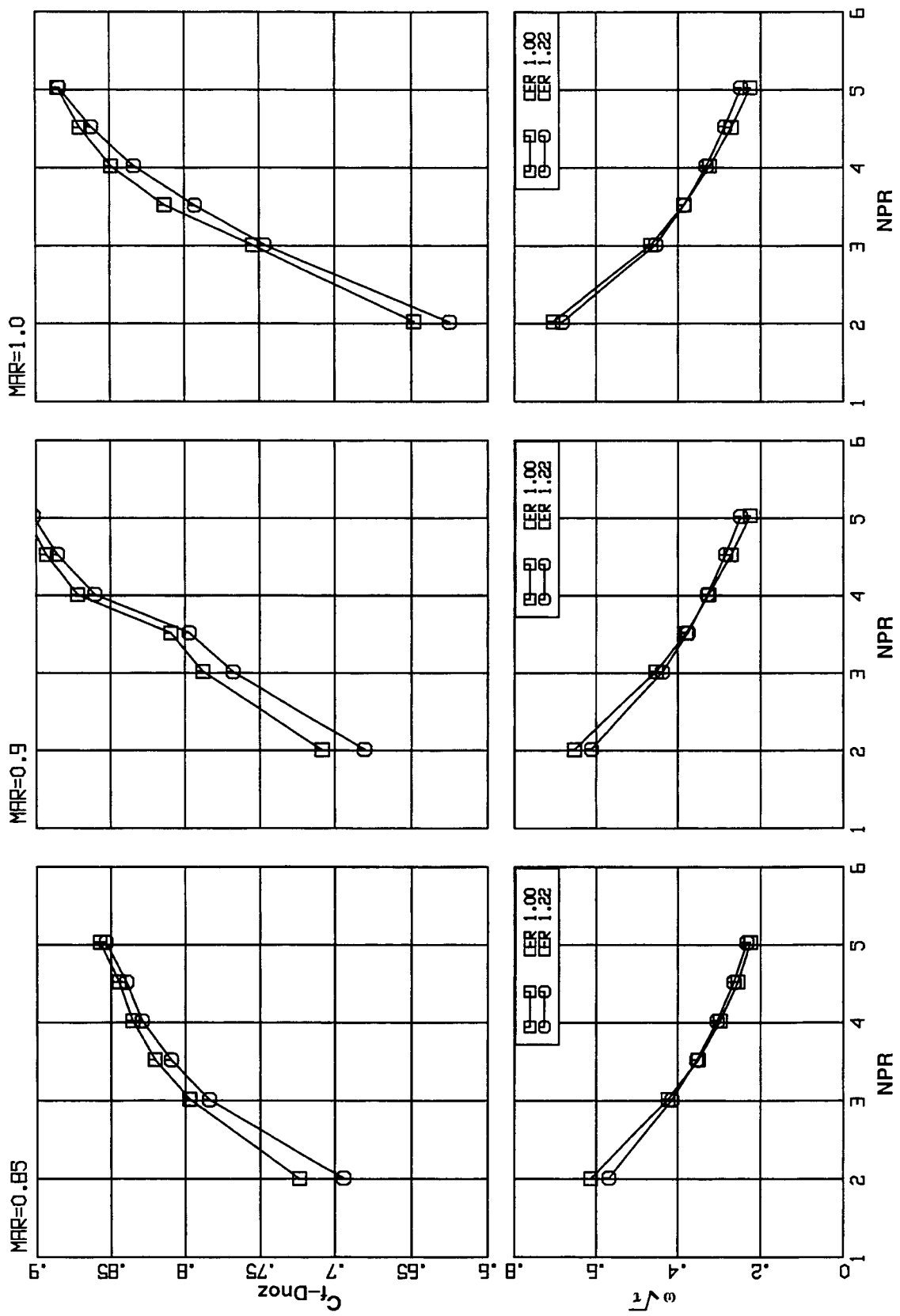

Figure 50. Effect of chute expansion ratio on ejector nozzle performance.
SAR 2.8, Staggered chutes, Long Flap configuration at M_0=0.70

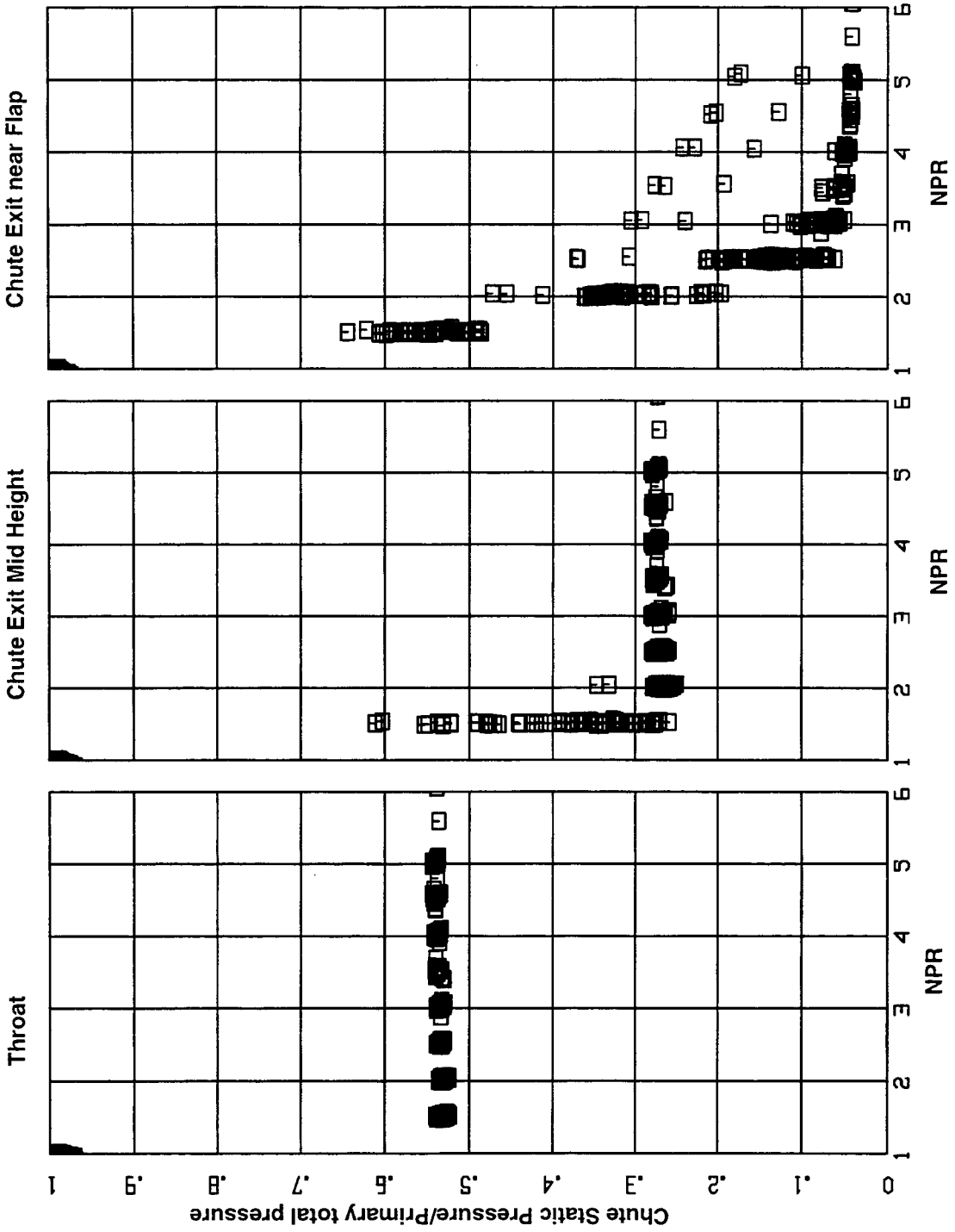

Figure 51. Chute static pressures at various Nozzle pressure ratios, all MARs and Mach numbers. SAR 3.3, CER 1.22, Aligned Chute, Long Flap configuration.

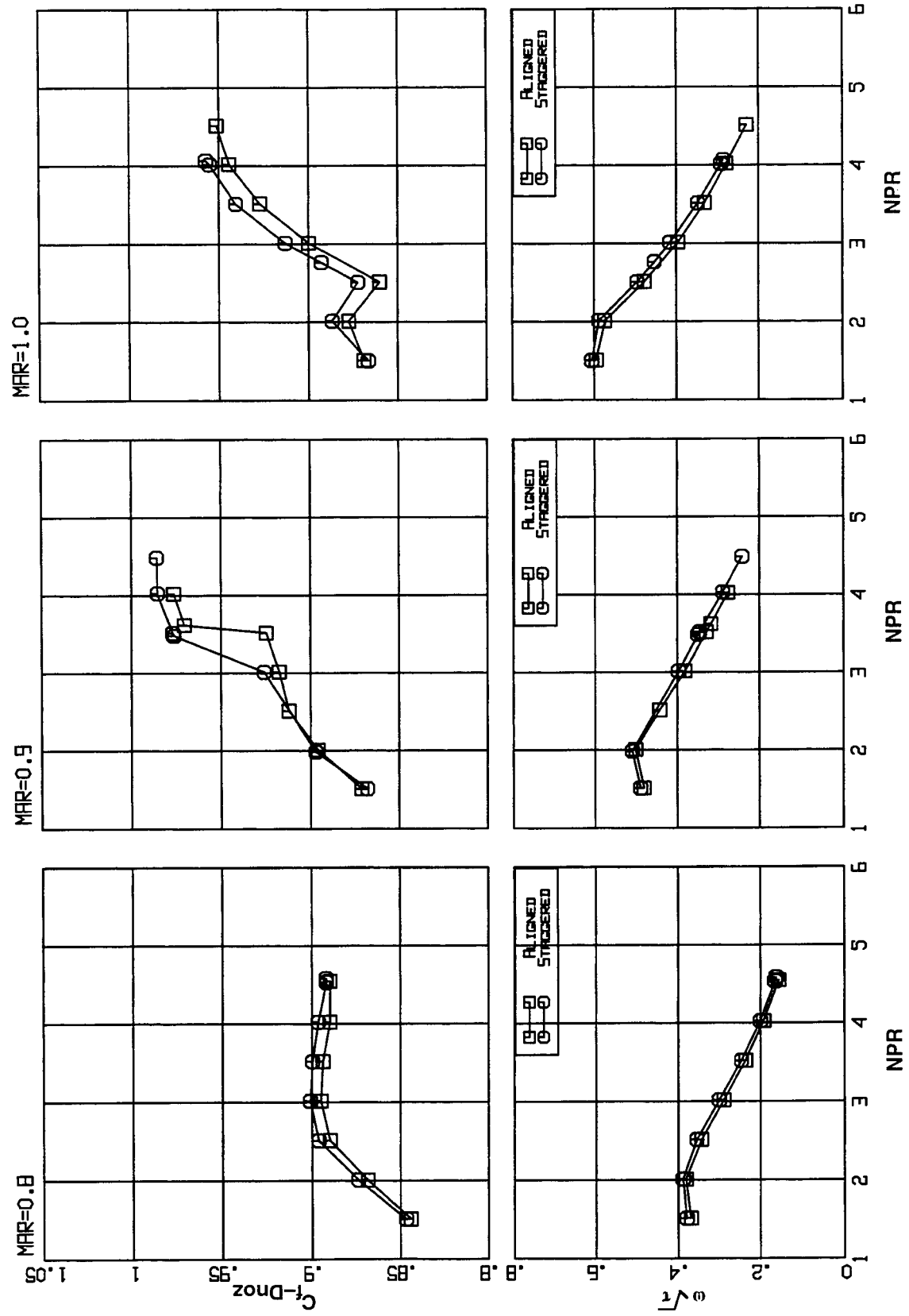

Figure 52. Effect of chute alignment on ejector nozzle performance. SAR 2.8, CER 1.22, Long Flap configuration at M_0=0.00

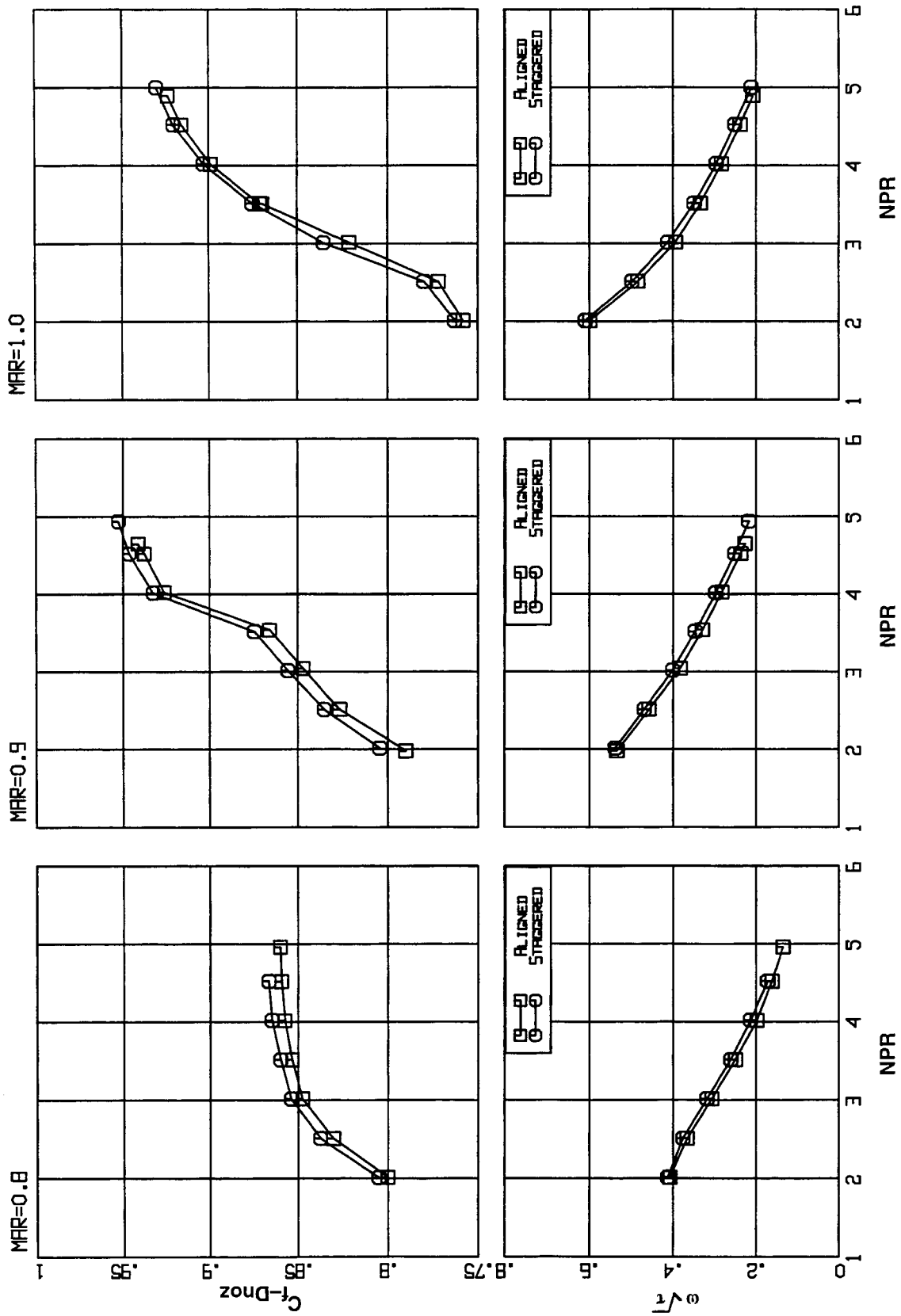

Figure 53. Effect of chute alignment on ejector nozzle performance. SAR 2.8, CER 1.22, Long Flap configuration at M_0=0.32

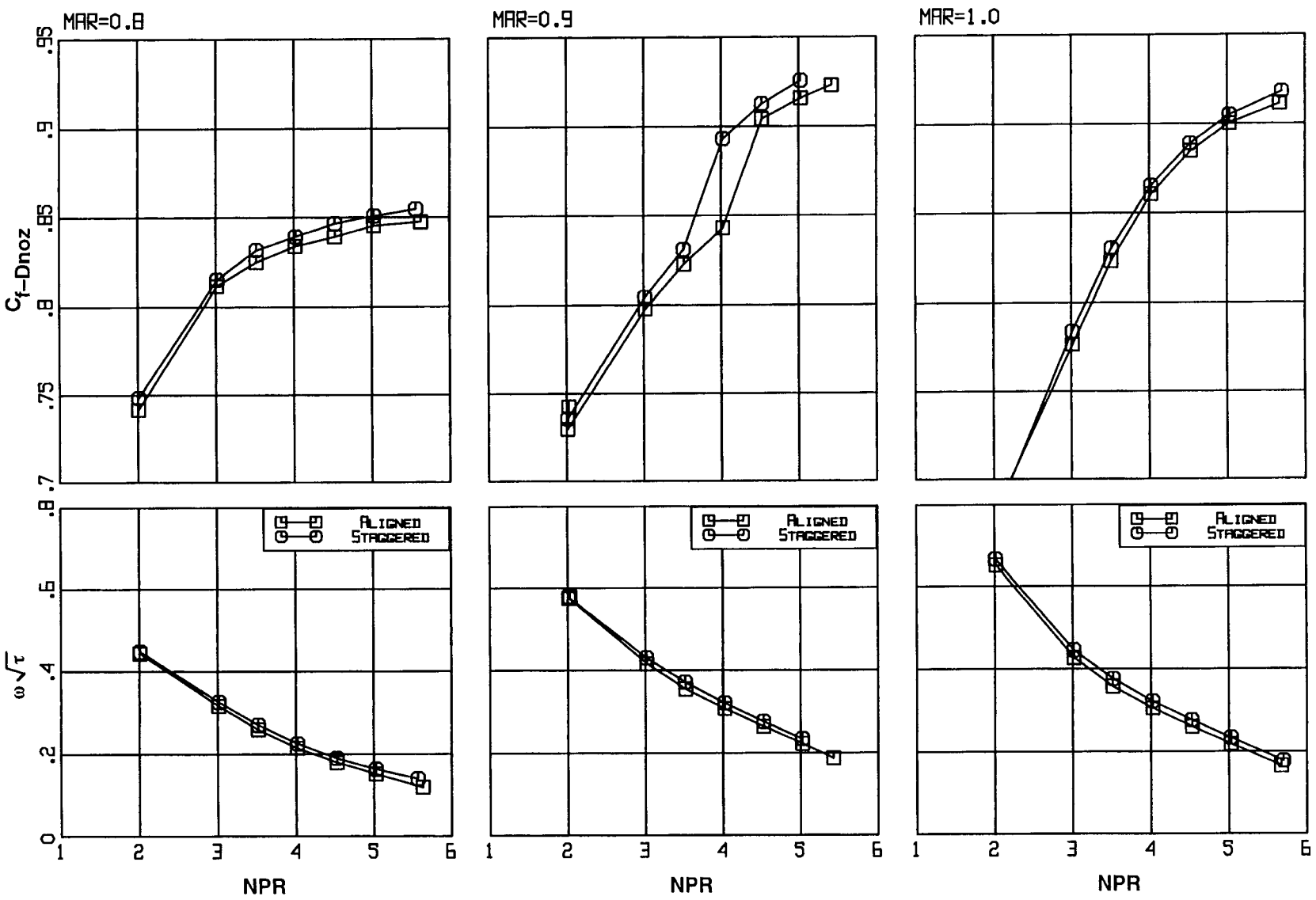

Figure 54. Effect of chute alignment on ejector nozzle performance. SAR 2.8, CER 1.22, Long Flap configuration at M_0=0.55

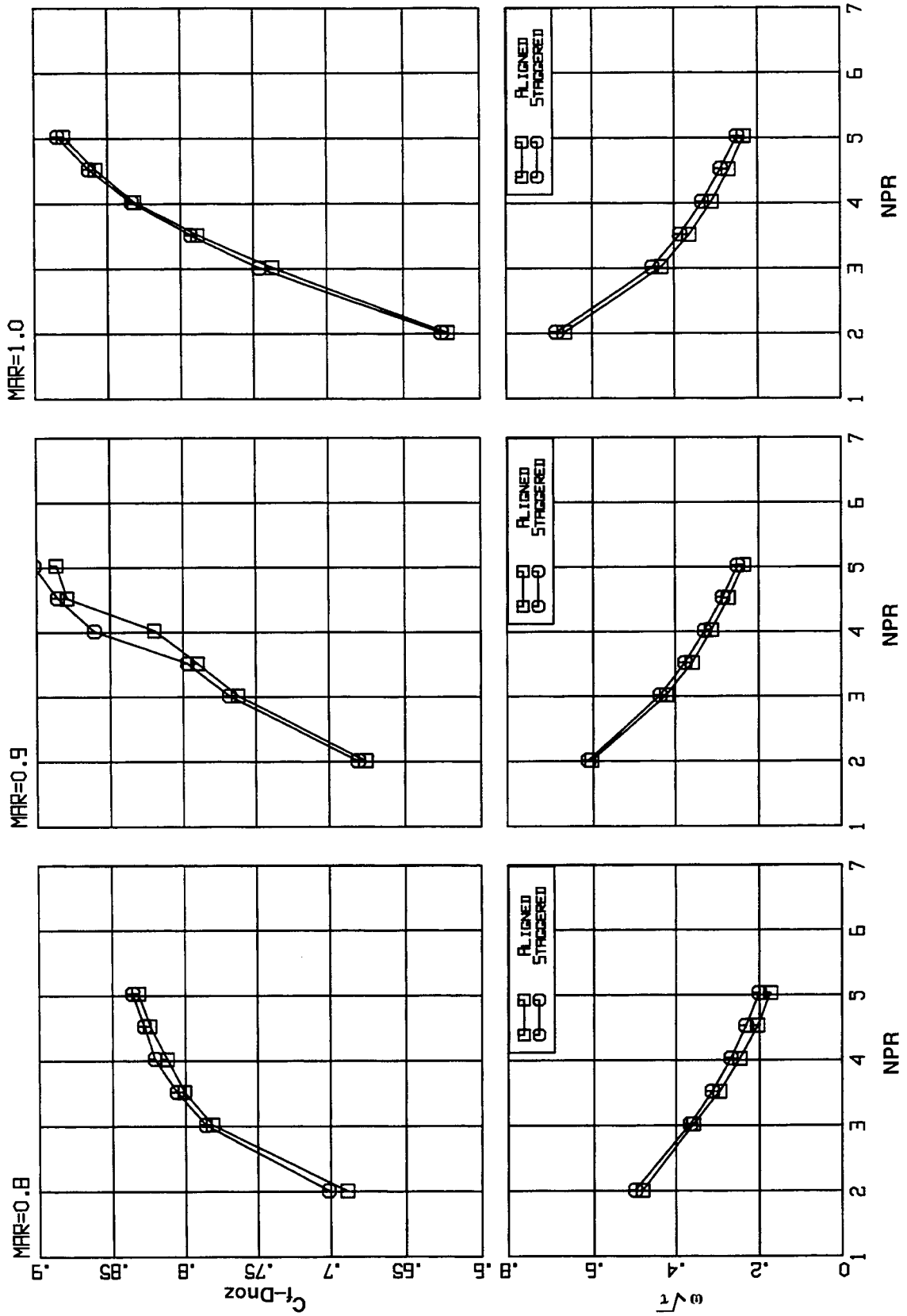

Figure 55. Effect of chute alignment on ejector nozzle performance. SAR 2.8, CER 1.22, Long Flap configuration at M_0=0.70

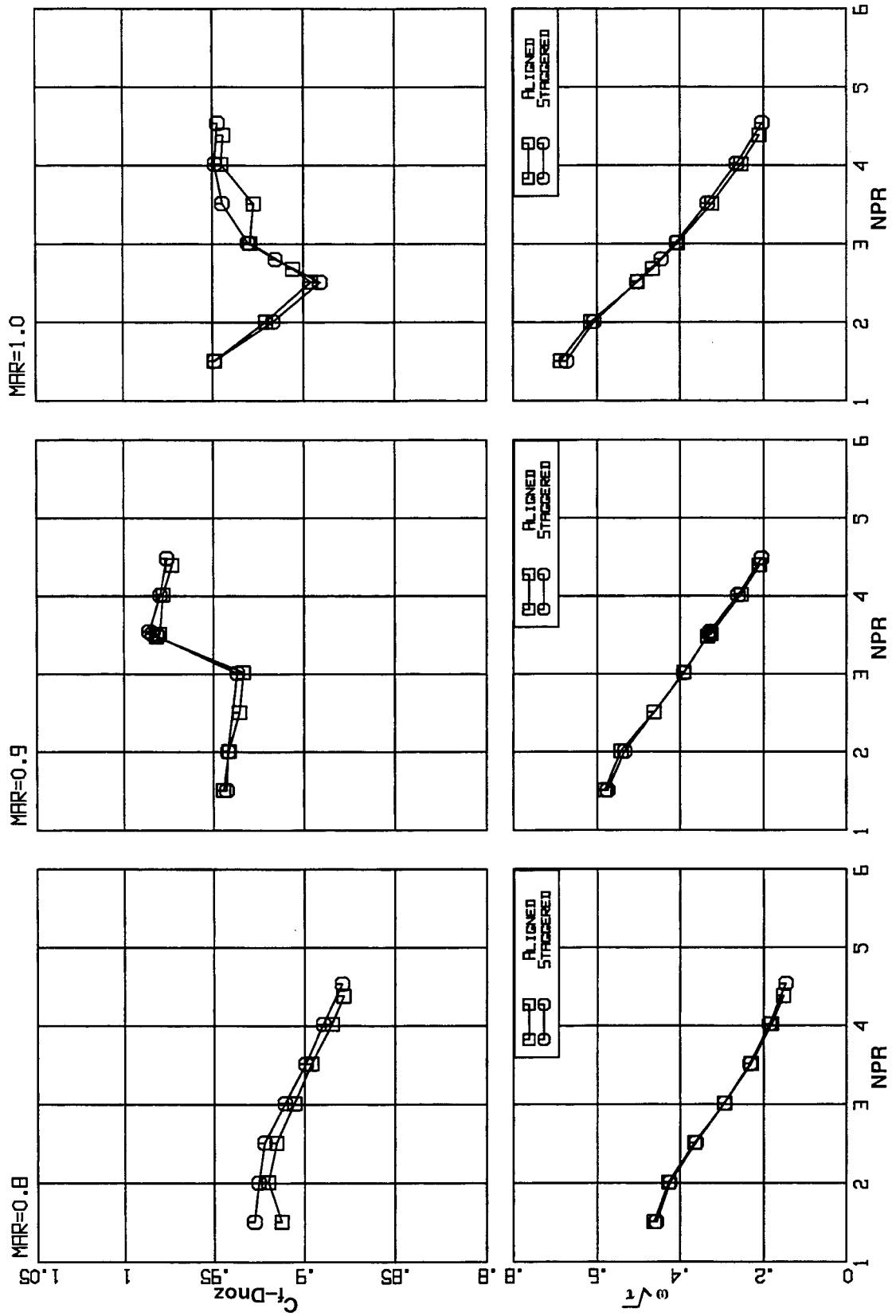

Figure 56. Effect of chute alignment on ejector nozzle performance.
SAR 2.8, CER 1.00, Long Flap configuration at M_0=0.00

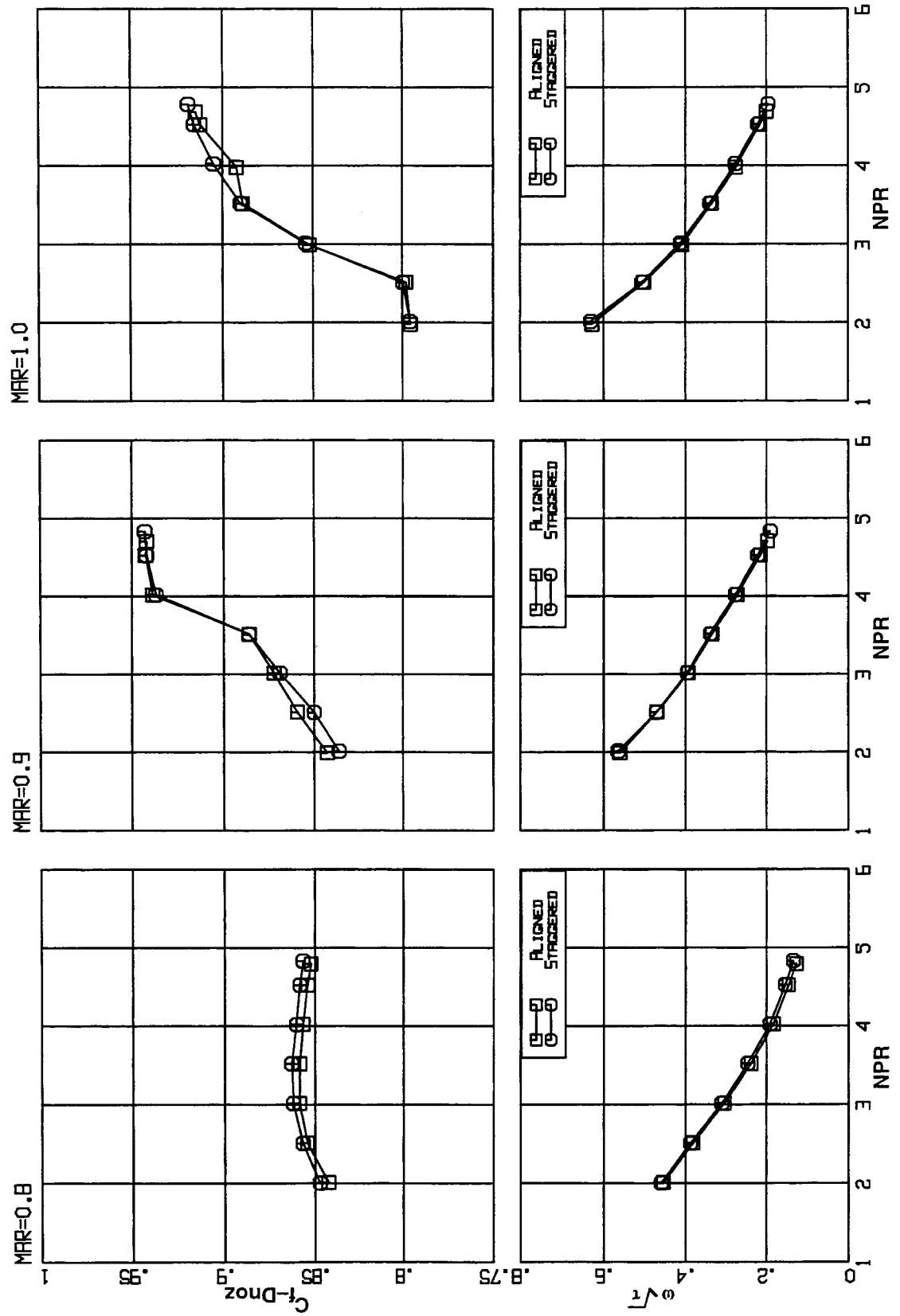

Figure 57. Effect of chute alignment on ejector nozzle performance. SAR 2.8, CER 1.00, Long Flap configuration at M_0=0.32

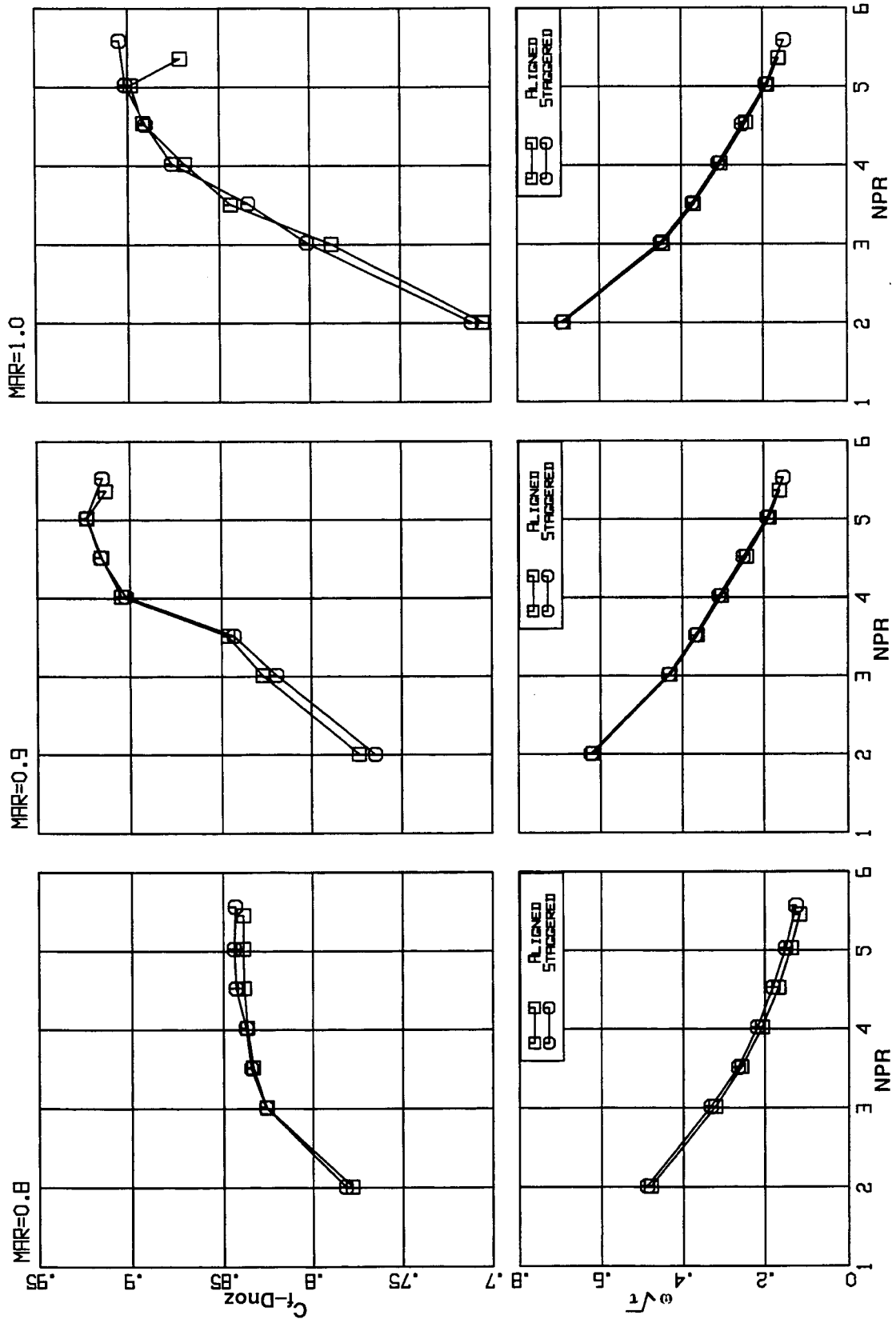

Figure 58. Effect of chute alignment on ejector nozzle performance. SAR 2.8, CER 1.00, Long Flap configuration at M_0=0.55

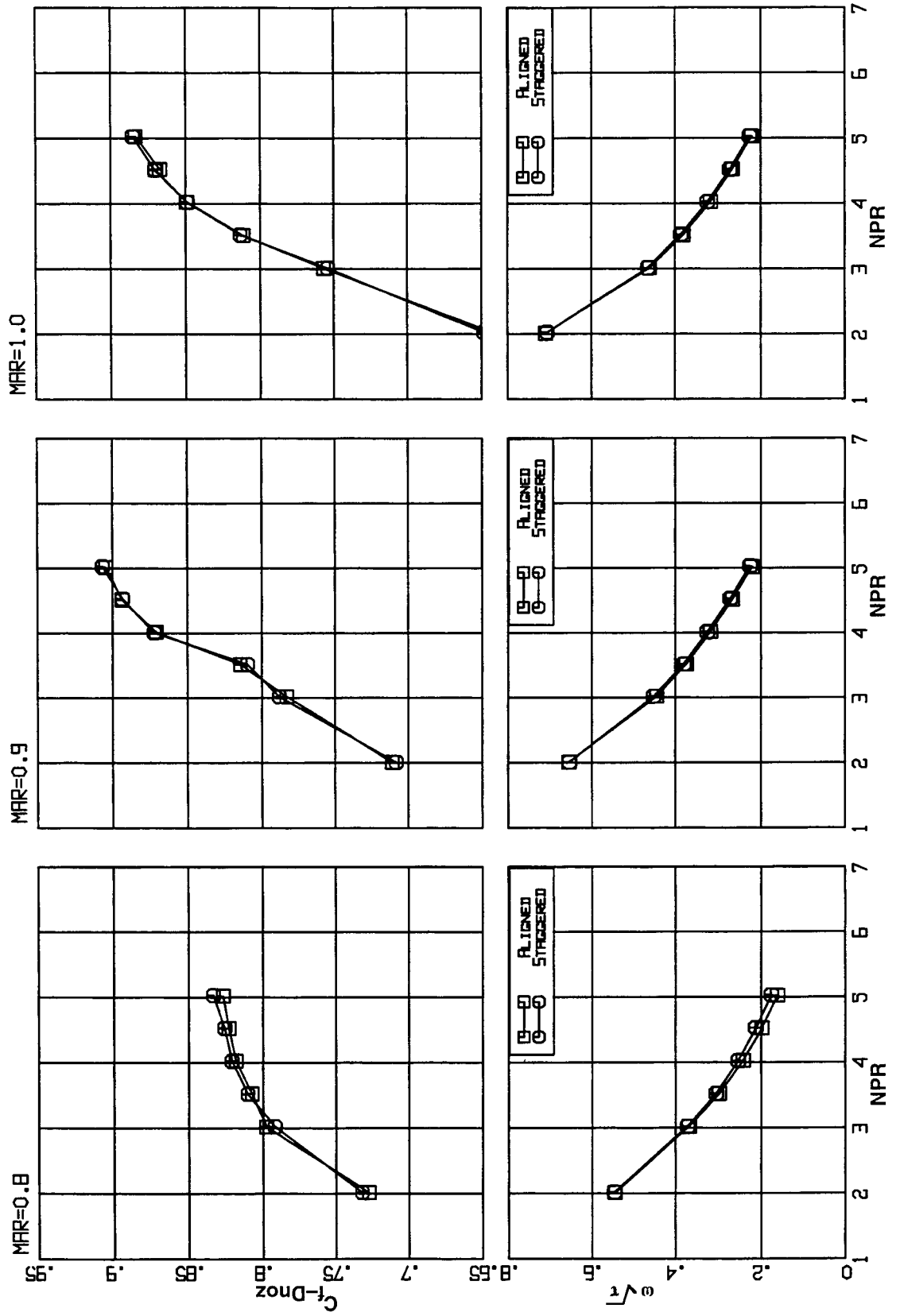

Figure 59. Effect of chute alignment on ejector nozzle performance. SAR 2.8, CER 1.00, Long Flap configuration at M_0=0.70

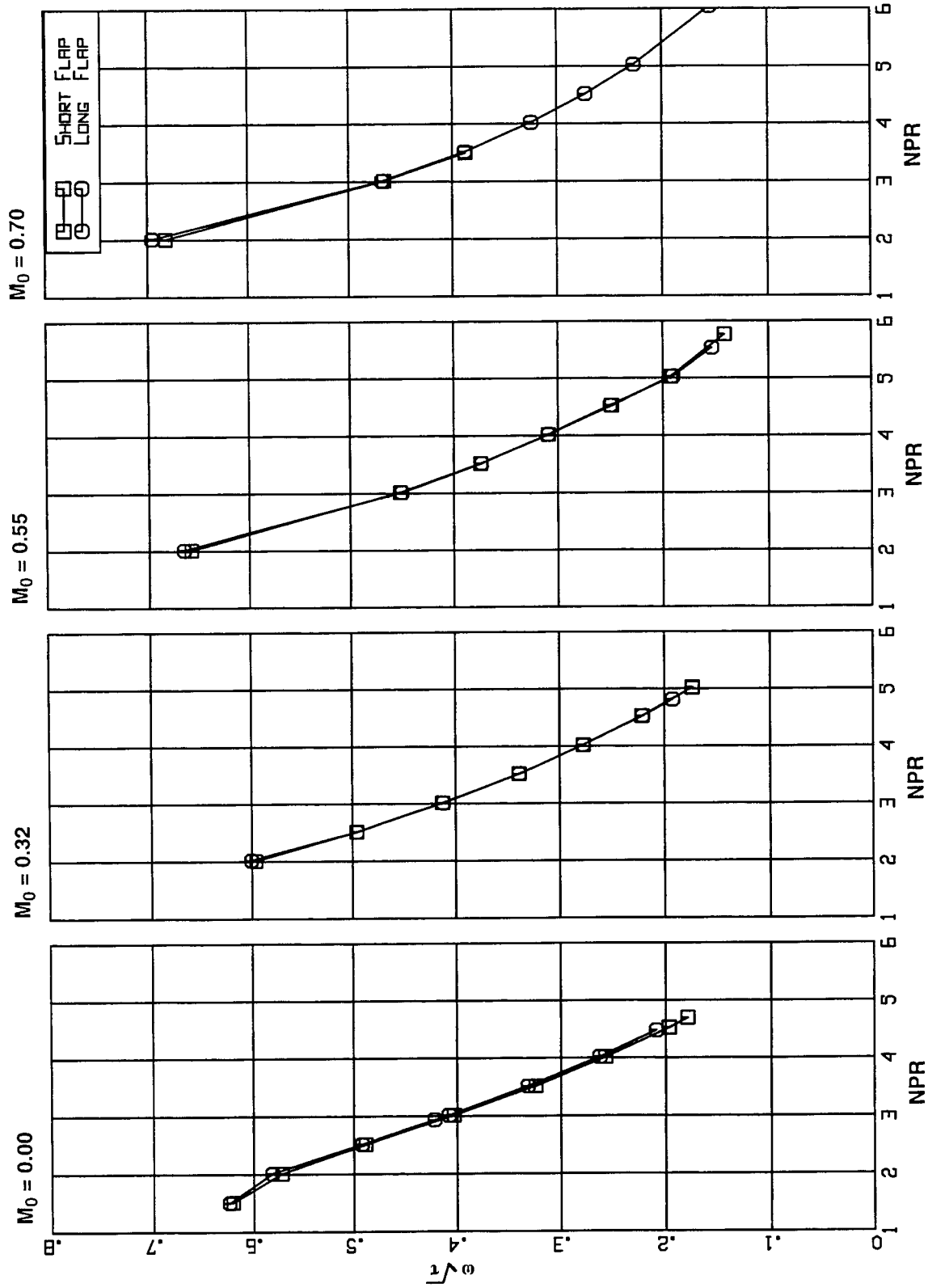

Figure 60. Effect of Flap length on ejector nozzle pumping characteristics. SAR 2.8, CER 1.00, Staggered Chute, MAR 0.95 configuration.

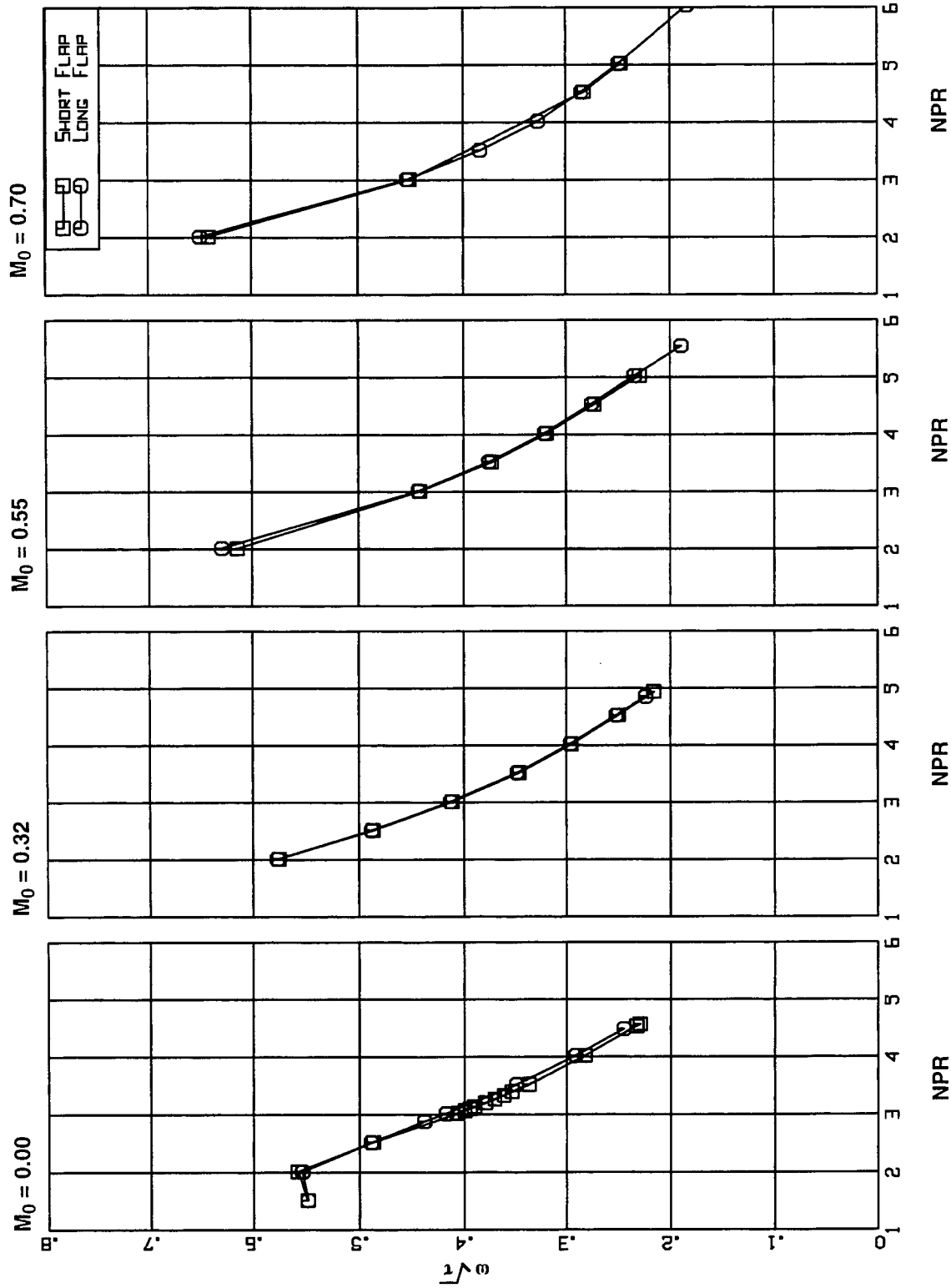

Figure 61. Effect of Flap length on ejector nozzle pumping characteristics. SAR 2.8, CER 1.22, Staggered Chute, MAR 0.95 configuration.

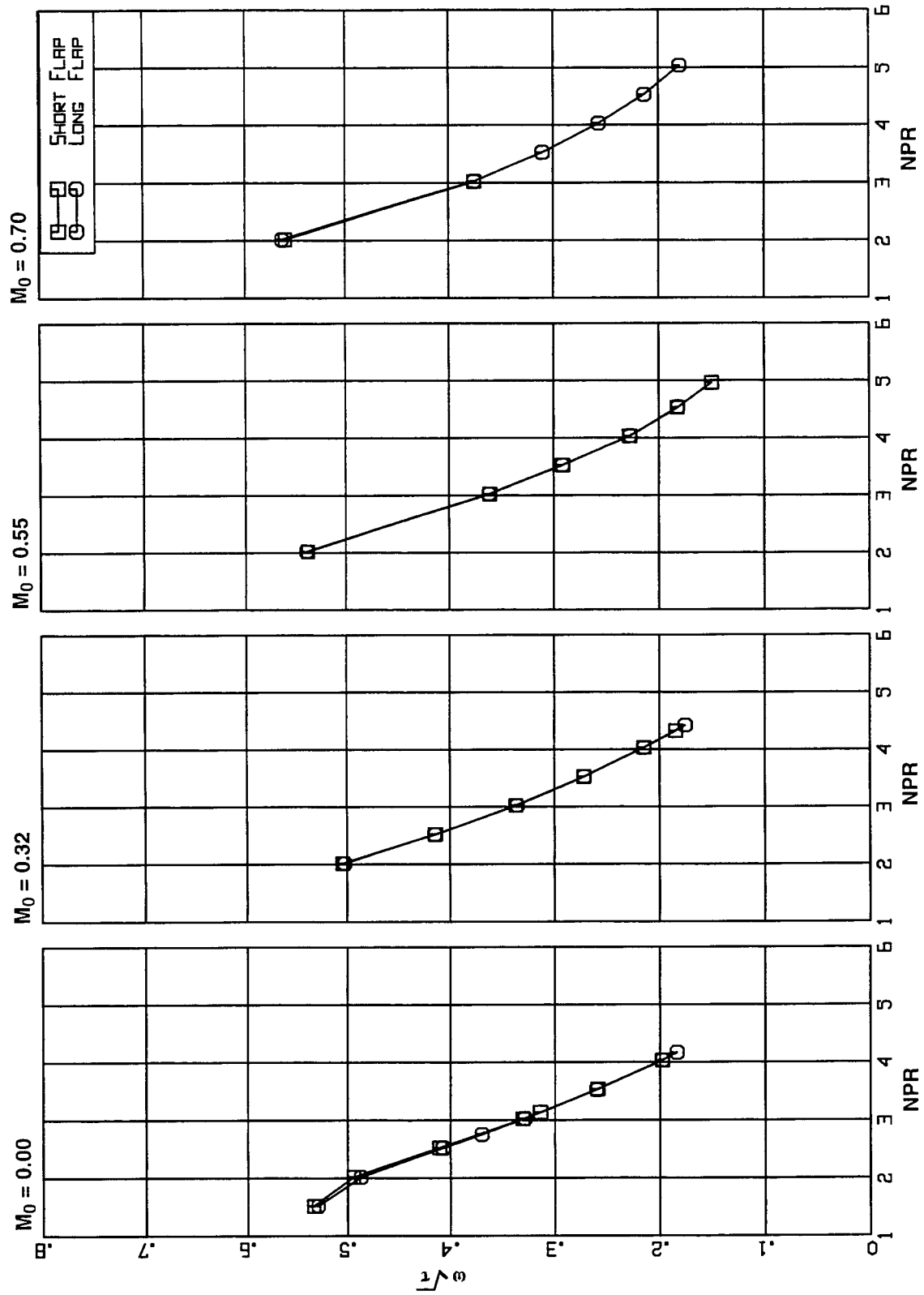

Figure 62. Effect of Flap length on ejector nozzle pumping characteristics. SAR 2.5, CER 1.00, Staggered Chute, MAR 0.95 configuration.

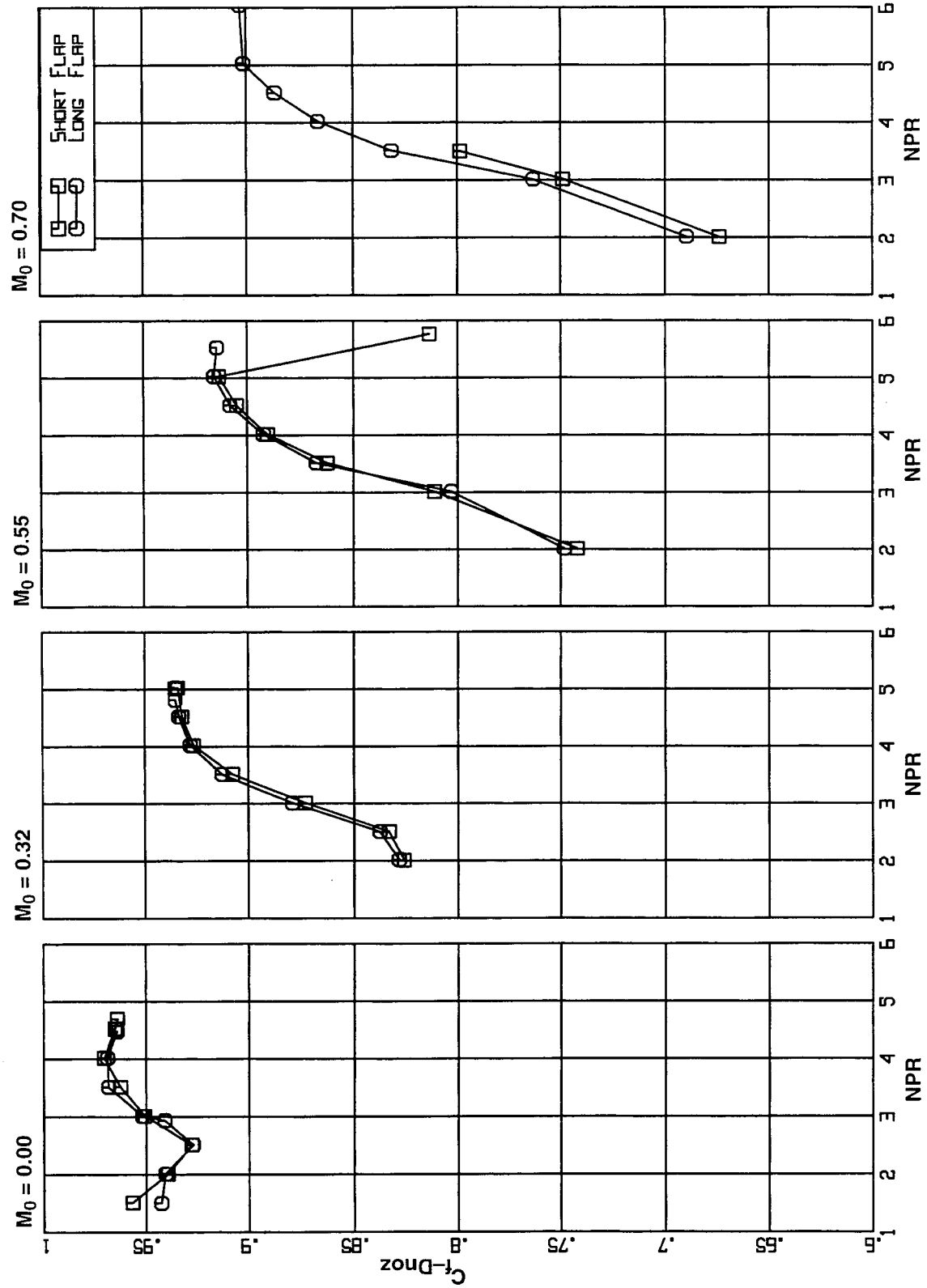

Figure 63. Effect of Flap length on ejector nozzle performance. SAR 2.8, CER 1.00, Staggered Chute, MAR 0.95 configuration.

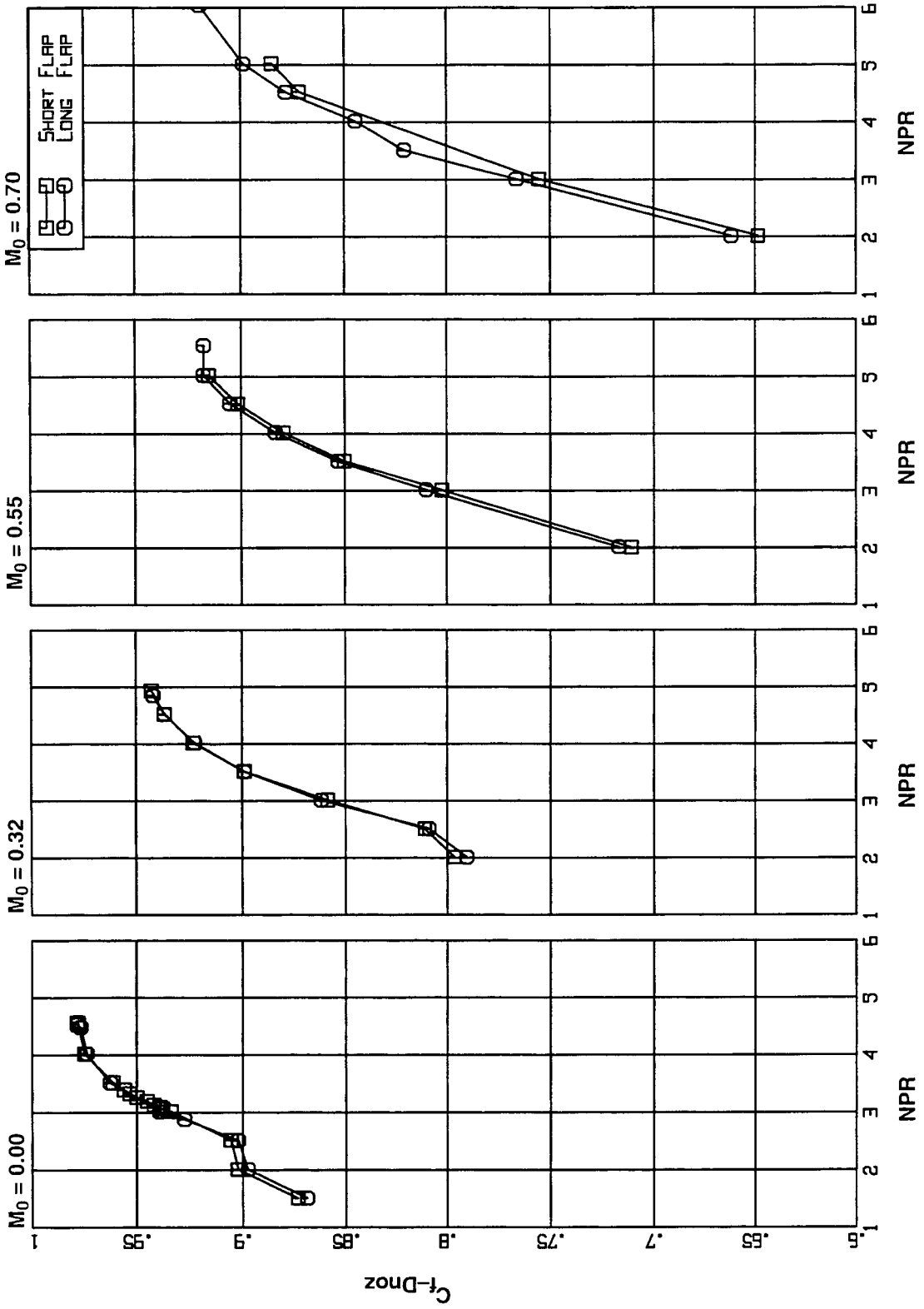

Figure 64. Effect of Flap length on ejector nozzle performance. SAR 2.8, CER 1.22, Staggered Chute, MAR 0.95 configuration.

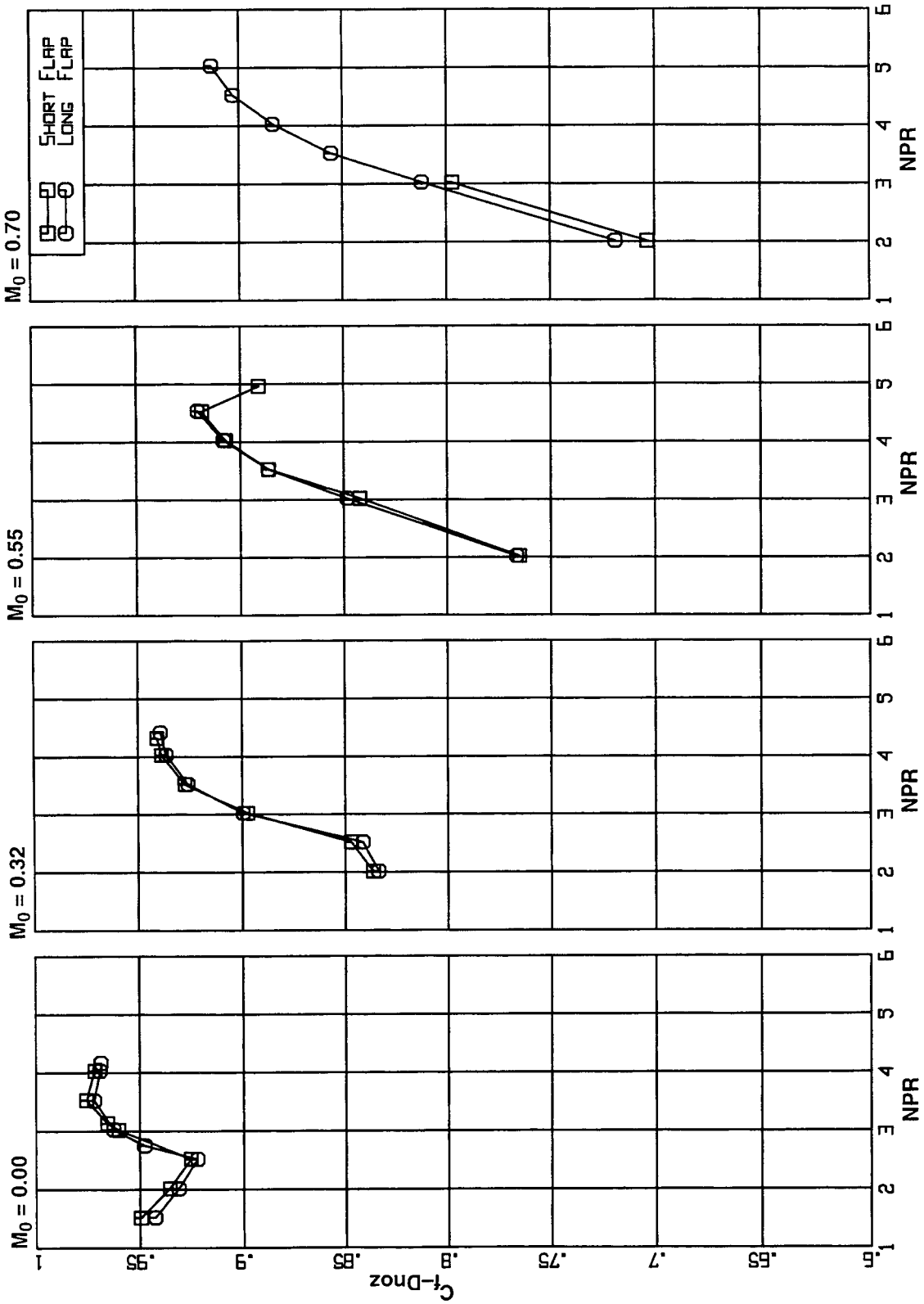

Figure 65. Effect of Flap length on ejector nozzle performance. SAR 2.5, CER 1.00, Staggered Chute, MAR 0.95 configuration.

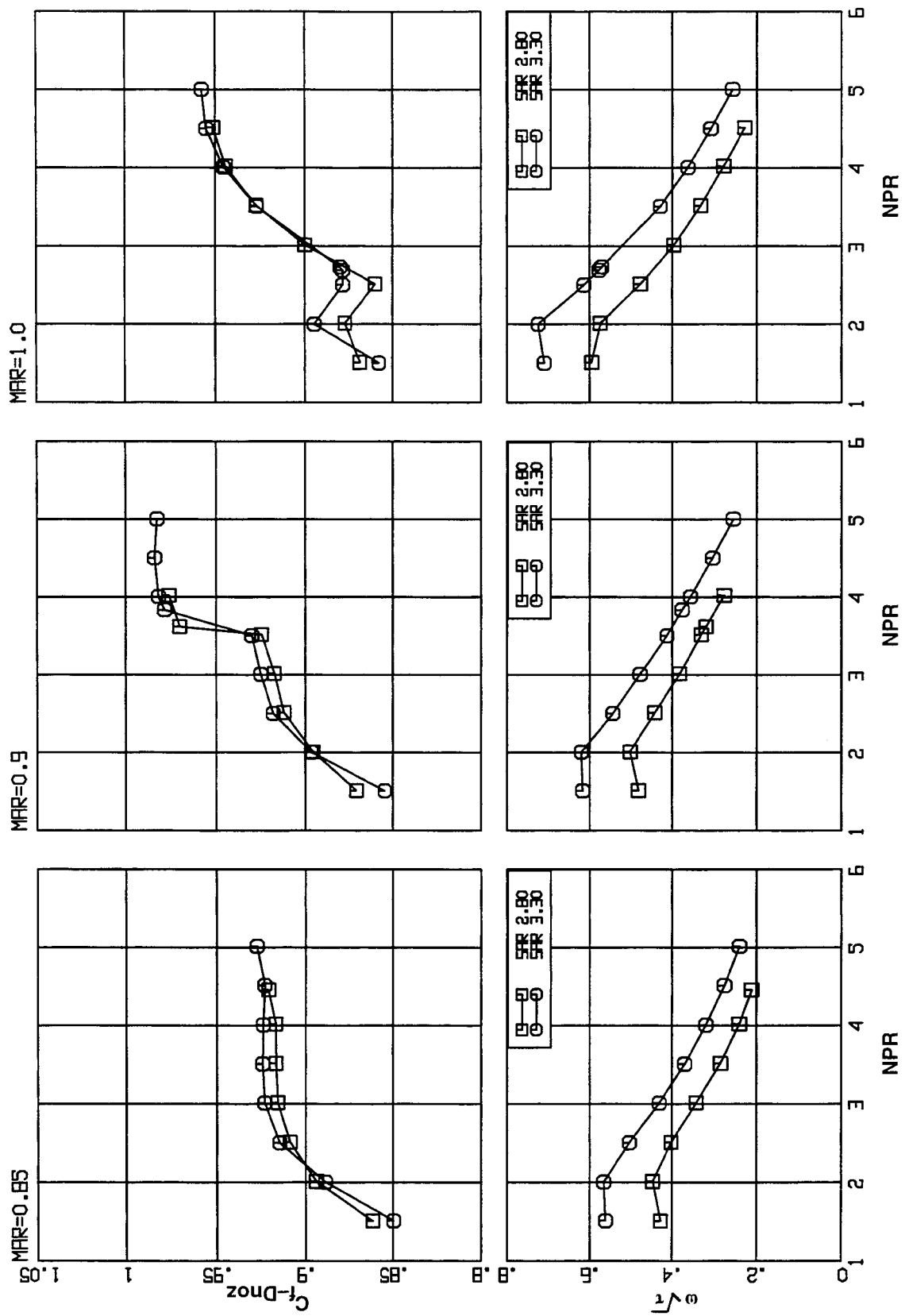

Figure 66. Effect of Suppressor Area Ratio (SAR) on ejector nozzle performance. CER 1.22, Aligned Chute, Long Flap configuration at M_0=0.00

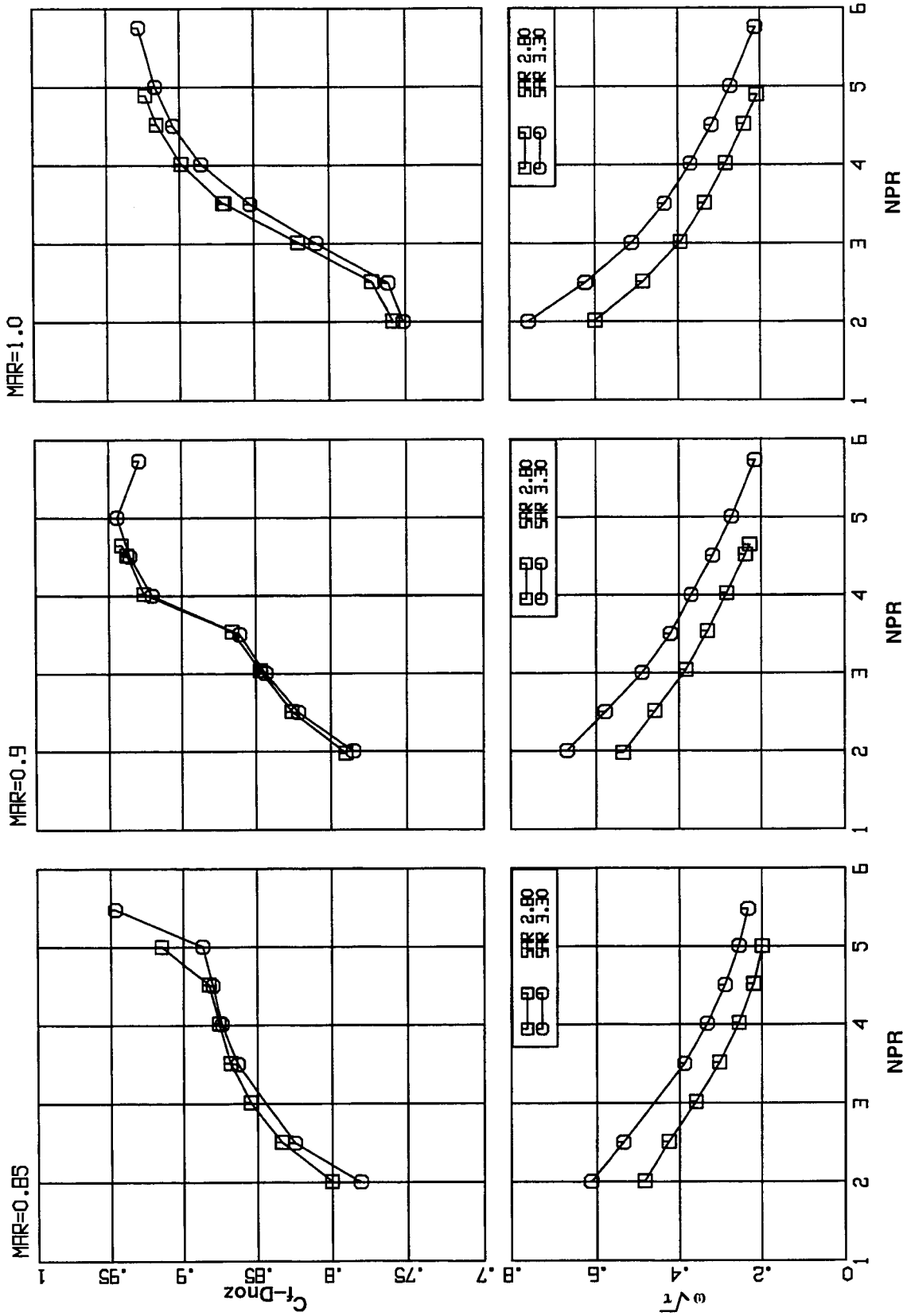

Figure 67. Effect of Suppressor Area Ratio (SAR) on ejector nozzle performance. CER 1.22, Aligned Chute, Long Flap configuration at M_0=0.32

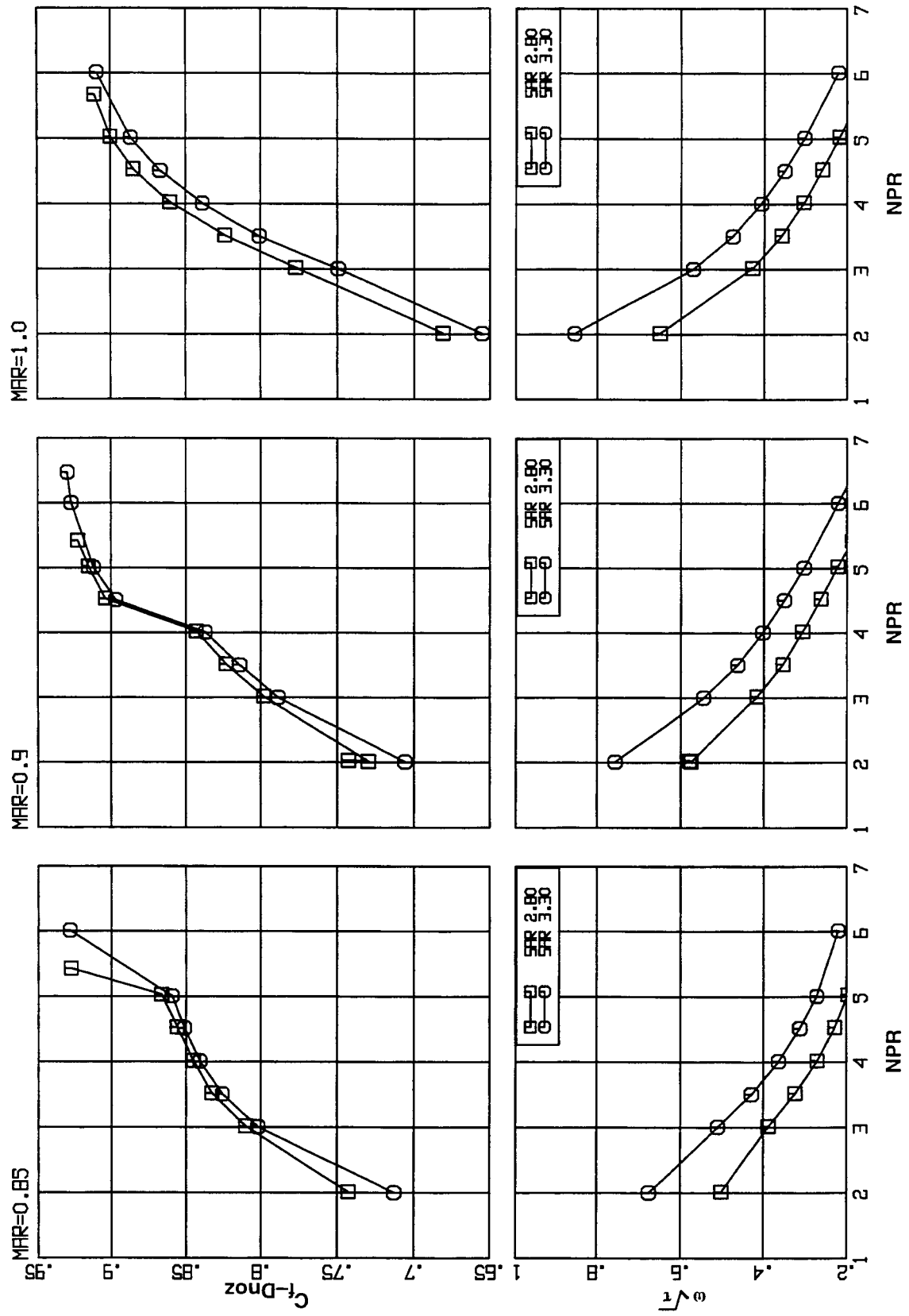

Figure 68. Effect of Suppressor Area Ratio (SAR) on ejector nozzle performance. CER 1.22, Aligned Chute, Long Flap configuration at M_0=0.55

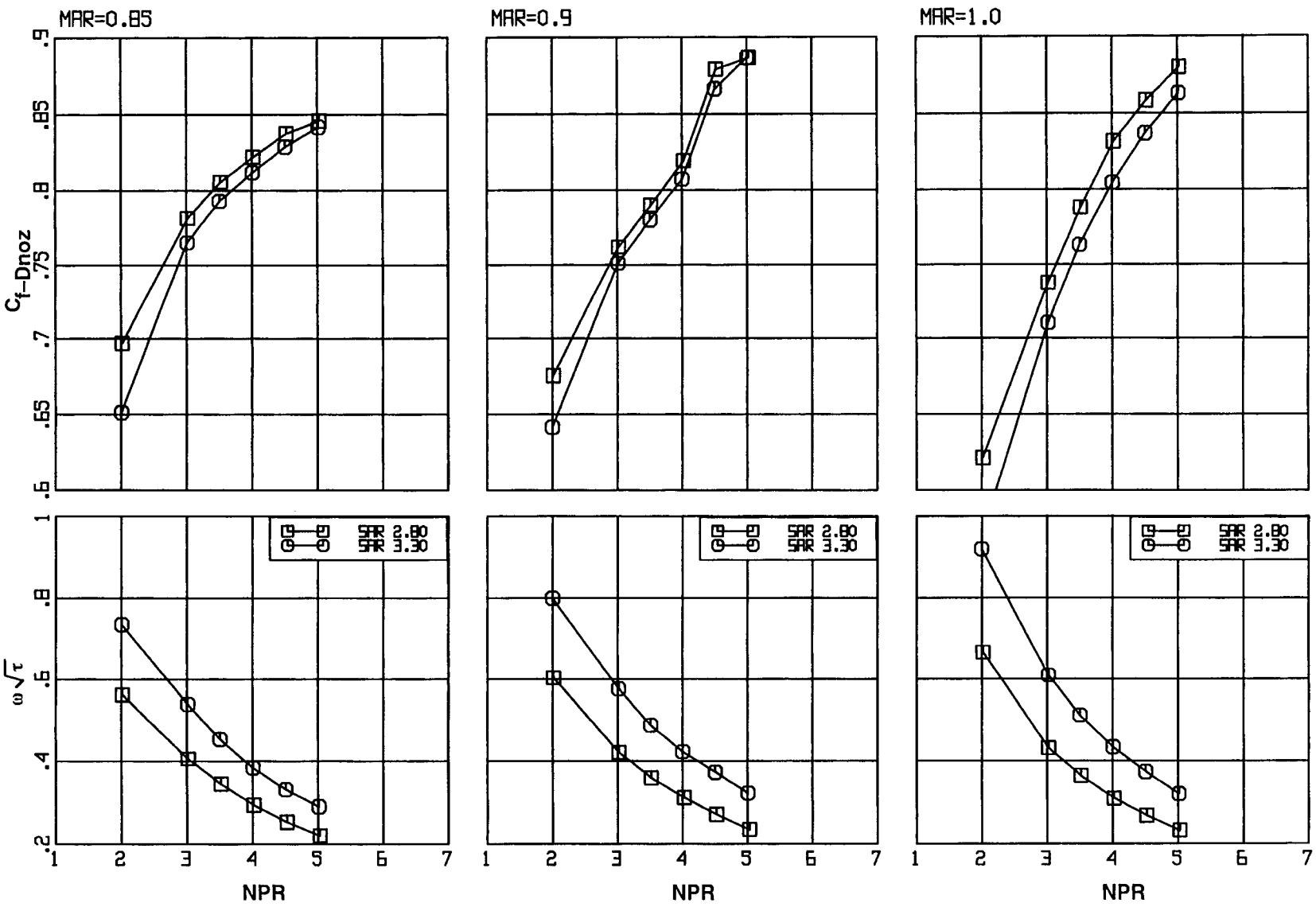

Figure 69. Effect of Suppressor Area Ratio (SAR) on ejector nozzle performance. CER 1.22, Aligned Chute, Long Flap configuration at M_0=0.70

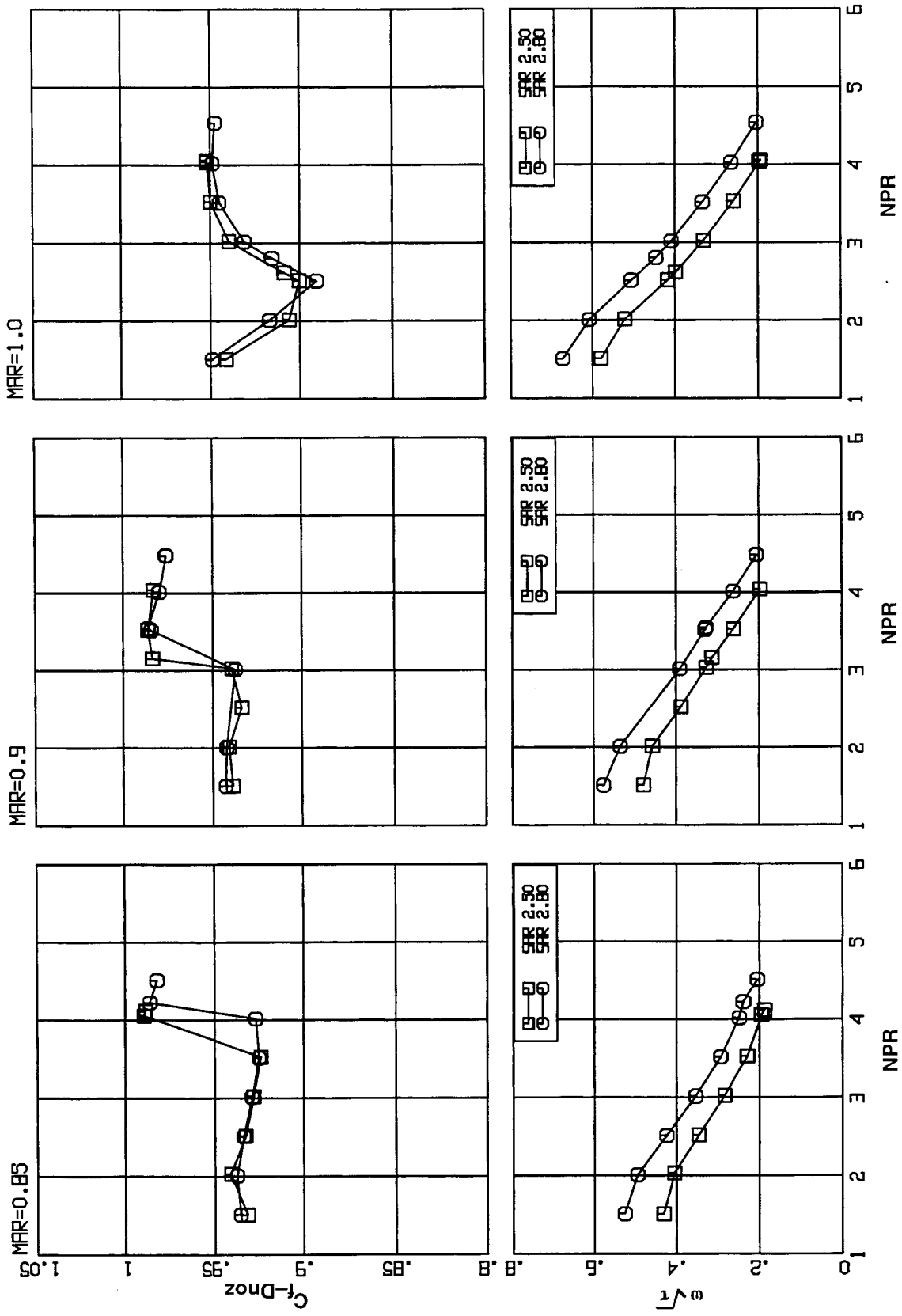

Figure 70. Effect of Suppressor Area Ratio (SAR) on ejector nozzle performance. CER 1.00, Staggered Chute, Long Flap configuration at M_0=0.00

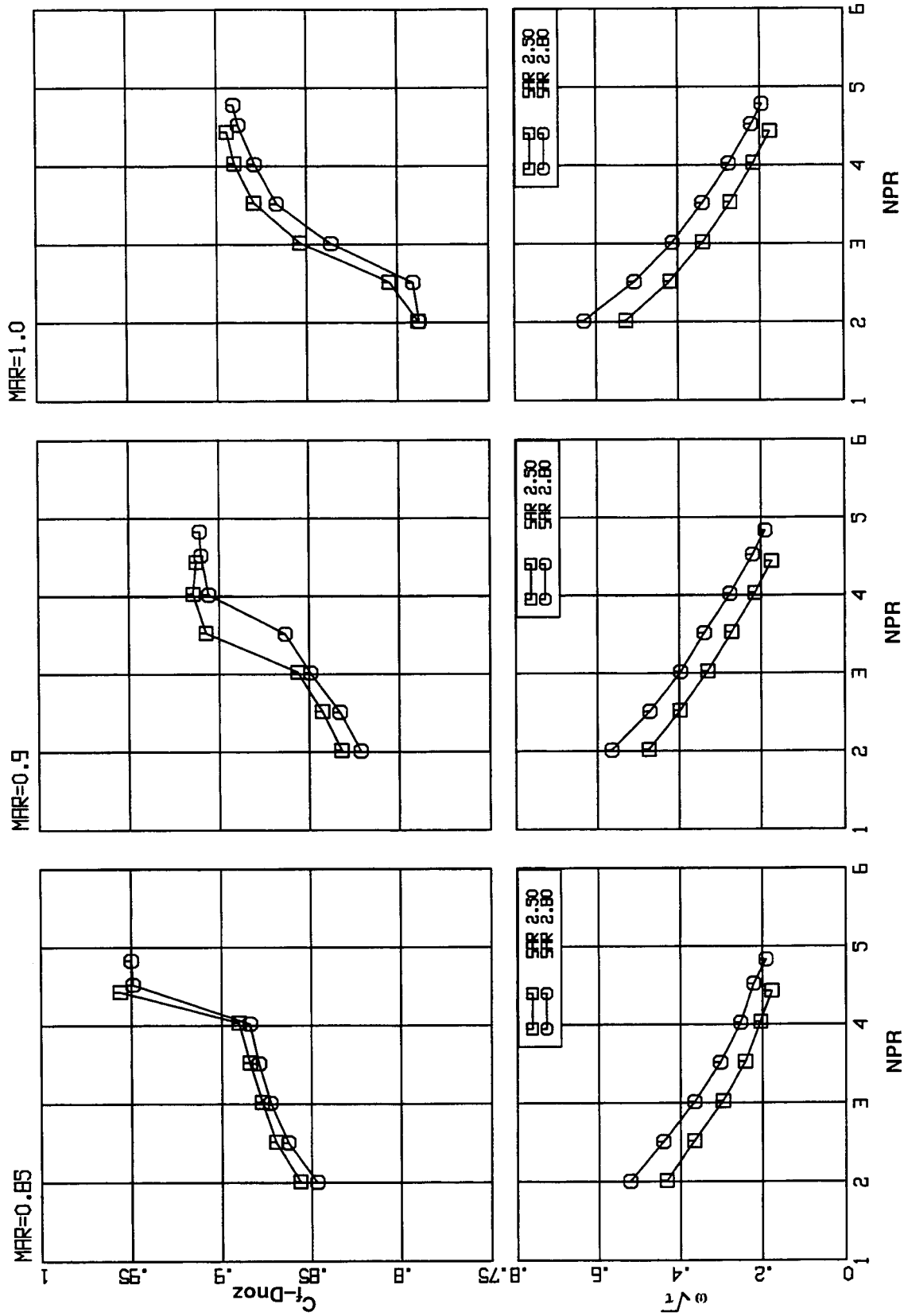

Figure 71. Effect of Suppressor Area Ratio (SAR) on ejector nozzle performance. CER 1.00, Staggered Chute, Long Flap configuration at M_0=0.32

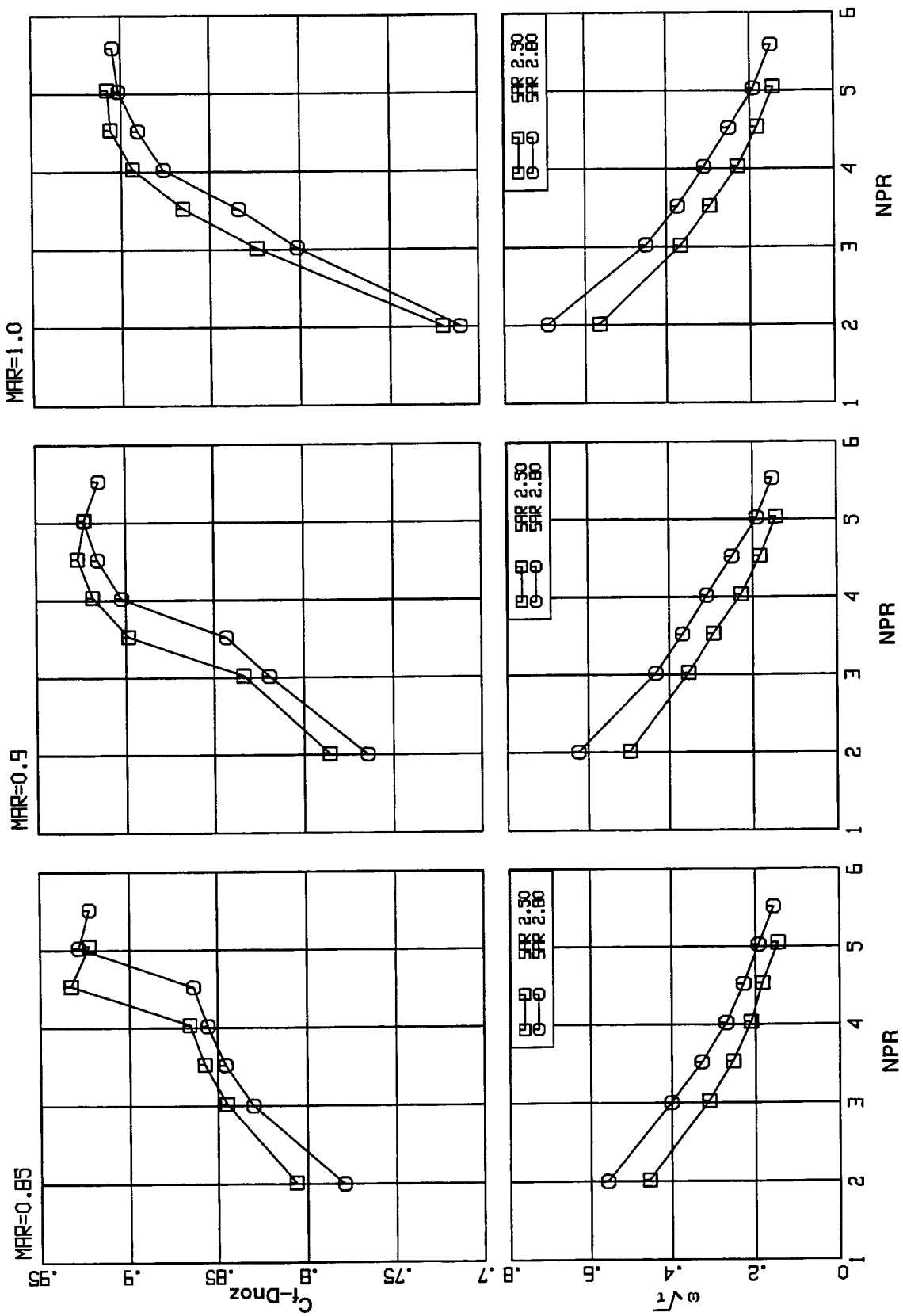

Figure 72. Effect of Suppressor Area Ratio (SAR) on ejector nozzle performance. CER 1.00, Staggered Chute, Long Flap configuration at M_0=0.55

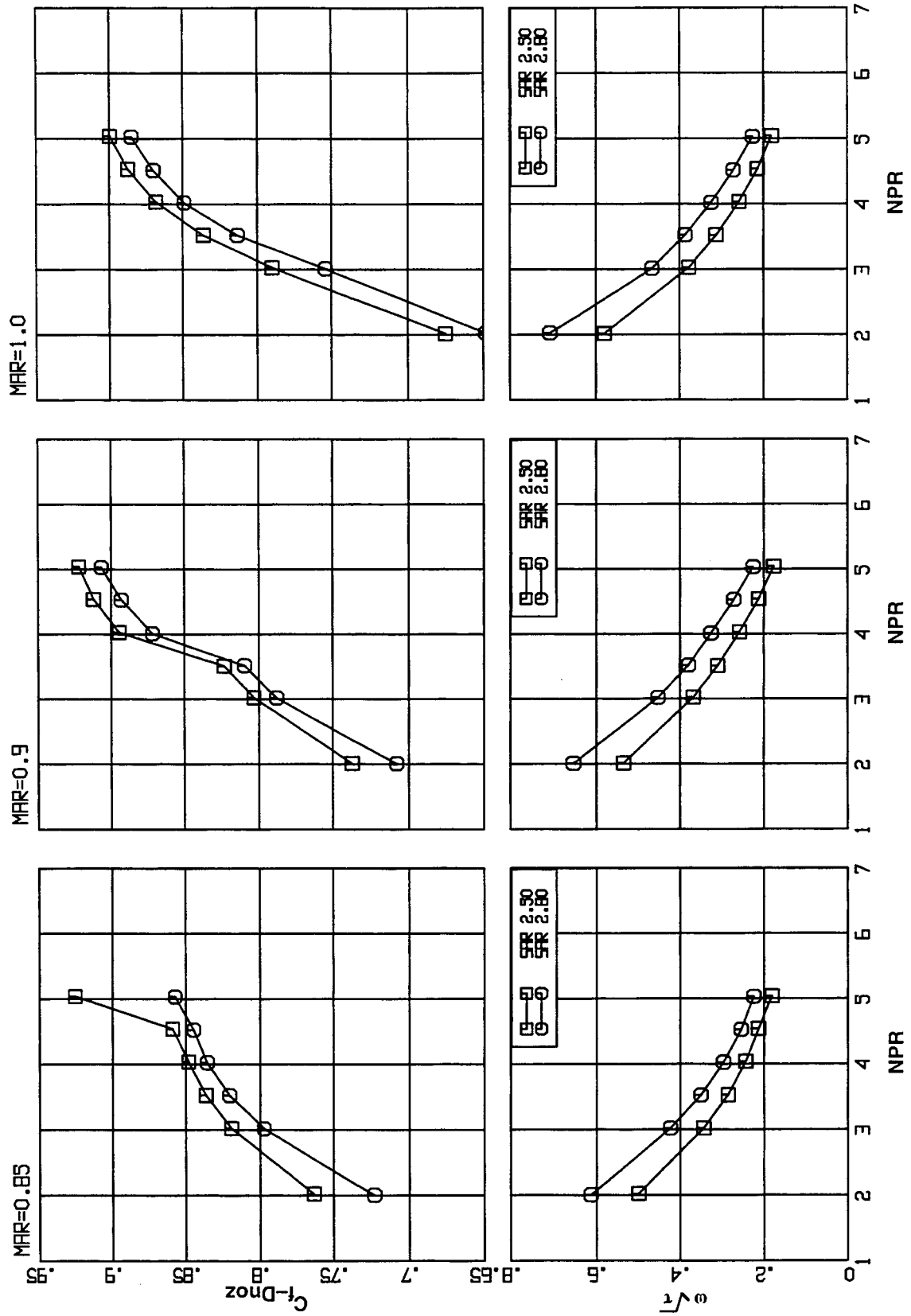

Figure 73. Effect of Suppressor Area Ratio (SAR) on ejector nozzle performance. CER 1.00, Staggered Chute, Long Flap configuration at M_0=0.70

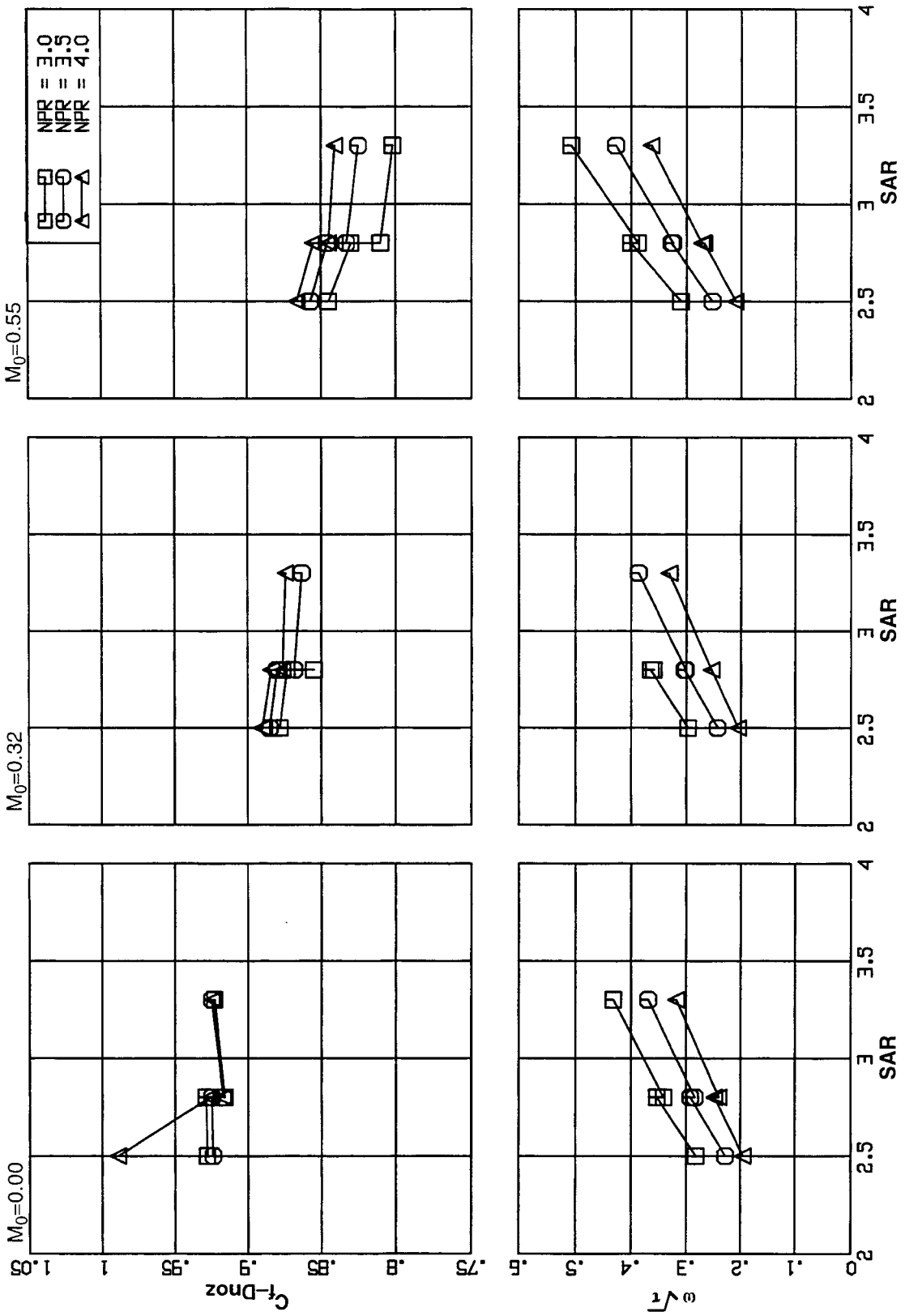

Figure 74. Effect of Suppressor Area Ratio (SAR) on ejector nozzle performance. MAR 0.85, Long flap configurations.

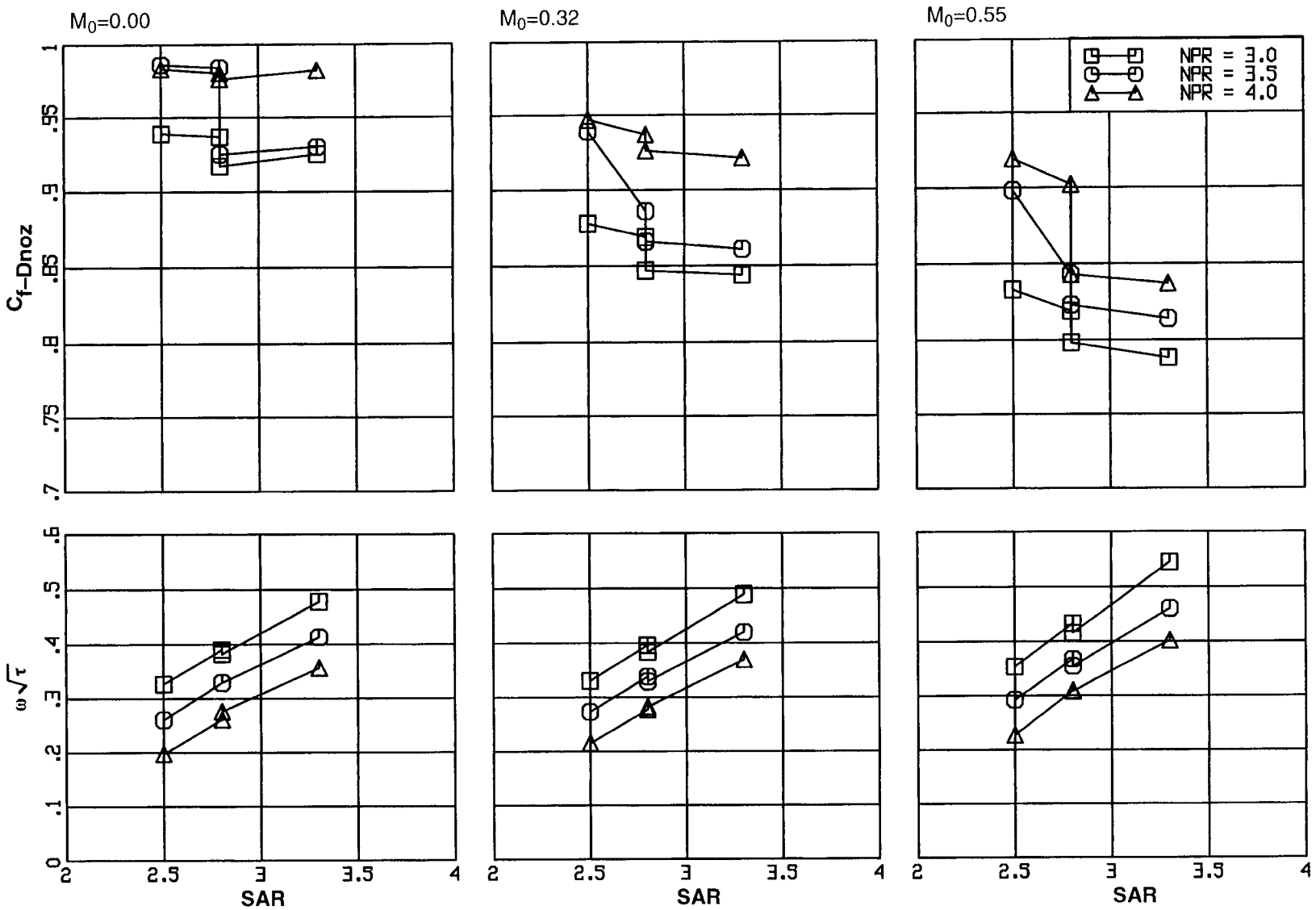

Figure 75. Effect of Suppressor Area Ratio (SAR) on ejector nozzle performance. MAR 0.90, Long flap configurations.

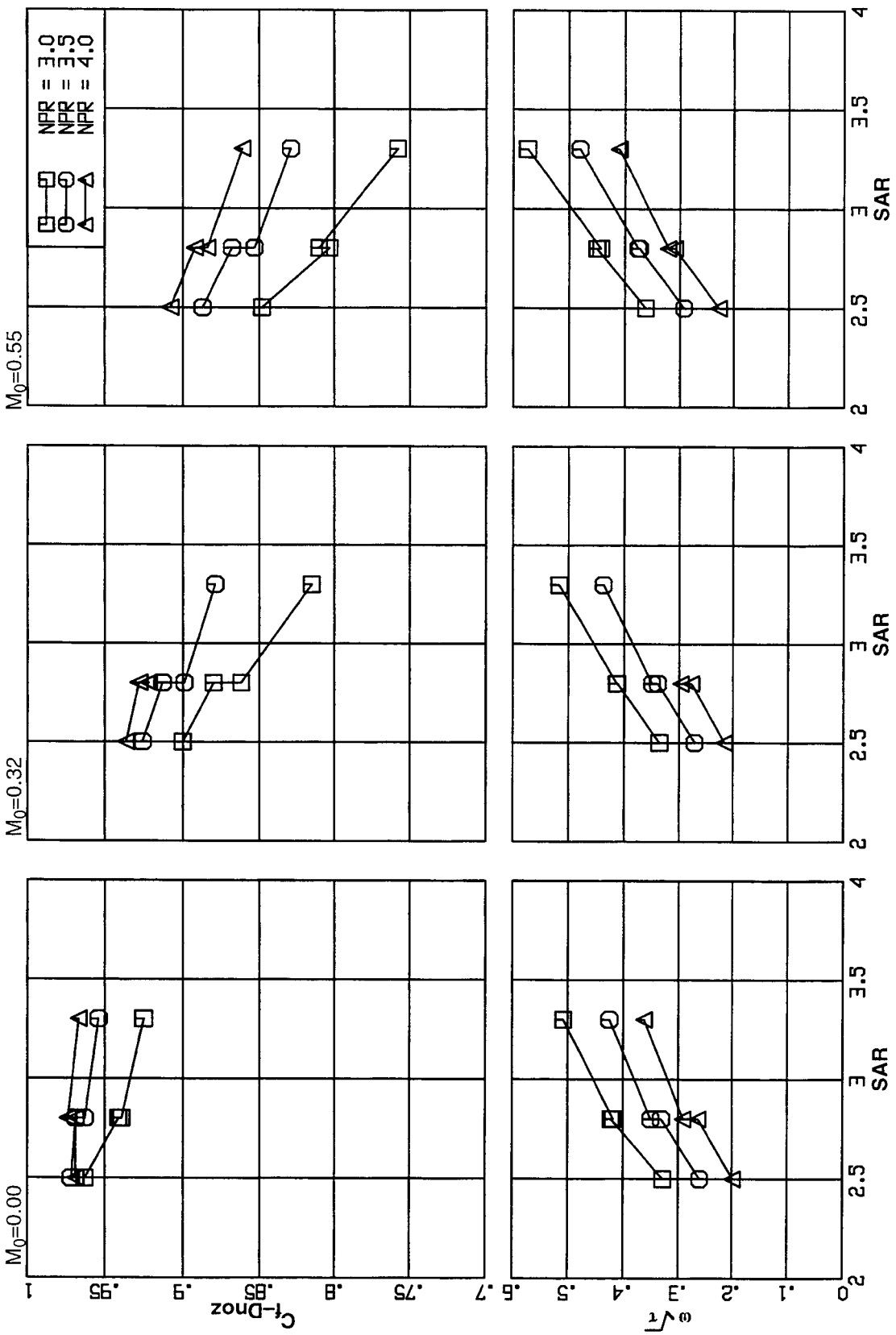

Figure 76. Effect of Suppressor Area Ratio (SAR) on ejector nozzle performance. MAR 0.95, Long flap configurations.

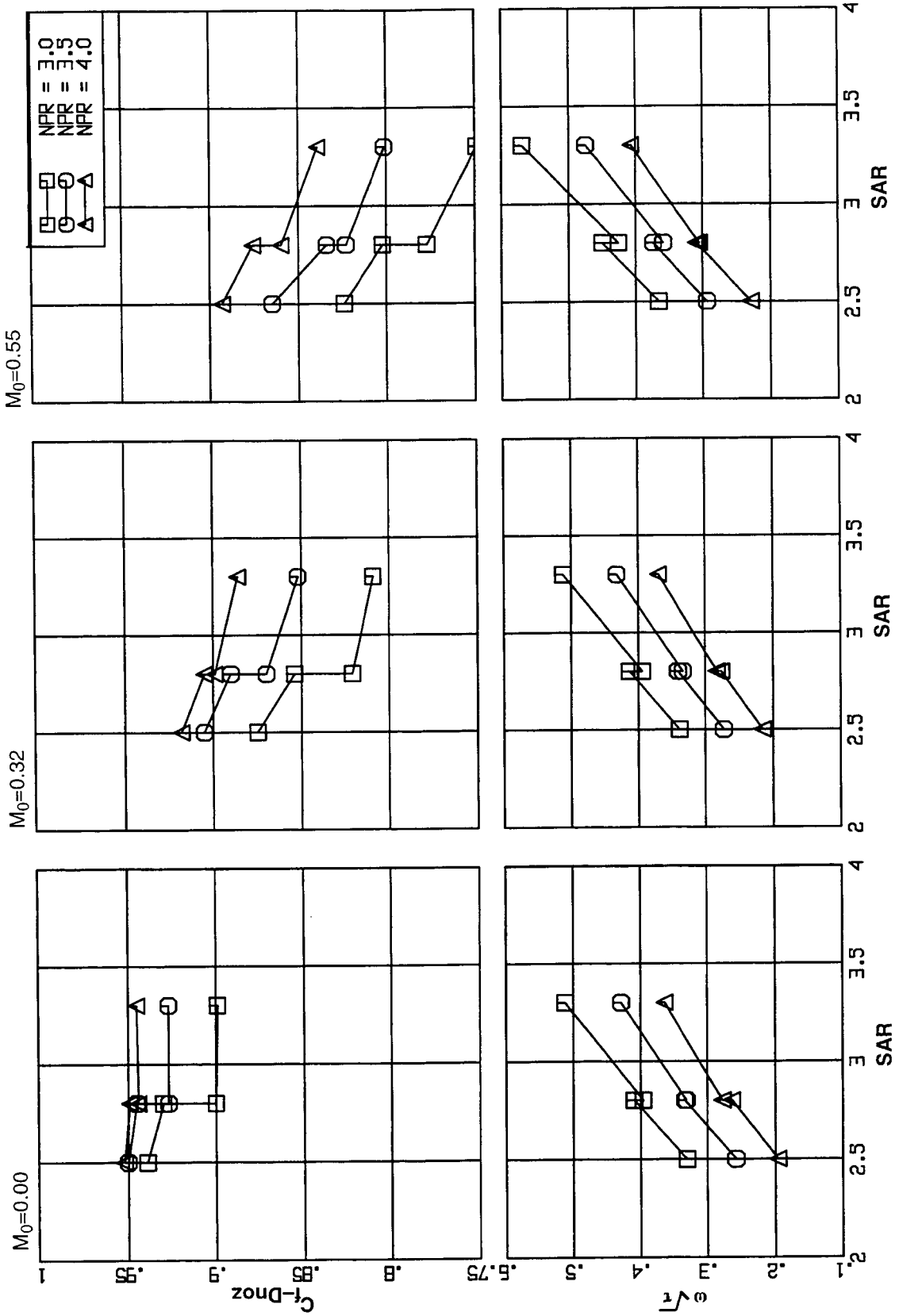

Figure 77. Effect of Suppressor Area Ratio (SAR) on ejector nozzle performance. MAR 1.0, Long Flap configurations.

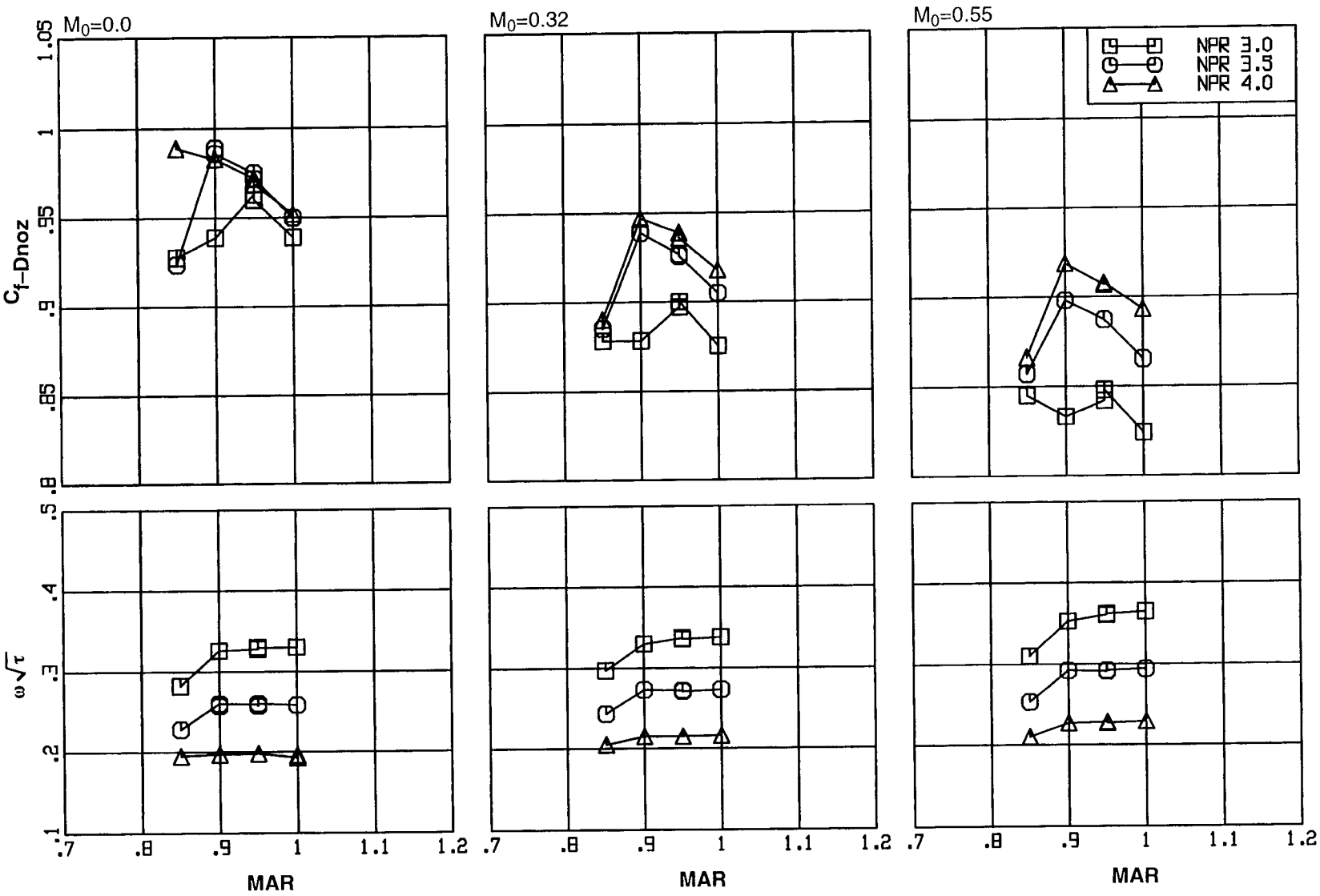

Figure 78. Effect of Mixing Area Ratio (MAR) on ejector nozzle performance. SAR 2.5, CER 1.00, Staggered Chute, Long Flap configuration.

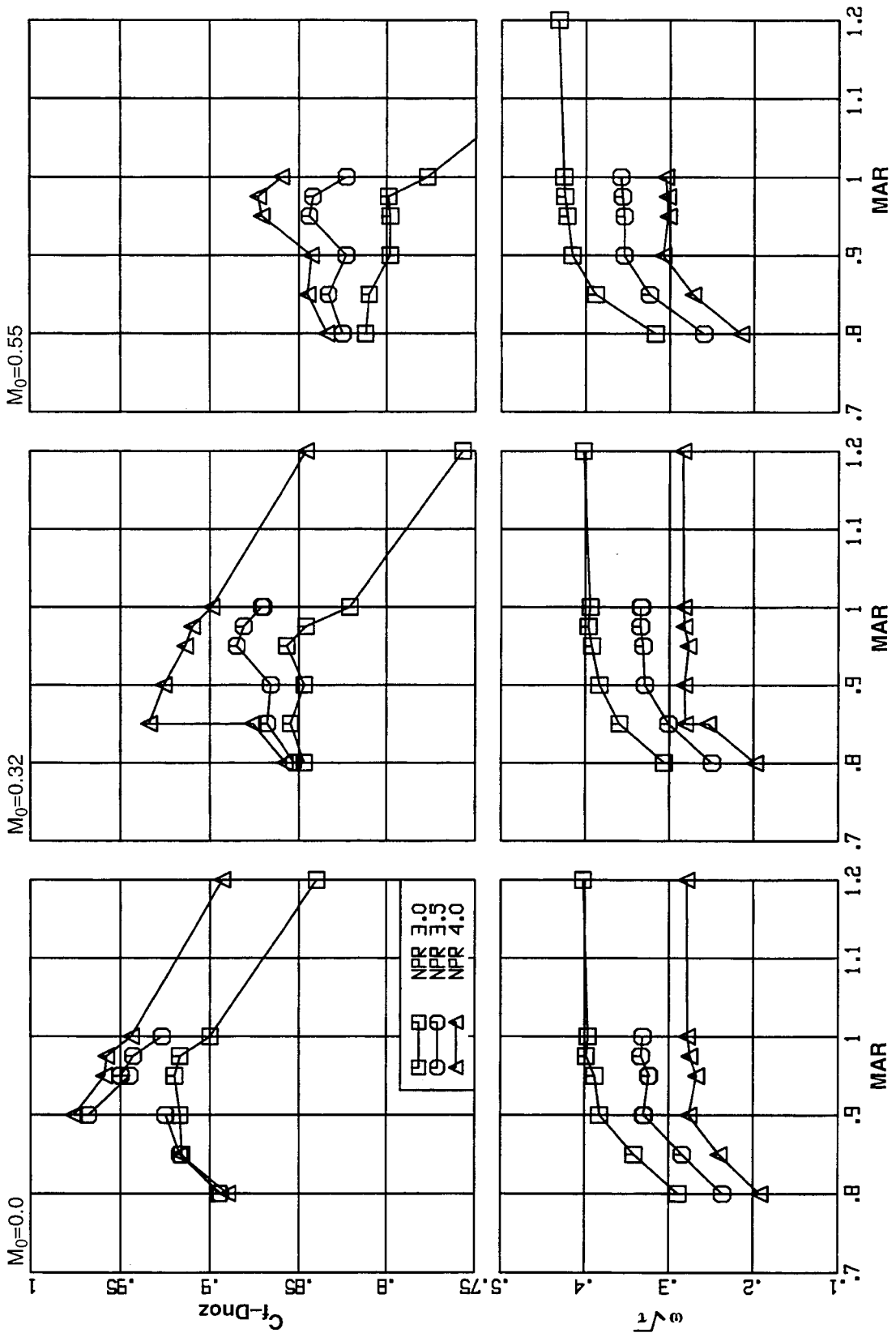

Figure 79. Effect of Mixing Area Ratio (MAR) on ejector nozzle performance. SAR 2.8, CER 1.22, Aligned Chute, Long Flap configuration.

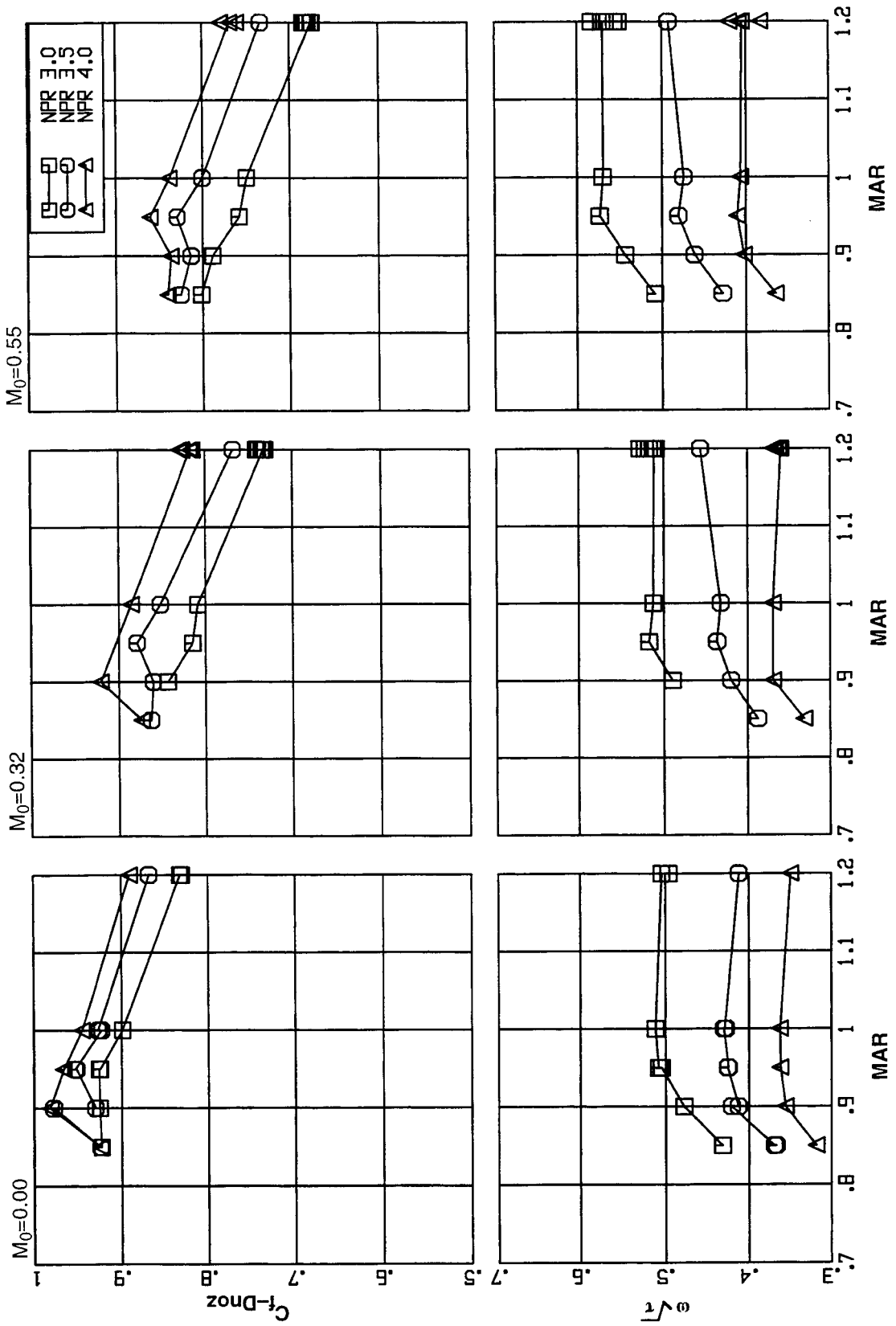

Figure 80. Effect of Mixing Area Ratio (MAR) on ejector nozzle performance. SAR 3.3, CER 1.22, Aligned Chute, Long Flap configuration.

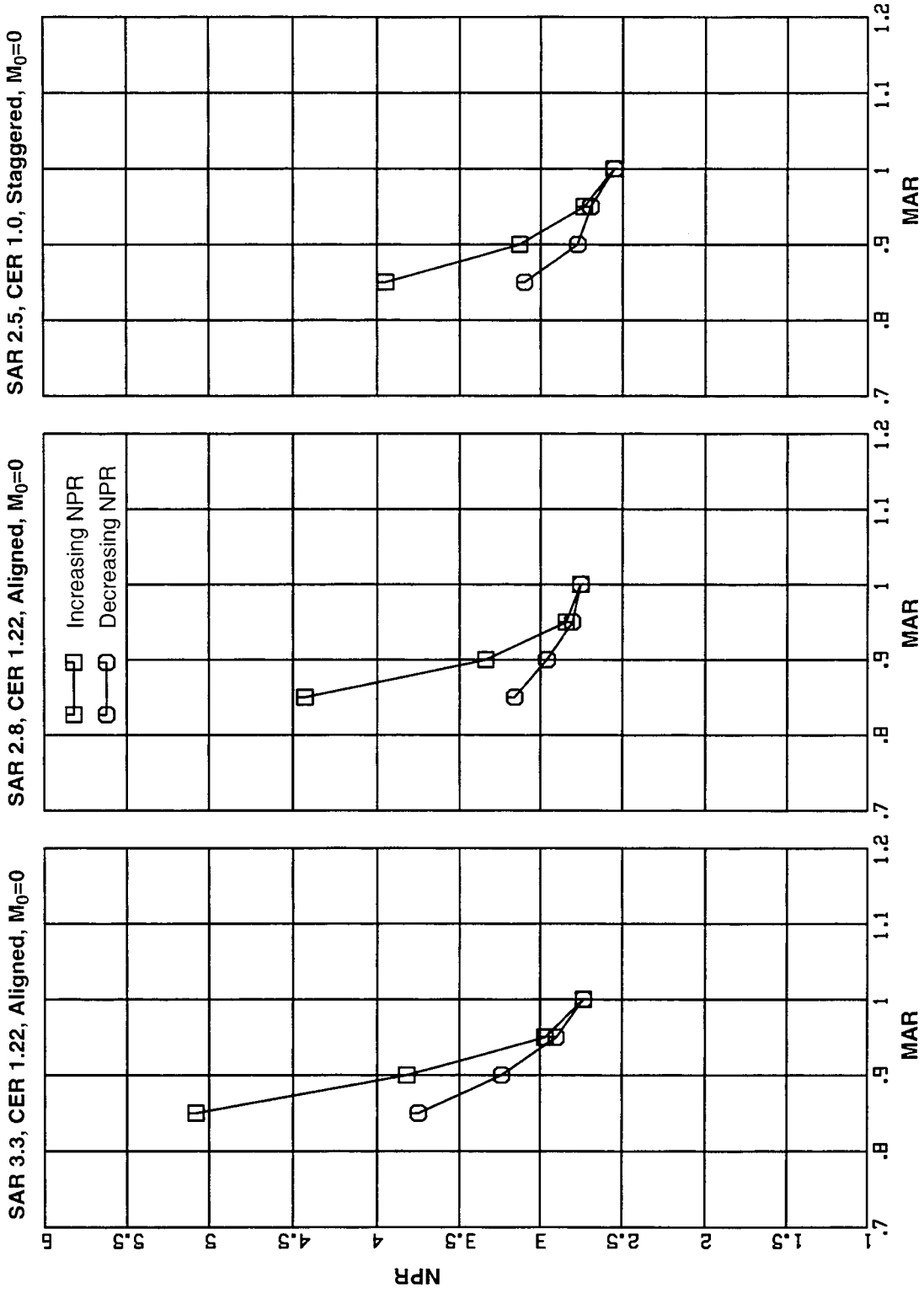

Figure 81. Effect of Mixing Area Ratio (MAR) on ejector nozzle transition pressure ratio. Long Flap configurations at static condition.

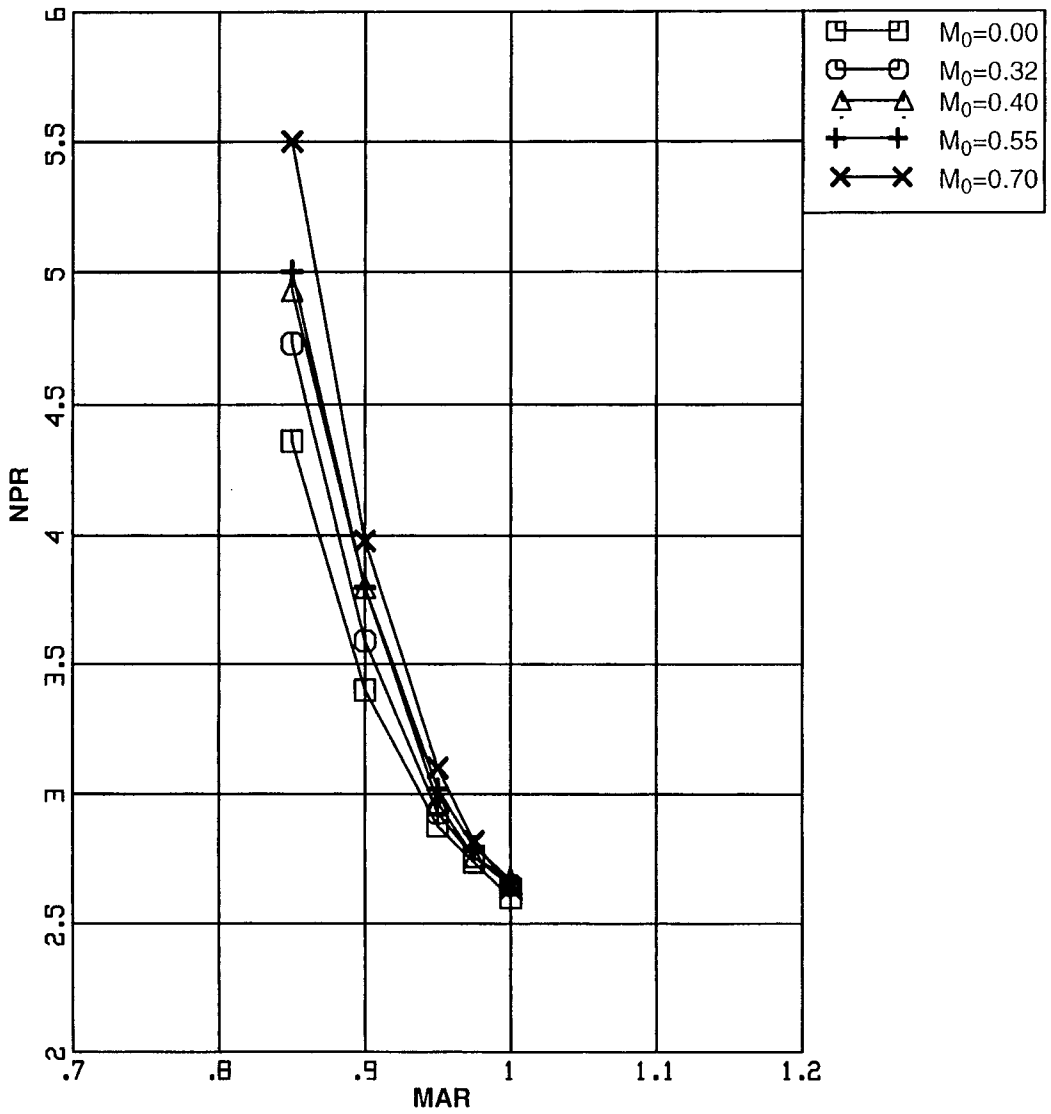

Figure 82. Effect of free stream Mach number on ejector nozzle transition pressure ratio. SAR 2.8, CER 1.00, Staggered Chute, Long Flap configurations.

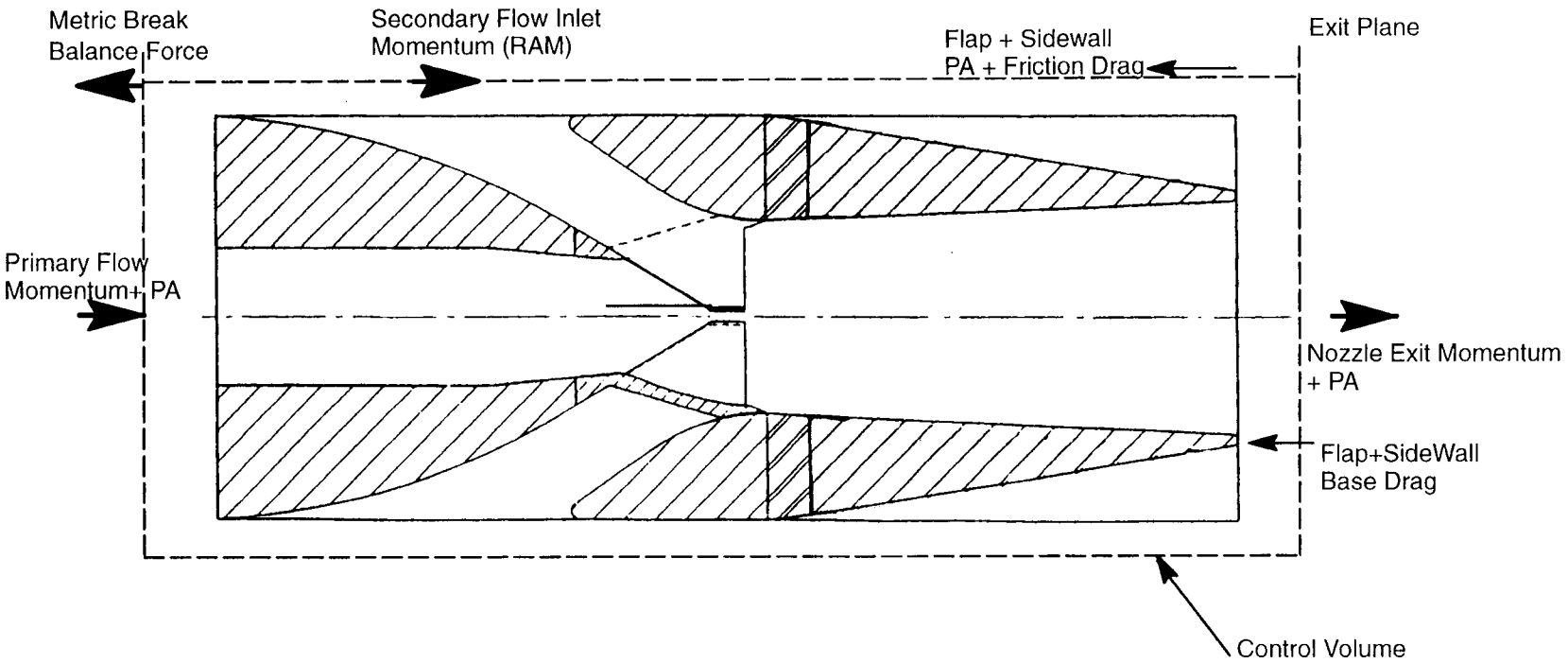

Balane Force = (Nozzle Exit Momentum+ PA) – (Primary Flow Inlet Momentum +PA) – Secondary Flow Inlet Mometum
– (Flap + SideWall PA+ Friction Drag) – (Flap + Side Wall Base Drag)
Gross Thrust = (Nozzle Exit Momentum+ PA)
Thrust Minus Drag = (Balance Force – Primary Flow (Inlet Momentum + PA)) =
= Nozzle Gross Thrust – Secondary Flow RAM – (Side wall +Flap (PA + Friction+Base) Drag)
Thrust Minus Ram Drag = Gross Thrust – Secondary Flow Inlet Momemtum

Figure 83. Schematic of various forces acting on the mixer ejector nozzle scale model and the thrust definitions.

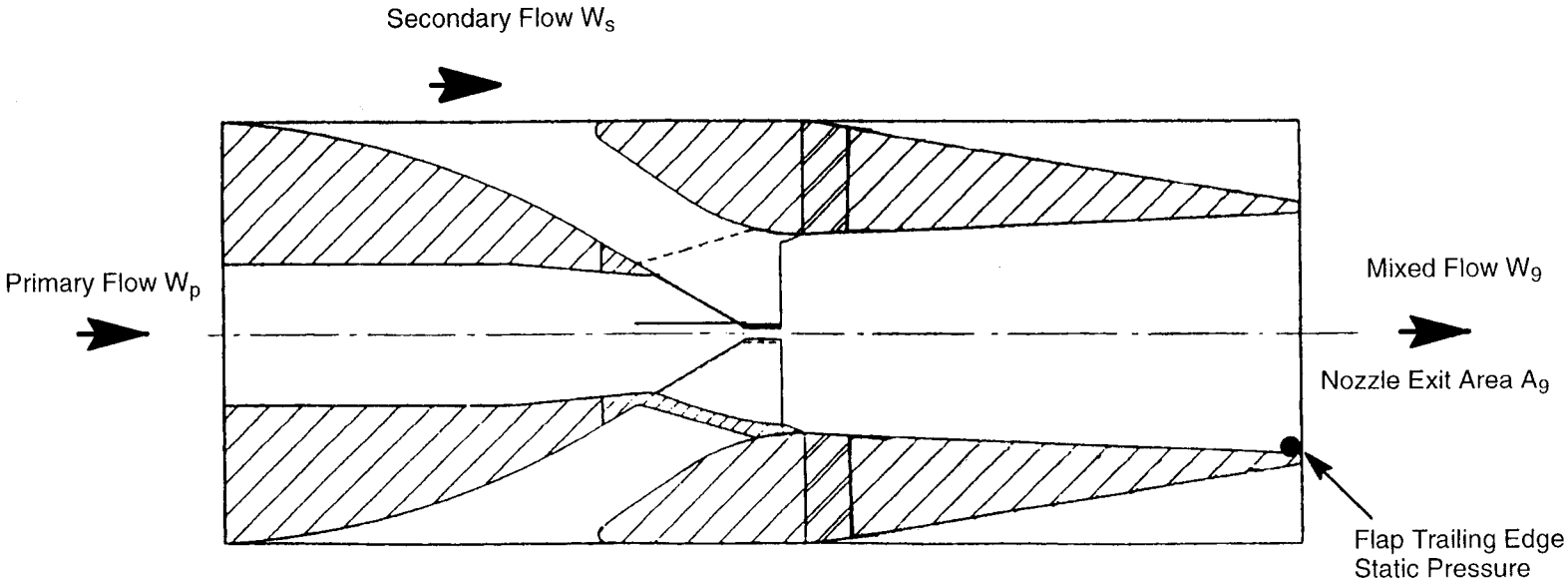

Continuity: $W_9 = W_p + W_s$

Energy: $T = (C_p W_p T_p + C_{ps} W_s T_s)/W$

Nozzle Exit Area: A_9

Estimate Nozzle Exit V_9(Velocity) and M_9 (Mach Number) under following assumptions
Subsonic Flow

Exit Static Pressure = Pambient for M < 1.0
Exit Static Pressure > Pambient for M = 1.0

Supersonic Flow

Exit Static Pressure = Measured Last Flap Static Pressure

1D Gross Turust = W_9V_9+(Pstatic$_9$ – Pambient)A_9

Figure 84. Schematic of 1D thrust estimation.

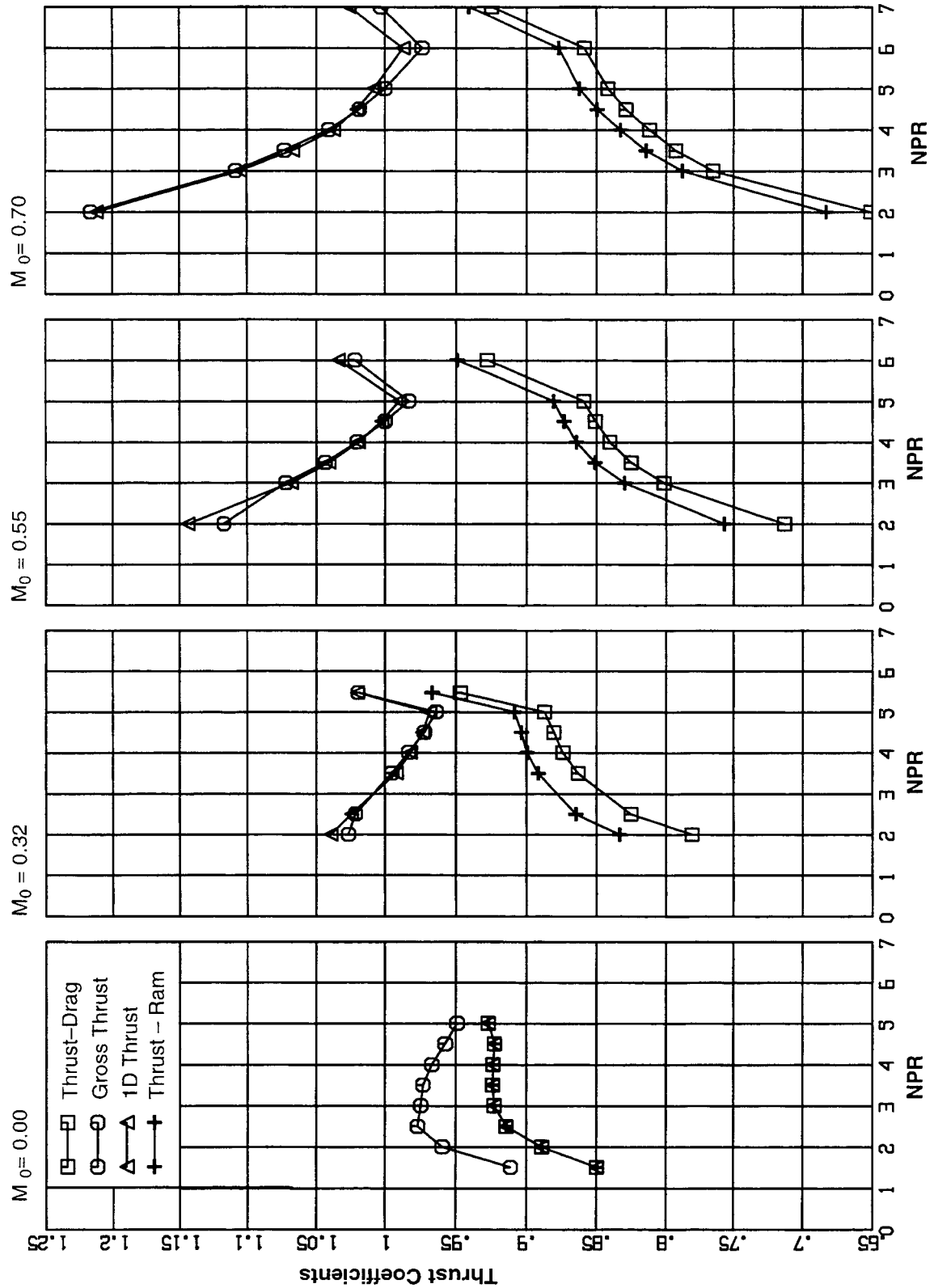

Figure 85. Comparison of estimated thrust coefficients SAR 3.3, CER 1.22, MAR 0.85 Aligned Chute, Long Flap Configuration.

REPORT DOCUMENTATION PAGE

Form Approved
OMB No. 0704-0188

1. AGENCY USE ONLY (*Leave blank*)	2. REPORT DATE	3. REPORT TYPE AND DATES COVERED
	January 2005	Final Contractor Report

4. TITLE AND SUBTITLE

Cold Aero Performance of a Two-Dimensional Mixer Ejector Nozzle

5. FUNDING NUMBERS

WBS–22–714–09–46
NAS3–26617

6. AUTHOR(S)

C. Balan

7. PERFORMING ORGANIZATION NAME(S) AND ADDRESS(ES)

GE Aircraft Engines
One Neumann Way, MD B–5
Cincinnati, Ohio 45125–1988

8. PERFORMING ORGANIZATION REPORT NUMBER

E–14647

9. SPONSORING/MONITORING AGENCY NAME(S) AND ADDRESS(ES)

National Aeronautics and Space Administration
Washington, DC 20546–0001

10. SPONSORING/MONITORING AGENCY REPORT NUMBER

NASA CR—2005-213134

11. SUPPLEMENTARY NOTES

This research was originally published internally as HSR055 in August 1997. Responsible person, Diane Chapman, Ultra-Efficient Engine Technology Program Office, NASA Glenn Research Center, organization code PA, 216–433–2309.

12a. DISTRIBUTION/AVAILABILITY STATEMENT

Unclassified - Unlimited
Subject Categories: 01, 05, and 07 Distribution: Nonstandard

Available electronically at http://gltrs.grc.nasa.gov

This publication is available from the NASA Center for AeroSpace Information, 301–621–0390.

12b. DISTRIBUTION CODE

13. ABSTRACT ***(Maximum 200 words)***

Since 1986, NASA and the U.S. aerospace industry have been assessing the economic viability and environmental acceptability of a second-generation supersonic civil transport, or High Speed Civil Transport (HSCT). Environmental acceptability in terms of airport community noise and economic viability are critical elements in this endeavor. Development of a propulsion system that satisfies strict airport noise regulations (FAR36 Stage III levels), at acceptable performance and weight, is critical to the success of any HSCT program. Two-dimensional mixer-ejector (2DME) exhaust systems are one approach in achieving this goal. In support of HSCT development, GEAE (GE Aircraft Engines), under contract to the NASA Glenn Research Center (contract NAS3–26617), conducted this test program at the NASA Langley 16 ft transonic wind tunnel to evaluate the cold aerodynamic performance aspects of the 2DME exhaust system concept. The effects of SAR (SAR, suppressor area ratio, = mixed-flow area ÷ primary nozzle throat area), MAR (MAR = overall exhaust system exit ÷ mixing-plane area), flap length, CER (suppressor chute expansion ratio), chute alignment, and free stream Mach number were investigated on a 1/11th cold aerodynamic scale model of a 2DME exhaust system.

14. SUBJECT TERMS

High speed civil transport; Mixer-ejector exhaust systems; Suppressor area ratio; Flap length; Suppressor chute expansion ratio; Chute alignment; Free stream Mach number

15. NUMBER OF PAGES

123

16. PRICE CODE

17. SECURITY CLASSIFICATION OF REPORT	18. SECURITY CLASSIFICATION OF THIS PAGE	19. SECURITY CLASSIFICATION OF ABSTRACT	20. LIMITATION OF ABSTRACT
Unclassified	Unclassified	Unclassified	